Chapter 4

Feasibility study for the ISOL production of ^{64}Cu and ^{67}Cu

"Tali [facili da intendersi] sono tutte le cose vere, doppo che son trovate; ma il punto sta nel saperle trovare"

"So [easy to understand] are all truths, once they are discovered; the point is in being able to discover them."

Galileo Galilei (Italian polymath, 1564 – 1642), *Dialogo sopra i due massimi sistemi del mondo,* day 2.

4.1 Introduction

The possibility to label the same biological vectors with pairs of radionuclides of the same element – one β^+-emitter for PET imaging and one β^--emitter for metabolic radiation therapy – is at the basis of the so called theranostics. Among the radionuclides of medical interest that could be produced with the ISOL technique, ^{64}Cu and ^{67}Cu are a promising theranostic pair [4.1]. ^{64}Cu can be used both for diagnostic (PET) and therapeutic use, thanks to its co-emission of β+ and β− particles ($t_{1/2}$ = 12.701 h) and is currently under preclinical and clinical development [4.2]. The common production routines for ^{64}Cu foresee the use of medical cyclotrons, impinging a proton beam on a nickel target (usually a ^{64}Ni enriched target, since the natural abundance of ^{64}Ni is lower than 1%) via the preferable ^{64}Ni(p,n)^{64}Cu reaction [4.3], obtaining a high quality and intense production. In addition, other possible production methods have been investigated, such as the ^{64}Zn(d,2p)^{64}Cu reaction, which is considered when less

activity is required [4.4]. In general, the production of ^{64}Cu via the aforementioned techniques can be satisfactory.

^{67}Cu is a β^- emitter ($t_{1/2}$ = 2.58 d, Eβ−av 162 keV) ideal for therapeutic applications. In addition, its low-energy gamma co-emission (185 keV, intensity 48.7%) makes it appropriate for SPECT applications, thus allowing the follow-up of the disease treatment. Finally, it represents a perfect matched pair for theranostics with the PET isotope ^{64}Cu, since the diagnosis and the subsequent therapy can be performed using chemically identical molecules [4.1]. Despite its highly potential use for the clinics, its use is nowadays very limited, due to shortage in the production. Indeed, the most investigated production routine is through the reaction ^{68}Zn(p,2p)^{67}Cu [4.5], but high proton energies (70 MeV or more) are required, in order to both avoid the excessive side production of other copper isotopes that decrease the specific activity, consequently regular small medical cyclotron with maximum proton energy ranging from 11 to 17 MeV cannot be used [4.6, 4.7]. Furthermore, since the cross sections of such reactions are generally low [4.8], an intense production is hardly achievable.

Whereas the traditional techniques can efficiently produce only ^{64}Cu, the ISOL technique could have the potential to simultaneously produce reasonable amounts of both ^{67}Cu with ^{64}Cu, using the same appropriate production target, but thanks to mass separation it would be possible to recover them independently [4.9]. However, such isotopes are barely produced with the Uranium Carbide target, already designed and studied for SPES.

Consequently, in the framework of ISOLPHARM, a feasibility study was performed in order to both identify the most suitable ISOL target for the simultaneous production of ^{64}Cu and ^{67}Cu, and to evaluate the capability of SPES technologies to ionize and recover copper beams.

Such feasibility study is reported in detail in the following chapter.

4.2 Zirconium Germanide as possible ISOL target material

When a new ISOL target material has to be chosen several requirements have to be followed. Firstly, the available primary beam characteristics in terms of maximum energy and beam particle types have to be considered, in order to identify the possible nuclear reactions that can generate the desired products. Indeed at SPES the installed cyclotron is capable of delivering a high intensity proton beam with energy in the range of 35-70 MeV [4.10]. With such primary beam, the most common nuclear reaction may be the light-ion induced fusion reaction, but also some less probable spallation or fragmentation reactions might occur if the proton energy is closer to the maximum available value. As a consequence, the target material should include stable nuclides as closest as possible to the desired products. TENDL-2015 [4.11] database was

deeply investigated in order to find appropriate candidates among the stable nuclei close to ^{64}Cu and ^{67}Cu and Zinc, Gallium and Germanium isotopes were finally considered.

A second requirement for an ISOL target is the high limiting temperature, required to allow the target to work at high temperature, as close as possible to 2000°C, in vacuum, in order to boost the temperature dependent release process. Additionally, at SPES only solid target are accepted, since the irradiation of liquid targets foresees stricter safety requirements. Consequently, only refractory materials should be used for the ISOL targets at SPES. Since none of the identified target elements (Zinc, Gallium, Germanium) is refractory in the form of a pure metal, binary refractory compounds were searched. The best identified candidate was Zirconium Germanide, that is described in detail in the next paragraph.

4.2.1 The Zirconium Germanide target material

Molten germanium targets were tested at ISOLDE, but a solid refractory germanium-containing target has never been developed, except for very preliminary investigations using Hf_5Ge_3 and Zr_5Ge_3 [4.12]. The high melting points of such germanium intermetallic compounds indicate that they may be suitable for the use in an ISOL system, thus they were considered as potential targets in this work and further developed.

The phase diagram of Zr-Ge system (figure 4.1) includes five intermetallic compounds (Zr_3Ge, Zr_5Ge_3, Zr_5Ge_4, ZrGe and Zr_2Ge) [4.13]. In particular, the phases Zr_5Ge_4 and ZrGe are characterized by the highest melting point and are expected to melt at about 2500 K (the other phases liquefy at less than 2000 K), thus they might be appropriate as an ISOL target material.

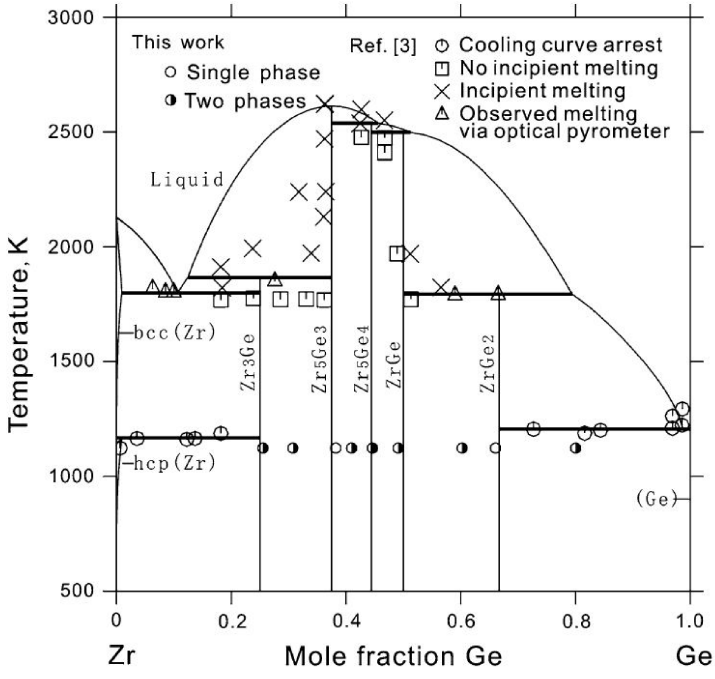

***Figure 4.1**: Zr-Ge system phase diagram* [4.13]

As declared in literature, zirconium germanides chemical resistance is not comparable with the carbides usually employed as target material. In fact, they dissolve in solfuric acid, hydrochloric, nitric acid (Zr_3Ge is an exception, indeed it remains practically unchanged), and white spirit, but in organic (acetic, oxalic, and citric) acids and in water, they are stable [4.14]. For this reason, it will be important to verify the stability of such materials at high temperature in vacuum, once a proper method for their synthesis is identified.

In literature three different methods to synthesize the zirconium germanide were briefly described [4.15, 4.16]:

- Synthesis from simple substances. This is one of the basic methods of producing germanides. It consists either in sintering a mixture of germanium and metal powders in argon or vacuum at comparatively low temperatures or in melting such a mixture in an electric arc or induction furnace provided with an inert gas (argon or helium) atmosphere. The overall reaction is:

$$mMe + nGe \rightarrow Me_mGe_n \tag{4.1}$$

- The germanothermic reduction. It consists in the vacuum-thermic reduction of transition metal oxides by germanium, which yields germanide phases of comparatively high purity;
- The Zirconium hydride method. The specimens can be prepared heating under vacuum powders of zirconium hydride and germanium.

The two latter methods were tested [4.17], and the Zirconium hydride method was chosen as the best candidate to produce the first ZrGe samples. Indeed, Germanothermic reduction, that could be realized using as precursors ZrO_2 and Ge, not convenient, because most of Ge was lost due to GeO side formation (59,6%). Moreover, another Ge fraction evaporated because of high temperatures required to boost the chemical reaction with ZrO_2.

Zirconium hydride method provided better results than the germanothermic reduction, indeed by heat treating pellets made of ZrH_2 and metallic Ge ZrGe was obtained without an excessive Ge loss. Figure 4.2 shows samples of the Zirconium Germanide as synthetized at LNL[4.18].

***Figure 4.2**: ZrGe samples after synthesis* [4.18]

As shown in figure 4.2, after synthetization the samples didn't present a regular shape, indeed the chemical reactions involved in the process released Hydrogen based gasses, thus creating macroscopic defects into the microstructure that cause its embrittlement. In order to improve the mechanical properties of the produced samples, the obtained ZrGe was subsequently grinded, and an additional sintering treatment was set. The samples obtained after the second sintering treatment showed an improved microstructure, as shown in figure 4.3.

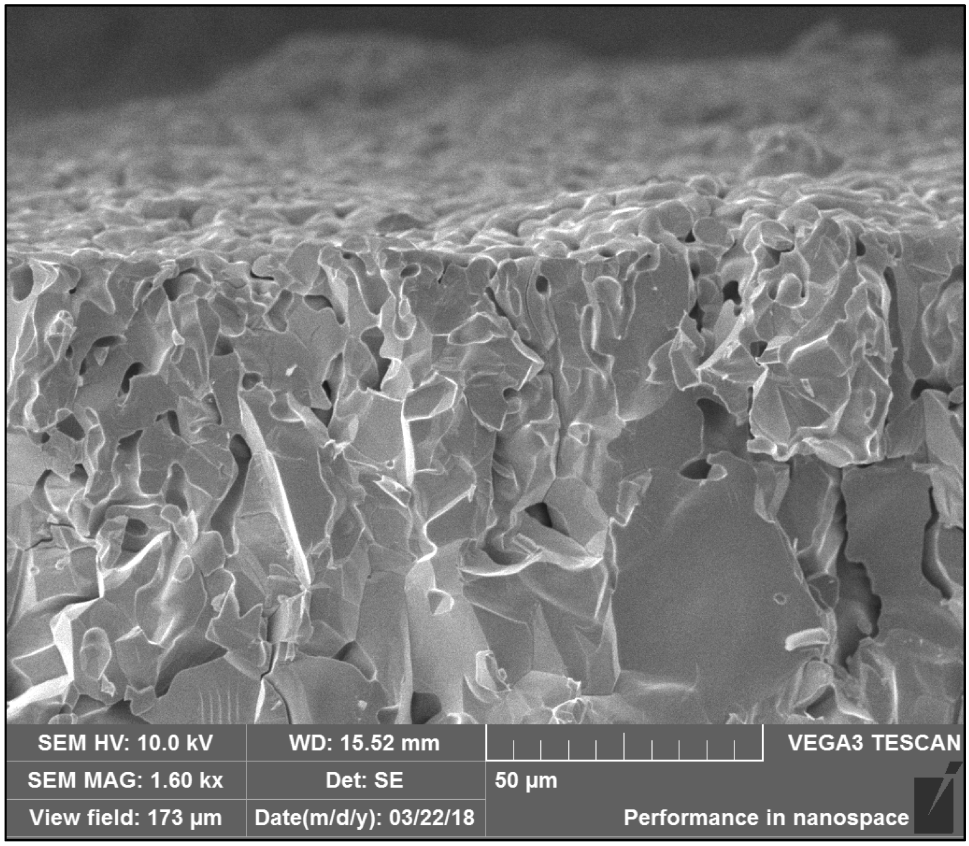

***Figure 4.3**: the microstructure of the ZrGe sample after re-sintering* [4.18].

In addition, the microstructure showed the presence of pores, a desired feature in ISOL targets since it promotes the release of the in-target produced nuclides.

Life tests at various temperatures were performed in order to evaluate the stability of the produced ZrGe samples in vacuum. Tests at 1900°C generally showed a gradual degradation of the ZrGe molecules on the surface of the samples, and the consequent evaporation of the unbound metallic Germanium. On the contrary, the samples that were treated at 1700°C didn't present a significant weight loss, since an excessive thermal decomposition of the ZrGe molecule didn't occur. Such working temperature, even if lower than the preferable 2000°C for the UC_x target [19], is still acceptable, since copper isotopes are expected to be released at even lower temperatures.

4.2.2 Yields from a ZrGe target

Once the feasibility of a suitable ISOL Germanium-based target was proved, and the first ZrGe samples were produced, the following step was the characterization of the expected yields from such target. A preliminary evaluation of the cross section of the reactions ^{nat}Ge(p, X)^{64}Cu and ^{nat}Ge(p, X)^{67}Cu was performed according to the data published in TENDL-2015 database [4.11], as indicated in figure 4.4. Such trends were obtained from the weighted average of the single contributes, reported in the database for each stable isotope of Germanium, that are ^{70}Ge (nat. abundance 20.52%), ^{72}Ge (nat. abundance 27.45%), ^{73}Ge (nat. abundance 7.76%), ^{74}Ge (nat. abundance 36.52%) and ^{76}Ge (nat. abundance 7.75%), using as weight the respective natural abundances.

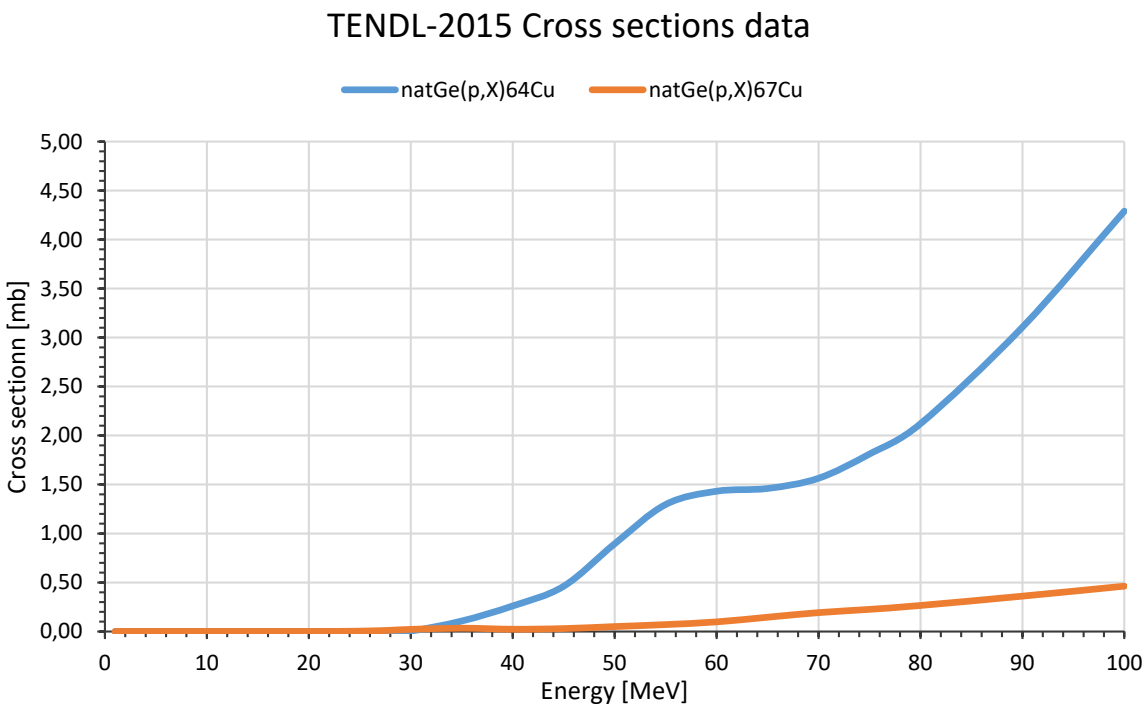

Figure 4.4: *cross section data taken form TENDL-2015* [4.11]

As shown in figure 4.4, generally, the higher is the proton energy, the higher is the cross section for both reactions. Moreover, for proton energy lower than 30 MeV, no ^{64}Cu and ^{67}Cu production is expected. For these reasons, a proton beam with energy as close as possible to the maximum available at SPES (70 MeV) should be foreseen for the ZrGe target. However, even at 70 MeV the cross sections presented in figure 4.4 are generally low, approximately 1.6 mb for the ^{nat}Ge(p, X)^{64}Cu reaction and 0.2 mb for the ^{nat}Ge(p, X)^{67}Cu reaction. Anyway, since normally SPES targets will also act as proton beam dump, the whole beam energy can be exploited, thus the yields are depending on the integrated cross section from the maximum available proton energy to zero, and not on the punctual cross section value corresponding to precise proton energy. In addition, the multi-foil target architecture proposed at SPES is suitable

to sustain intense proton beams (up to 200 μA) by splitting the power deposition into a certain amount of disks [4.20]. Since the same architecture will be adopted for the ZrGe target concept, the subsequent yields estimations were performed considering a 70 MeV 100 μA proton beam. A preliminary investigation of the expected in-target yields was performed by means of the Monte Carlo code FLUKA [4.21] (version 2011.2x.2). A simplified 4 cm diameter cylindrical geometry was considered for the Zirconium Germanide target with a hypothesized material density of 4 g/cm^3 (in accordance with the expected density of the ZrGe samples). A target thickness of 5cm was used, for ensuring the dumping of the beam within the production target. For the 70 MeV 100 μA (6.242E+14 p/s) proton beam a Gaussian profile was used with rms of 0.5 cm in both transverse axes. Figure 4.5 summarizes the so-calculated yields.

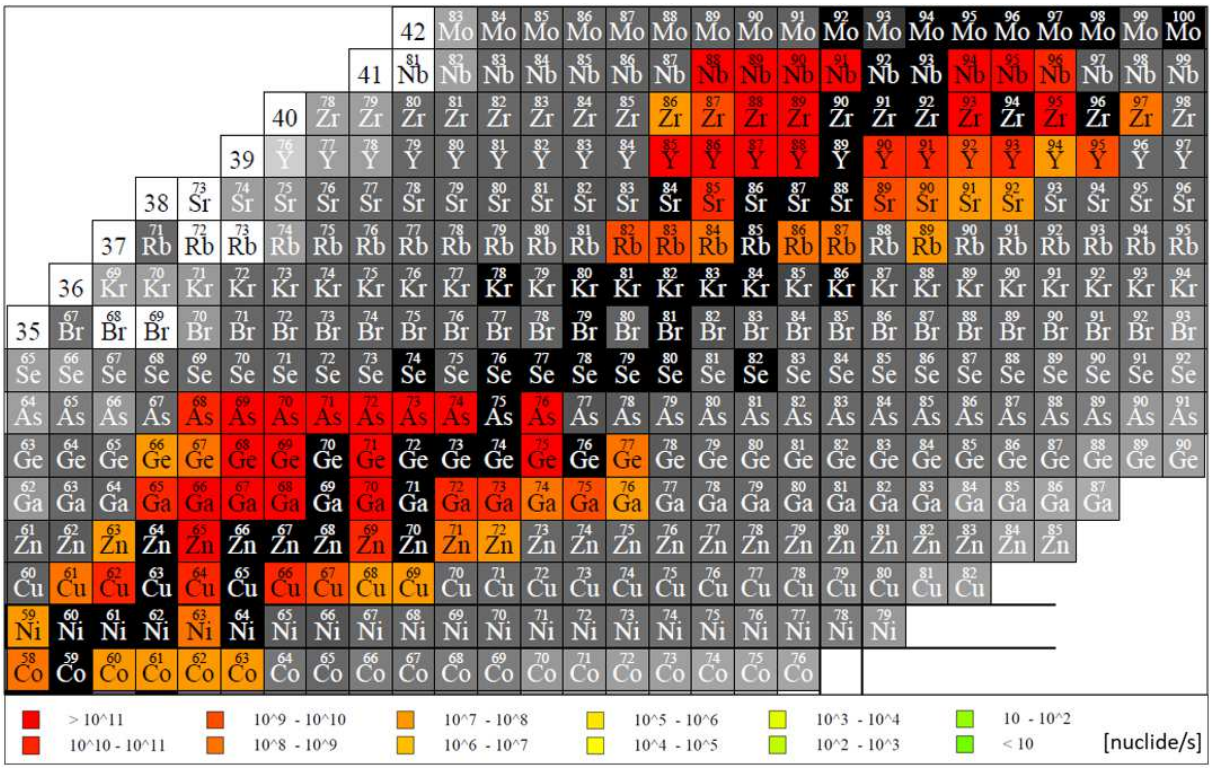

***Figure 4.5**: estimated in-target yields according to FLUKA*

As shown in figure 4.5 the expected nuclide production ranges from Cobalt to Arsenic for the nuclear reactions involving Germanium as target nucleus, whereas the proton induced reactions on Zirconium generate products from Rubidium to Niobium.

The excitation functions considered by FLUKA are based on the PEANUT nuclear interaction model. Since such model may have large uncertainties for lesser studied nuclear reactions, a more accurate investigation was necessary in order to increase the reliability of the results.

Consequently, other simulations were launched considering different excitation functions models. For such additional investigations, the Monte Carlo toolkit Geant4 (version 4.10.04.p02) [4.22] was used, since it allows the selection of different Physics Lists, that correspond to different nuclear interaction models.

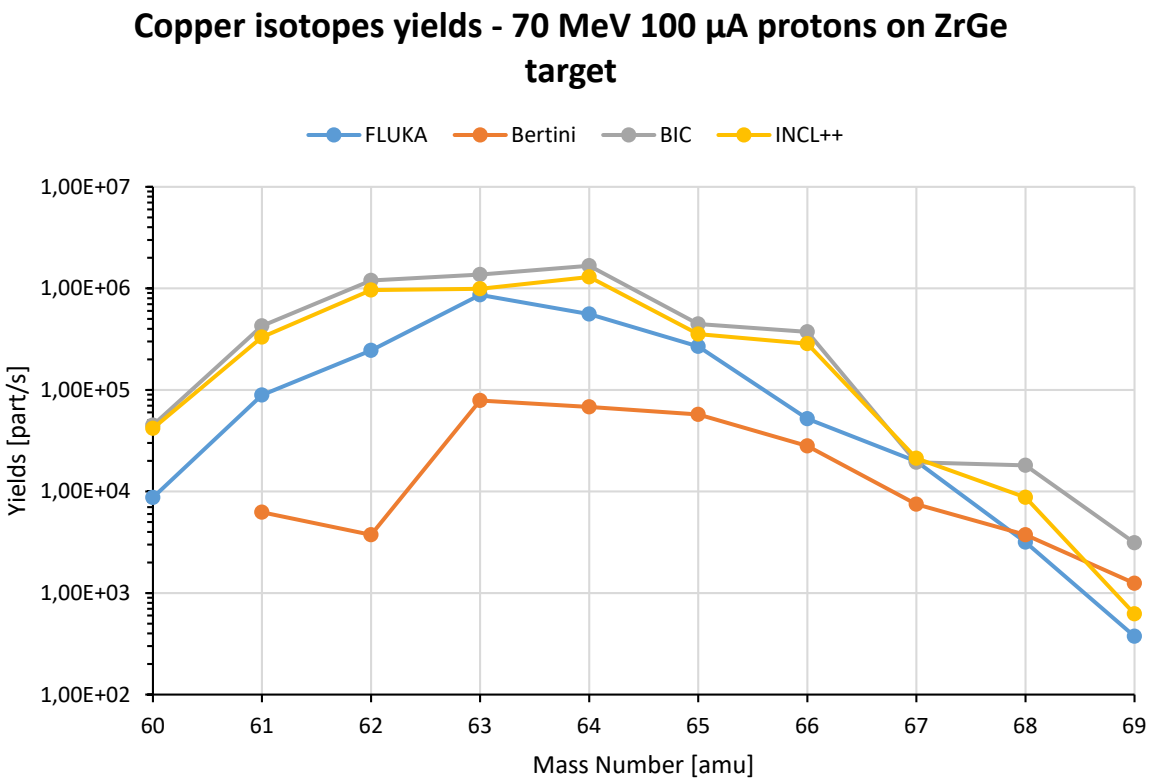

Figure 4.6: *Copper isotopes yields according to different models for a 70 MeV 100 µA proton beam on a ZrGe target*

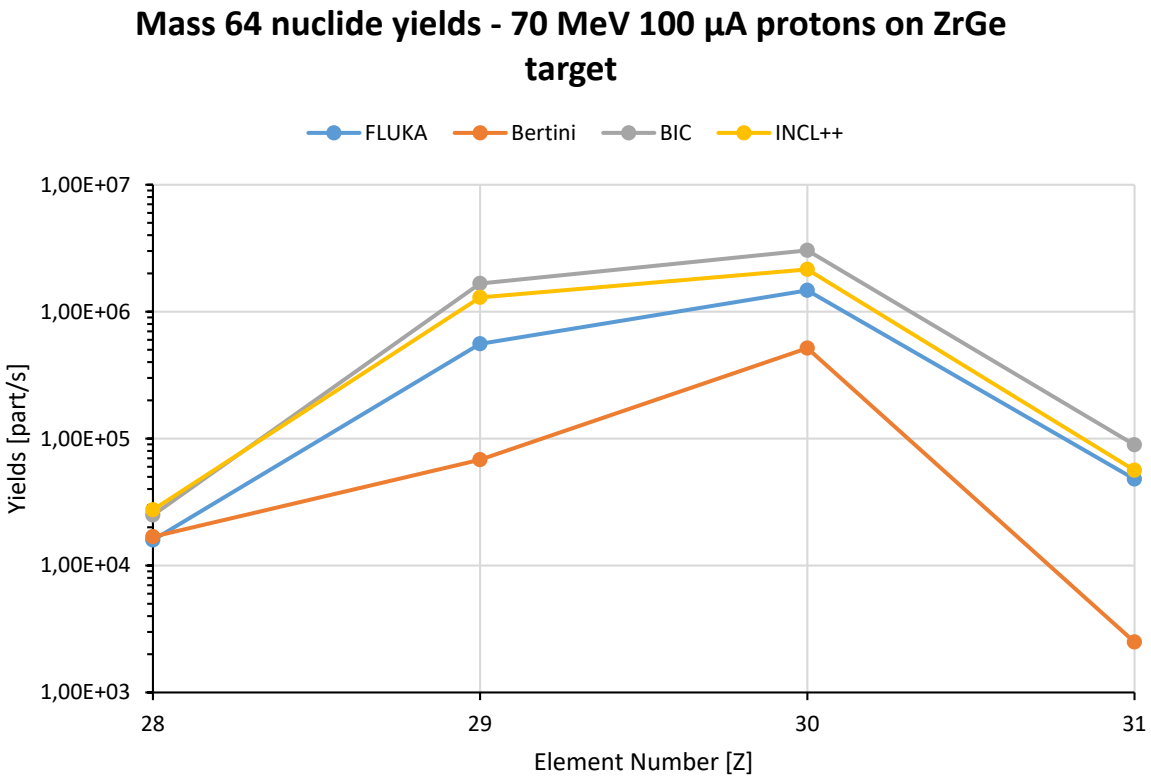

Figure 4.7: *Mass 64 nuclide yields according to different models for a 70 MeV 100 µA proton beam on a ZrGe target*

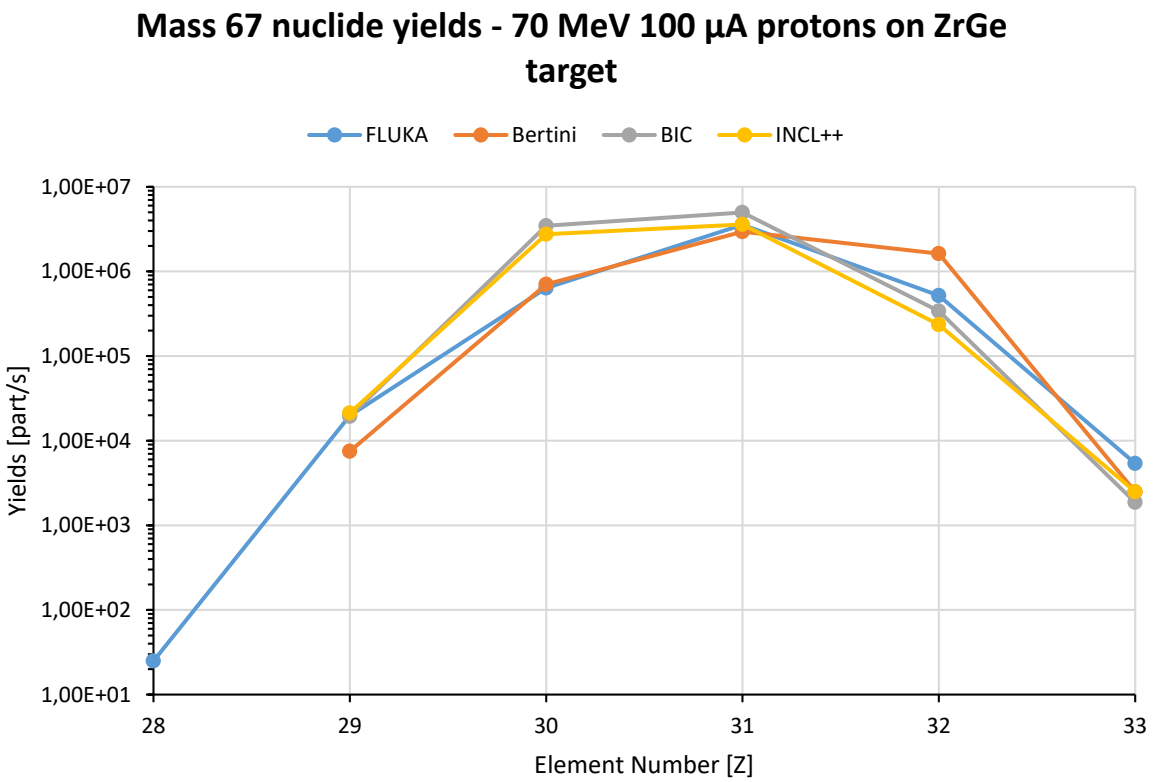

Figure 4.8: *Mass 67 nuclide yields according to different models for a 70 MeV 100 µA proton beam on a ZrGe target*

Figure 4.6, 4.7 and 4.8 summarize the comparison between the various nuclear models used in the simulations, with a focus on the yields for respectively the copper isotopes, for the mass 64 nuclides and for the mass 67 nuclides. In addition to the FLUKA-PEANUT results, the nuclear interaction models considered with Geant4 were the Bertini cascade model [4.23, 4.24], the Binary Cascade model (BIC) [4.23, 4.25] and the Liège intranuclear cascade model (INCL++) [4.26].

In particular, the activated Geant4 Physics Lists were FTFP_BERT for the Bertini cascade, QGSP_BIC for the BIC model, and QGSP_INCLXX for INCL++. In addition, in order to increase the reliability of the results at low energies, the electromagnetic option EMZ was activated [4.27].

As a general consideration, the various models produced a set of disperse results, in some cases with an order of magnitude difference. This is, for example, the case of the ^{64}Cu yields, were according to the Bertini cascade model approximately 7E+04 particles/s are produced, whereas the BIC model indicates a production of 1.7E+06 particles/s. For such reasons a detailed study of the excitation functions for the desired reactions was foreseen in order to estimate the in-target production with more precision. Anyway, for the subsequent preliminary evaluation of the in-target produced activities, the FLUKA results were taken into account, since the closest to the average between the various models.

4.2.3 Preliminary study of the $^{nat}Ge(p,X)^{64}Cu$ and $^{nat}Ge(p,X)^{67}Cu$ reactions

As already introduced, various nuclear interaction models were taken into account in order to estimate the ^{64}Cu and ^{67}Cu in target yields, but they produced different results. In addition in the EXFOR database [4.28] no experimental data for the reactions $^{nat}Ge(p,X)^{64}Cu$ and $^{nat}Ge(p,X)^{67}Cu$ in the energy range 0 -100 MeV were found, consequently a different approach was considered. The MC code FLUKA was taken as reference and its results were compared with the data calculated by means of dedicated codes as TALYS [4.11].

Figures 4.9 and 4.10 summarize the final results of such study for both nuclear reactions taken into account. In particular, the cross section calculations were performed for all natural isotopes of Germanium, namely ^{70}Ge (nat. abundance 20.52%), ^{72}Ge (nat. abundance 27.45%), ^{73}Ge (nat. abundance 7.76%), ^{74}Ge (nat. abundance 36.52%) and ^{76}Ge (nat. abundance 7.75%), and the final results for ^{nat}Get were calculated as the average of the single contributions of each stable Ge nuclide, considering the respective natural abundance as weight. Concerning FLUKA the cross sections were calculated in two different ways. Firstly, several simulations with a thin Ge (thickness 10 μm), in order to preserve the beam energy, were preformed and the cross section was calculated indirectly from the outputted yield. Such simulations were performed with proton beam energy steps of 5 MeV, and FLUKA version 2011.2x.2 was used. Secondly, the PEANUT model (FLUKA devel version 2018.0) was directly invoked [4.29]. Regarding TALYS (version 1.9), in addition to the data available in TENDL-2015 [4.30], both the default model and a version adjusted as suggested in literature [4.31] (TALYS mod data in figure 4.9 and 4.10) were used. More details regarding such study are presented in appendix C.

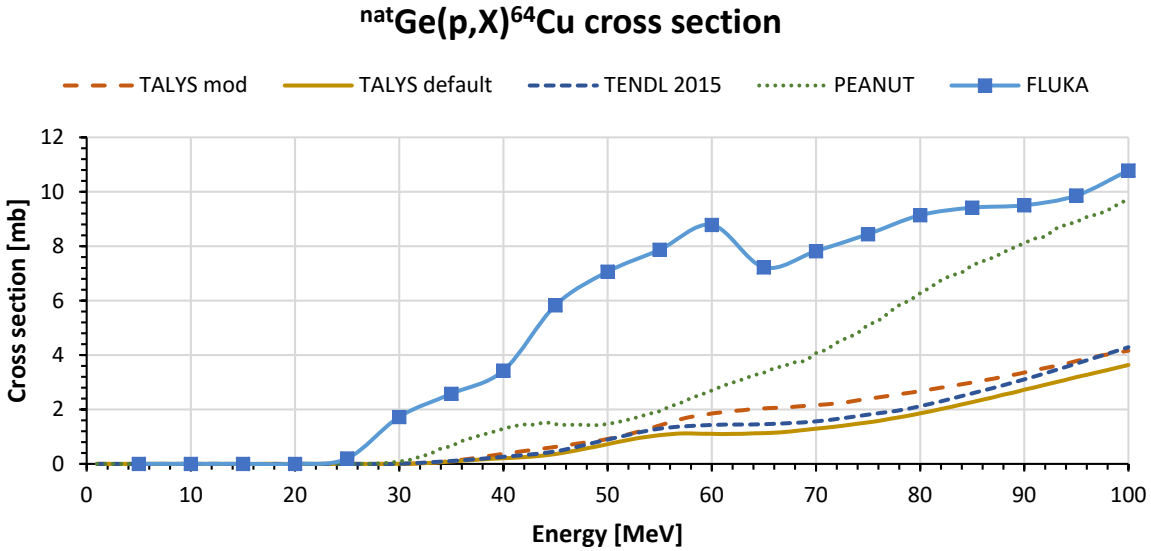

Figure 4.9: *cross section for the $^{nat}Ge(p,X)^{64}Cu$ reaction according to various models*

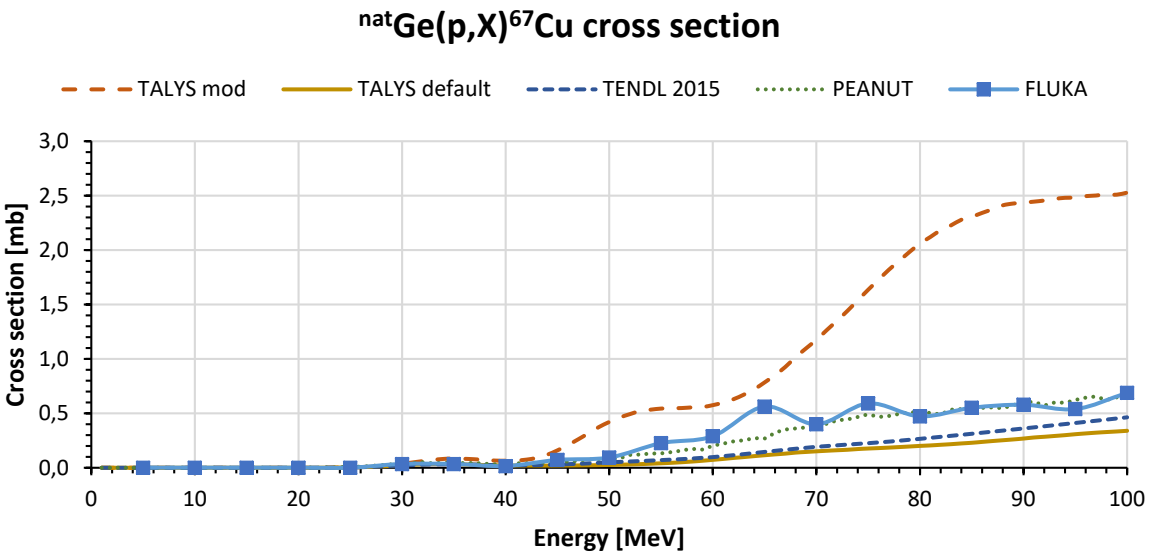

Figure 4.10: *cross section for the ^{nat}Ge(p,X)^{67}Cu reaction according to various models*

4.2.4 Expected in-target production of ^{64}Cu and ^{67}Cu

The MC code FLUKA, taken as reference for the evaluation of the expected yields, was also used to calculate the in-target produced activities at different irradiation times. In order to perform such simulations, the radioactive decays were activated, and timepoints of 0.5, 1, 2, 3, 4, 5 and 6 days were considered. Such timepoints are coherent with the maximum expected irradiation time for the SPES targets, namely 15 days. As for the yield simulations a primary beam of 70 MeV 100 µA protons was considered.

As shown in table 4.1 for ^{64}Cu the expected produced activity after 5 days of irradiation was 55.2 GBq, while for ^{67}Cu was 1.4 GBq. The production of the sole ^{64}Cu might not be competitive with the traditional accelerator-based techniques, however decent amounts of ^{67}Cu can be produced simultaneously.

Table 4.1: *the expected in-target activity for ^{64}Cu and ^{67}Cu at different irradiation timepoints*

ZrGe target (100 µA, 70 MeV protons)						
	^{64}Cu production ($t_{1/2}$: 61,83 h)			^{67}Cu production ($t_{1/2}$: 61,83 h)		
Time	**Activity**		**Nuclei**	**Activity**		**Nuclei**
[days]	[Bq]	[Ci]	[#]	[Bq]	[mCi]	[#]
0.5	2.66E+10	0.72	1.75E+15	2.37E+08	6.40	7.61E+13
1	4.03E+10	1.09	2.66E+15	4.44E+08	11.99	1.43E+14
1.5	4.75E+10	1.28	3.13E+15	6.24E+08	16.87	2.01E+14
2	5.12E+10	1.38	3.38E+15	7.82E+08	21.15	2.52E+14
3	5.42E+10	1.46	3.57E+15	1.04E+09	28.14	3.35E+14
4	5.50E+10	1.49	3.62E+15	1.24E+09	33.49	3.99E+14
5	5.52E+10	1.49	3.64E+15	1.39E+09	37.58	4.47E+14
6	5.52E+10	1.49	3.64E+15	1.51E+09	40.70	4.84E+14

4.2.5 Other nuclides of potential medical interest from the ZrGe target

In addition to the copper isotopes, other interesting radionuclides could be produced with this target material, such as Arsenic isotopes (figure 4.11), in particular ^{72}As ($t_{1/2}$=26 h, β^+ emission), ^{74}As ($t_{1/2}$=17.7 d, β^- Eβ' average =242.75 keV, 15.4% and Eβ''average 1352.8, keV 19.0%; β^+ $E\beta^+$average=408.0 keV, 26.1%) and ^{77}As (t1/2=38.79 h, β- $E\beta^-$average 228.8 keV, 97%).

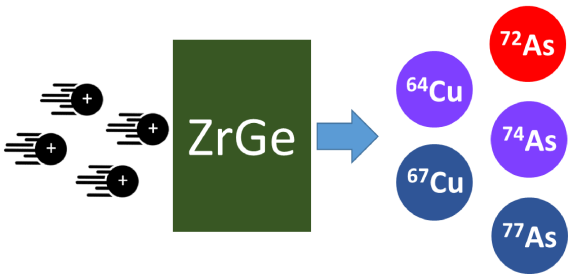

***Figure 4.11**: possible medical radionuclides from the ZrGe target.*

Preliminary studies for their possible implementation in biological studies were performed, along with measurements of the excitation functions of the reactions $^{nat}Ge(p, Xn)^{72}As$ and $^{nat}Ge(p, Xn)^{74}As$ [4.32]. Significant amounts of such radionuclides can be produced with the ZrGe target according to the FLUKA simulations, as shown in table 4.2.

***Table 4.2:** the expected in-target activity for ^{72}As, ^{74}As and ^{77}As at different irradiation timepoints.*

ZrGe target (100 μA, 70 MeV protons)									
	^{72}As production ($t_{1/2}$: 26 h)			^{74}As production ($t_{1/2}$: 17.7 d)			^{77}As production ($t_{1/2}$: 38.79 h)		
Time	Activity		Nuclei	Activity		Nuclei	Activity		Nuclei
[days]	[Bq]	[Ci]	[#]	[Bq]	[Ci]	[#]	[Bq]	[mCi]	[#]
0.5	6.33E+10	1.71	8.55E+15	1.57E+09	0.04	3.48E+15	5.55E+06	0.15	1.12E+12
1	1.09E+11	2.95	1.48E+16	3.11E+09	84.08	6.89E+15	1.22E+07	0.33	2.46E+12
1.5	1.43E+11	3.86	1.93E+16	4.62E+09	124.91	1.02E+16	1.85E+07	0.50	3.74E+12
2	1.67E+11	4.51	2.25E+16	6.10E+09	164.94	1.35E+16	2.41E+07	0.65	4.87E+12
3	1.97E+11	5.34	2.67E+16	8.98E+09	242.71	1.99E+16	3.28E+07	0.89	6.63E+12
4	2.13E+11	5.77	2.88E+16	1.17E+10	317.51	2.60E+16	3.87E+07	1.05	7.82E+12
5	2.22E+11	6.00	3.00E+16	1.44E+10	389.43	3.19E+16	4.26E+07	1.15	8.61E+12
6	2.26E+11	6.12	3.06E+16	1.70E+10	458.62	3.76E+16	4.52E+07	1.22	9.12E+12

4.3 Copper ionization tests with the offline SPES Front-End

After the evaluation of the expected in target yields and produced activities, a subsequent crucial step of the feasibility study for the production of copper medical isotopes at ISOLPHARM is the investigation of the ionization capabilities of SPES ion sources. Indeed, only a fraction of the amount of in-target produced copper isotopes will be ionized and extracted into a beam. Consequently, in order to evaluate the efficiency of the ionization process, tests with stable copper beams were performed with the SPES Front End prototype, as done in the

cases of Strontium, Yttrium, Iodine and Silver, as presented in chapter 3. The results obtained with the stable isotopes of copper are relevant also for the medical radioisotopes since the ionization efficiency is related only to the chemical properties of the element of interest.

The ionization tests were performed by loading precise amounts of stable copper (^{63}Cu 69.17%, ^{65}Cu 30.83%) into the ion source. Such tests were performed using the SPES FE in off-line modality, meaning that the proton beam and the production target are not assembled.

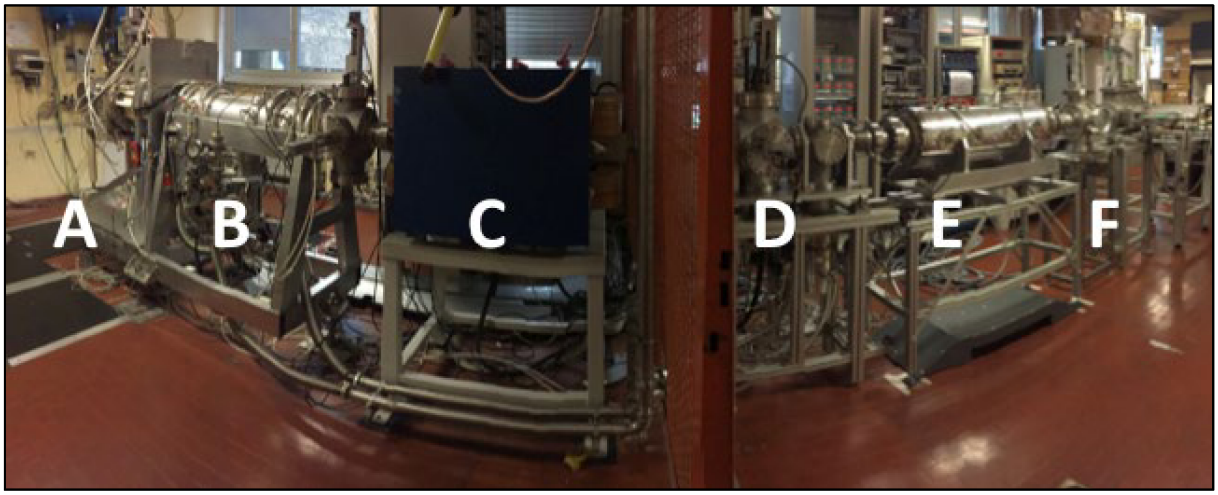

Figure 4.12: *the SPES Front End prototype used for the offline tests. (A) Target - Ion Source unit; (B) First triplet and steers unit and diagnostic device; (C) Mass separator, Wien Filter; (D) Second diagnostic unit; (E) Second triplet system; (F) Secondary target for beams recovery station.*

As introduced in chapter 3, the experimental apparatus used for the ionization tests is made of six main functional subsystems (figure 4.12): the Target - Ion Source (TIS) unit (A), the first beam optics subsystem, made up of four steers to align the beam with the focal plan and the triplets to focus the beam, and the first diagnostic box, that includes a Faraday cup for the beam current measurement and a beam profiler (B), the Wien filter (WF), a velocity selector used as mass separator (C), the second diagnostic box, including the slits, devices that can modify the aperture of the beamline after the WF and again a beam profiler and a Faraday cup (D), the second beam optic subsystem, namely the second triplets (E) and the secondary target station for the collection of the beam (F). The beamline pressure levels normally range between 10^{-5} and 10^{-6} mbar.

Copper was introduced inside the TIS unit by means of the Mass Marker (MM) technique [4.33], a method that foresees the surface deposition of a small amount of the desired element on a thin tantalum foil (the Mass Marker – MM), that is lately accurately folded and inserted inside a small tubular oven, that replaces the production target. The so-called oven can be stepwise heated by Joule effect up to a desired temperature level, allowing the atomization of the substrate previously deposed on the foil, and the migration of the neutrals towards the ion source through the transfer line. In the case of copper (first ionization energy 7.73 eV [4.34]), the SPES Plasma Ions Source (PIS) was used, which is capable to ionize a wide set of elements,

also the most electronegative [4.35]. The deposition of the copper load onto the MM was performed by dropping 40 µL of copper standard solution ($Cu(NO_3)_2$ 1 g/L, Fluka Analytics) on the tantalum foil, and the aqueous solvent was subsequently evaporated. The MM, after being accurately folded, was inserted into the oven at 80 mm distance from the opening. One extremity of the oven was then sealed, and the other open side was connected to the transfer line (figure 4.13).

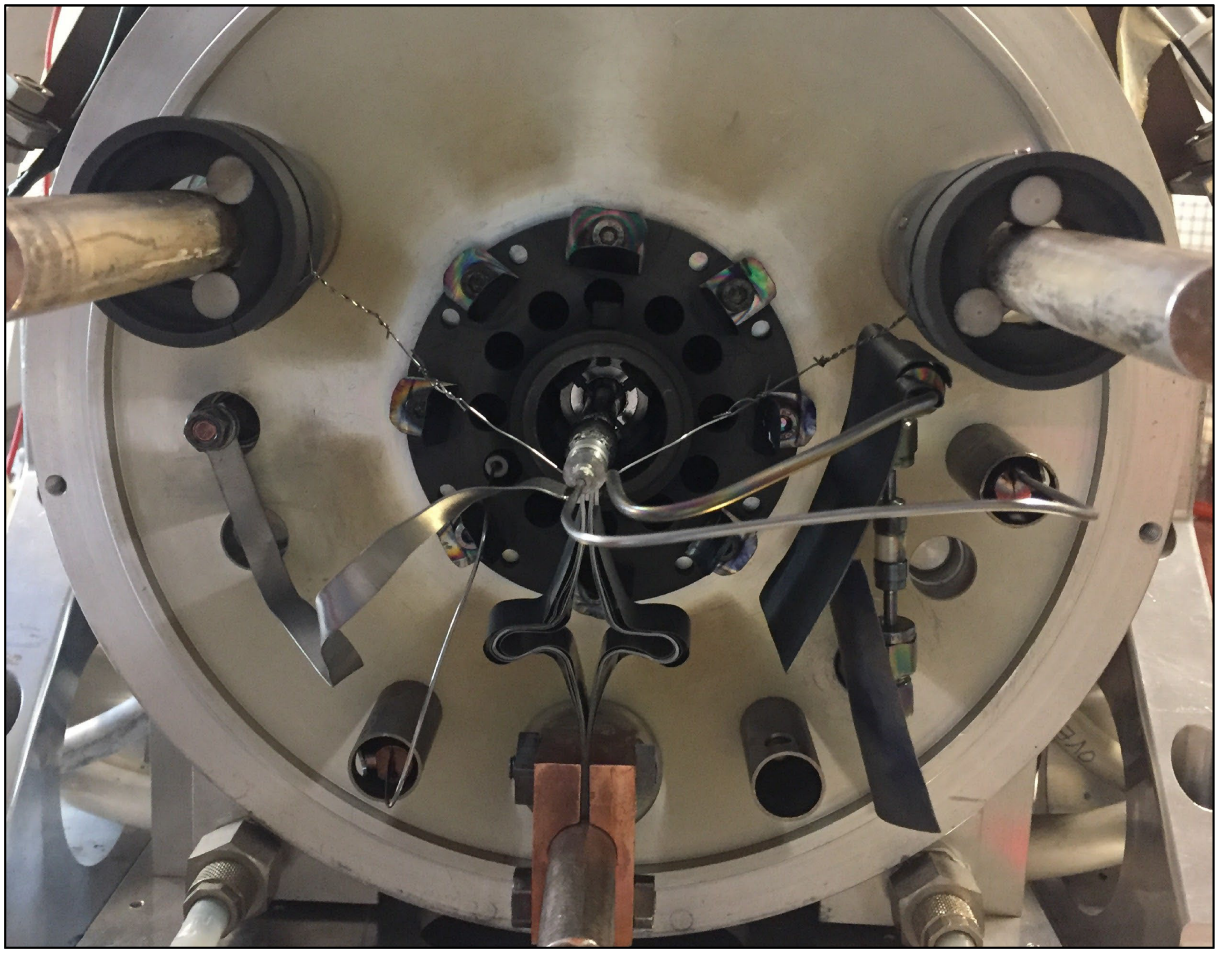

Figure 4.13: *the SPES PIS coupled with the oven containing a Cu-loaded MM*

The following parameters were used for the performance of the tests:

- The ion source and transfer line were heated by joule effect with a current intensity of 415 A, thus reaching a temperature level generally above 2000°C
- The oven maximum current was set to 80 A,
- The extraction electrode was positioned at 50% of its maximum stroke, and potential drop of 25 kV was applied between the latter and the TIS unit
- Regarding the first beam optics subassembly, the deflectors were left off (the beam was already aligned), whereas the three quadrupoles Q1, Q2 and Q3 forming the first triplet were set respectively at 875, 695 and 1398 V.

- The Wien Filter settings were studied in order to allow the selection of only ^{63}Cu, the most abundant stable isotope of copper. A constant electric field of 103.16 kV/m was set into the WF by means of two couple of electrodes, respectively at 590 V (pre-electrodes) and 2579 V (electrodes). The magnetic field was adjusted by means of the WF coil current, set at 111 A, thus only mass 63 atoms are not diverted. In case of mass 65 selection the WF coil current was set at 114 A.
- The slits were positioned leaving an aperture with 18 mm width, in order that all diverted particles are dumped
- The second Faraday Cup (FC2) was left into the beam line, in order to measure constantly the beam current.
- The subsequent triplets were left off, since the beam was dumped onto the second Faraday cup.

At the beginning of the tests all aforementioned parameters were set, except for the oven current, that was stepwise increased from 0A. ^{nat}Cu ionization occurred after heating the oven with a 30 A current, corresponding approximately to a 1200°C at the MM position. Subsequently the oven current was increased with 5 A steps, up to 80A, thus operating working in a temperature range of 1200-2000°C. The stepwise increase of the heating current, allowed to gradually release the loaded copper isotopes towards the ion source. Indeed, the copper current measured ranged between the 200 and 600 nA.

The effective presence of copper in the extracted beam composition was verified by means of the analysis of the ion masses transported along the beam line. A typical mass scan is reported in figure 4.14 [9].

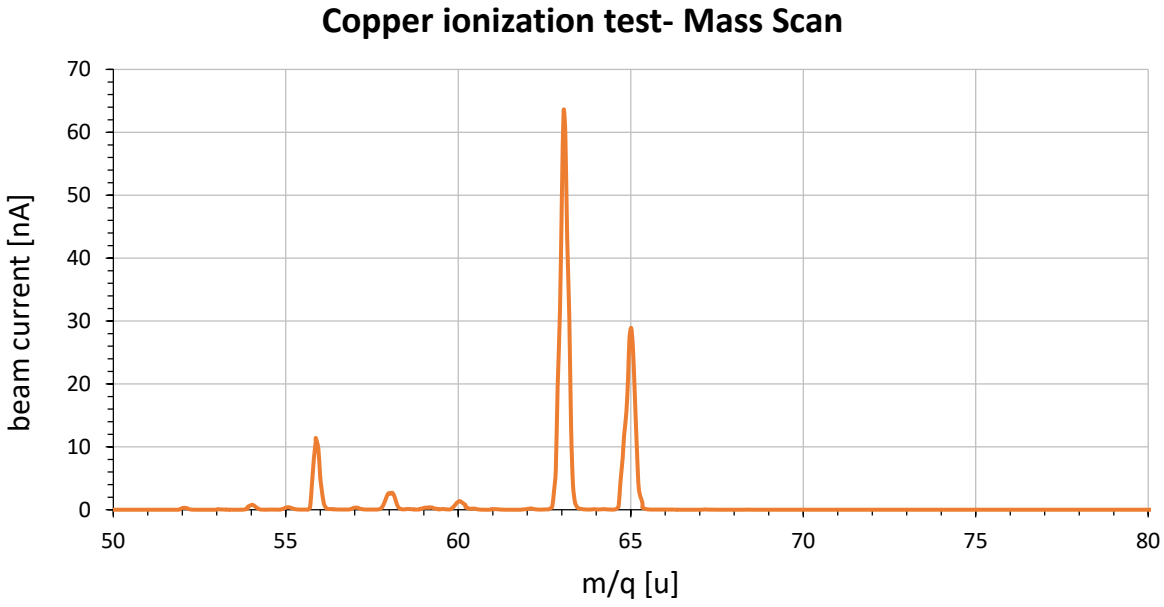

Figure 4.14: *mass scan performed during the copper ionization tests. Mass 63 and 65 correspond to the stable isotopes of copper ^{63}Cu and ^{65}Cu*

Copper was clearly identified thanks to the two peaks of masses 63 and 65. Indeed the isotopic abundances of the two stable copper isotopes were compared with the two peaks heights ratio, which gave a value of 68.7/31.3, very close to expected values of 69.2/30.8 from natural copper. The other peaks found on the mass scan were identified as beam impurities, typical for the assembly used for the tests. In fact, inside the apparatus some steel-alloy components are present and undergo heating. For this reason, they may release some of their chemical components, such as iron, ^{54}Fe and ^{56}Fe, being the latter the most common iron isotopes in nature, and ^{58}Ni and ^{60}Ni. These impurities are anyway not affecting the result of the tests, since they are deflected by the mass separator, and tend to disappear gradually after a long heating.
A single ionization tests was continued until all the copper load was evaporated and no more copper beam current was detected in the FC2, namely the test lasted approximately 4 hours keeping the Cu+ current at about 200 nA. Figure 4.15 shows the typical copper beam current trend for an ionization test. [4.9, 4.36]

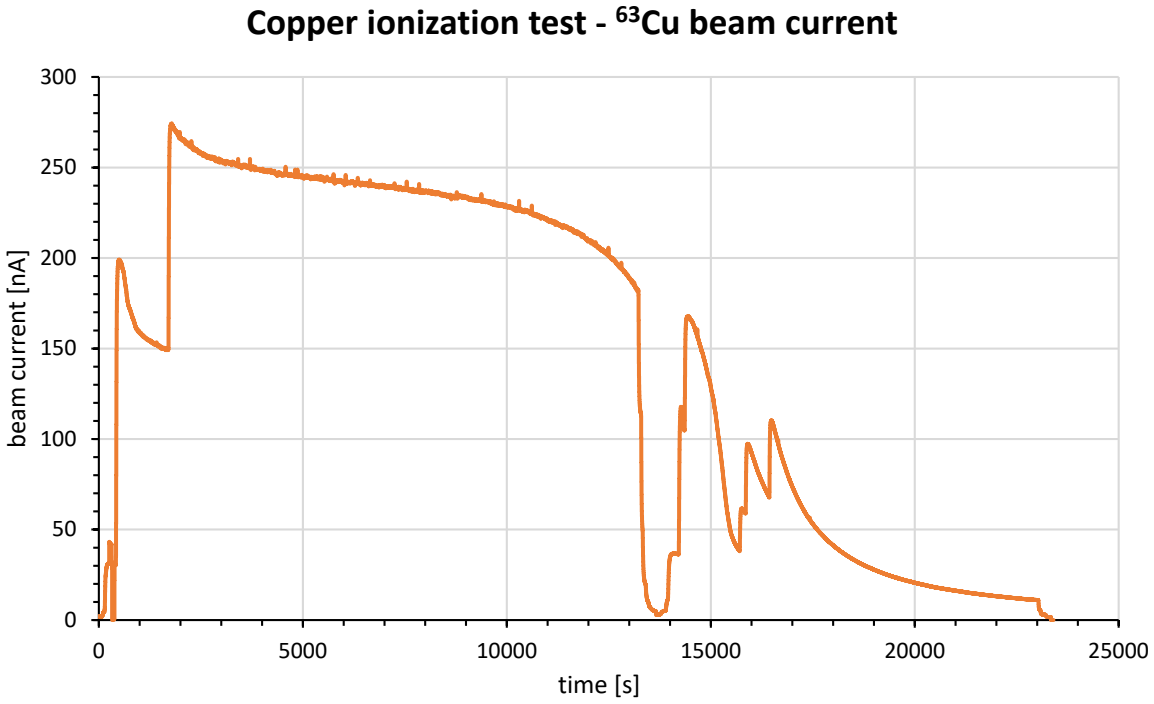

Figure 4.15: *the typical trend of copper beam in time during ionization tests*

In order to evaluate the copper ionization efficiency, the FC2 current was integrated in time and the total amount of copper ionized was consequently calculated. The ionization efficiency was then calculated as the percentage ratio between the integrated copper beam current and the initial amount of copper loaded into the MM.
Three independent ionization tests were performed, giving an average efficiency of 7.67±1.3%. Table 4.3 summarizes the results of the single tests.

Table 4.3: *the results of the three ionization tests*

Copper ionization efficiency tests					
Test number	Loaded charge (^{nat}Cu)	^{63}Cu natural abundance	Loaded charge (^{63}Cu)	Measured charge (^{63}Cu)	Efficiency
[#]	[C]	[%]	[C]	[C]	[%]
1	6.08E-02	69.17	4.20E-02	3.38E-03	**8.03E+00**
2	6.08E-02	69.17	4.20E-02	3.68E-03	**8.75E+00**
3	6.08E-02	69.17	4.20E-02	2.62E-03	**6.23E+00**

4.4 Copper deposition tests with the offline SPES Front-End

Once the capability to ionize copper beams was proven and the efficiency of such process was measured, the following step was to verify the feasibility of the collection of the ionized copper nuclides by dumping the beam on an appropriate secondary target, that could be subsequently recovered and dissolved. After dissolution the collected copper could be harvested and quantified.

In the cased of copper, sodium chloride disks were used as collection targets, and were assembled into the secondary target station. Such disks were prepared by pressing pure NaCl powders into a cylindrical dye [4.37]. The secondary target station used for such tests consists on a diagnostic box including a beam profiler and Faraday cup, that was opportunely modified to hold the target disk, as presented in chapter 3.

In the case of the deposition tests, the Mass Marker was loaded with 200 µL of copper nitrate (1 g/L), in order to recover an amount of copper that could be easily measured after the target dissolution. Even in this case the MM was inserted into the tubular oven at approximately 8 cm from the closed extremity. The settings used for the Front End were the same as for the ionization tests, with the exception that the FC2 was normally positioned out from the beam axis. The employed WF settings were aimed to alternatively select only mass 63 or 65, thus collecting on the NaCl substrate only either ^{63}Cu or ^{65}Cu. In addition, the quadrupoles QT1, QT2 and QT3 of the second triplets were turned on, and set at 1760, 850 and 1775 V, respectively. The best focalization settings were found thanks to the use of the beam profiler equipped in the secondary target station. The Faraday cup hosting the collection target was positioned in correspondence of the beam axis, thus intercepting the beam, whereas any other beam intercepting device was removed.

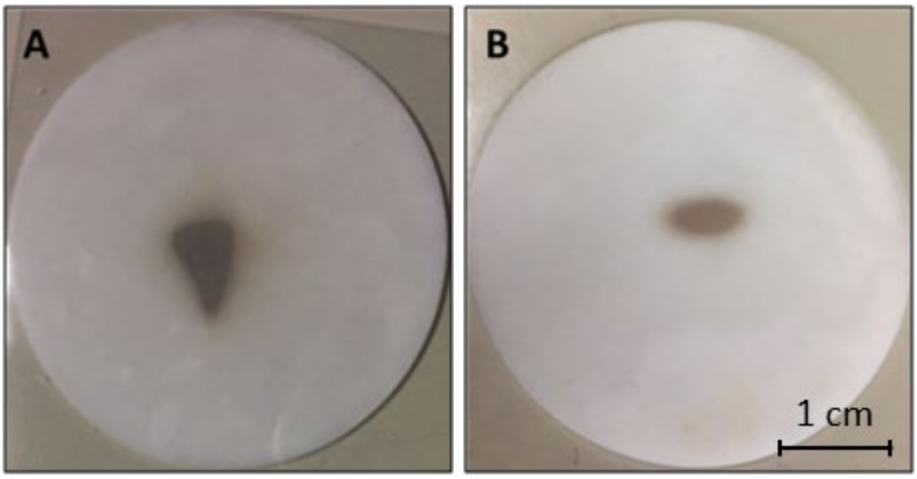

Figure 4.16: *a couple of NaCl collection targets after deposition. The spots in the center in figure A correspond to the ^{63}Cu collection, whereas the smaller spot in figure B correspond to the ^{65}Cu collection.*

The oven Joule heating was turned on employing currents up to 65 A, and the deposition tests was continued for approximately 4-5 hours. The Cu beam intensity was periodically measured by inserting in the beam line the FC2 for few seconds. Such measurements were performed every 20-30 minutes. By integrating in time the interpolating function of the measured values it was possible to estimate the total amounts of copper atoms reaching the NaCl target. Figure 4.16 shows samples of secondary targets after the deposition tests. It is possible to notice that the spot size corresponding to the deposition of ^{63}Cu (figure 4.16-A) is larger than the spot corresponding to the collection of ^{65}Cu (figure 4.16-B) coherently with the respective natural abundances, namely 69.17% and 30.83%.

After the deposition tests, the irradiated secondary targets were removed from the offline FE and prepared for the quantitative analysis of the deposed copper amounts. Indeed, since the beam spot was very clear and to reduce the sodium chloride amount, the portion of the disk where the copper was visible was separated from the rest, breaking the substrate, thus decreasing the quantity of solvent required for the subsequent dissolution in HNO3 (0.5 M).

Afterwards the samples were prepared for Graphite Furnace Atomic Absorption Spectroscopy (GF-AAS, Varian ©, lamp current = 4 mA, λ= 327.4 nm), and the amounts of recovered copper were thus measured. The deposition tests were repeated four times, two times collecting only ^{63}Cu (test #1, #2 and #4), and once deposing only ^{65}Cu (test #3)

Table 4.4 summarizes the results obtained with the aforementioned tests [4.9]: it is possible to notice that the first two tests, show a lower efficiency than the last two. Such difference might be due to the fact that in the case of the last two tests, the dissolved sample was concentrated before GF-AAS analysis by heating it at 180°C for 120 min, thus allowing a more precise quantification of the copper amounts in solution. For such reason, the last values should be considered as the most reliable recovery efficiency estimations [4.36].

Table 4.4: *the results of the three deposition tests*

Copper recovery efficiency tests			
Test number	Extracted Cu amount (integration of the beam current)	Measured Cu amount (via GF-AAS)	Efficiency
[#]	[µg]	[µg]	[%]
1	9.94	1.46	**14.69**
2	5.21	1.09	**20.92**
3	1.12	0.54	**48.21**
4	0.94	0.5	**53.19**

As additional deposition test, one more experiment was performed, where both masses of ^{nat}Cu, ^{63}Cu and ^{65}Cu, were recovered on the same secondary target, in order to prove the possibility of collecting simultaneously and in separated spots both ^{64}Cu and ^{67}Cu when the facility will be operating on-line [4.9].

For the performance of such test different FE parameters were used, in order to decrease the mass separation resolution and simultaneously transport both ^{63}Cu and ^{65}Cu. In particular, the deflectors on the first optics assembly S1, S2, S3 and S4 were set at respectively 50 v, 320 V, 10 V and 100 V, whereas the quadrupole triplet Q1, Q2 and Q3 were set at 500 V, 619 V and 1517 V, in order to inject the beam into the WF with the best focalization. The electric field into the WF was set at 56.12 kV/m by means of the pre-electrodes and electrodes, respectively at 257 V and 1403 V. The magnetic field was generated by means of the WF coil current, set at 60 A, thus both mass 63 and 65 particles are transported with a separation of approximately 10 mm. The second triplet quadrupoles, QT1, QT2 and QT3 were set respectively at 1820 V, 900 v and 1820 V, and the deposition was started by heating the MM by Joule effect.

The secondary target used for such test is presented in figure 4.17: the two spots corresponding to the two Copper isotopes are clearly identifiable. The smaller one, on the left corresponds to ^{65}Cu, whereas the bigger one, on the right, is related to the more naturally abundant ^{63}Cu.

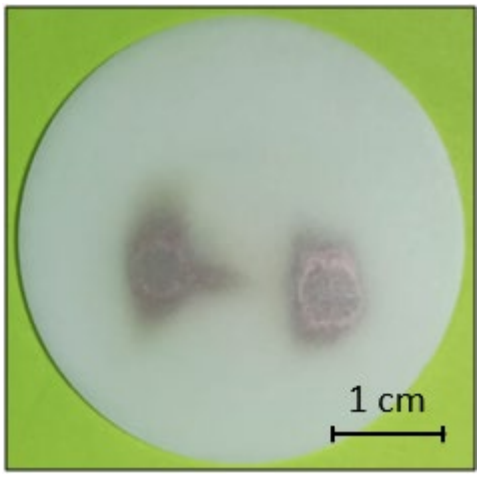

Figure 4.17: *The NaCl collection target after deposition of both ^{63}Cu and ^{65}Cu. The two spots clearly identify the two Copper isotopes.*

After deposition, the NaCl target was split in two parts, one of each spot, in order to analyze them independently. As for the other deposition tests, also these samples were analyzed through

GF-AAS, after target dissolution and solution concentration (as for test #3). It was possible to verify that the ^{63}Cu spot was 4.72 μg, while ^{65}Cu was 1.98 μg, the 70.5 and 29.5% of the total amount of copper recovered respectively, thus respecting the natural isotopic natural abundance of Copper.

4.5 Preliminary evaluations of the release of copper from a ZrGe substrate

As already introduced, the developed ZrGe target should not operate at temperatures higher than 1900°C, since the breaking of the molecule and the subsequent release of Ge atoms would lead to the fast degradation of the target material. Since normally ISOL targets should operate at the highest acceptable temperature level in order to boost the isotope release, thus generally above 2000°C, a tradeoff should be found in the case of ZrGe. Being ZrGe a custom made material, its limiting temperature in high vacuum environment (10^{-5} – 10^{-6} mbar) were not known and required dedicated experimental evaluations.

For the aforementioned reasons, preliminary effusion tests were performed, similarly to what was done for Ag, as presented in chapter 3. In such case, however, the aim was not to investigate the eventual formation of Copper compounds that could decrease the overall efficiency of the ISOL process, but the concern was to identify an optimal temperature level, where Cu is rapidly released, and the ZrGe degradation rate is still acceptable.

For the performances of such tests 40 μL of $Cu(NO_3)_2$ (1 g/L) were deposed on a 5x5 mm^2 ZrGe sample (thickness ≈ 0.7 mm), that was positioned directly in the transfer line of the SPES PIS, as shown in figure 4.18 [4.18].

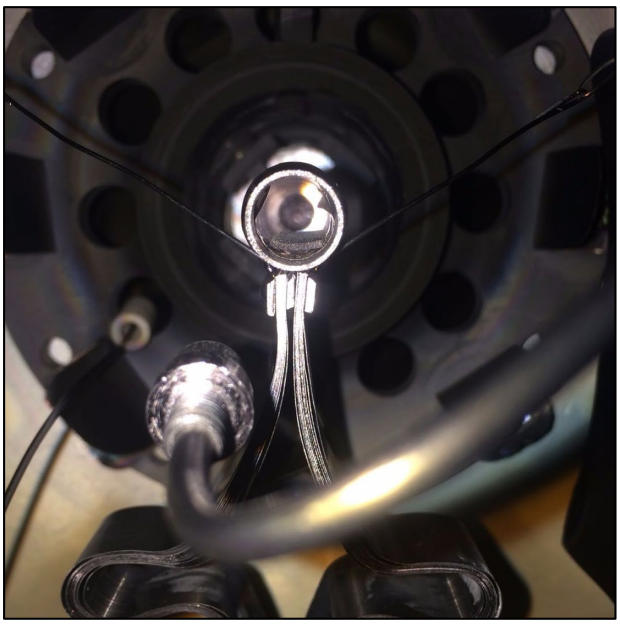

***Figure 4.18**: the ZrGe substrate with the Cu load, inserted directly in the ion source transfer line*

The ion source was lately heated up with current intensities from 375 A to 425 A, corresponding at temperature levels ranging from 1300°C to 2000°C and the out coming ion beam composition was monitored with the performance of Mass Scans.

Figure 4.19 and 4.20 report the mass scans corresponding to four different ion source heating current intensities, namely 390 A, 400 A, 410 A and 420 A.

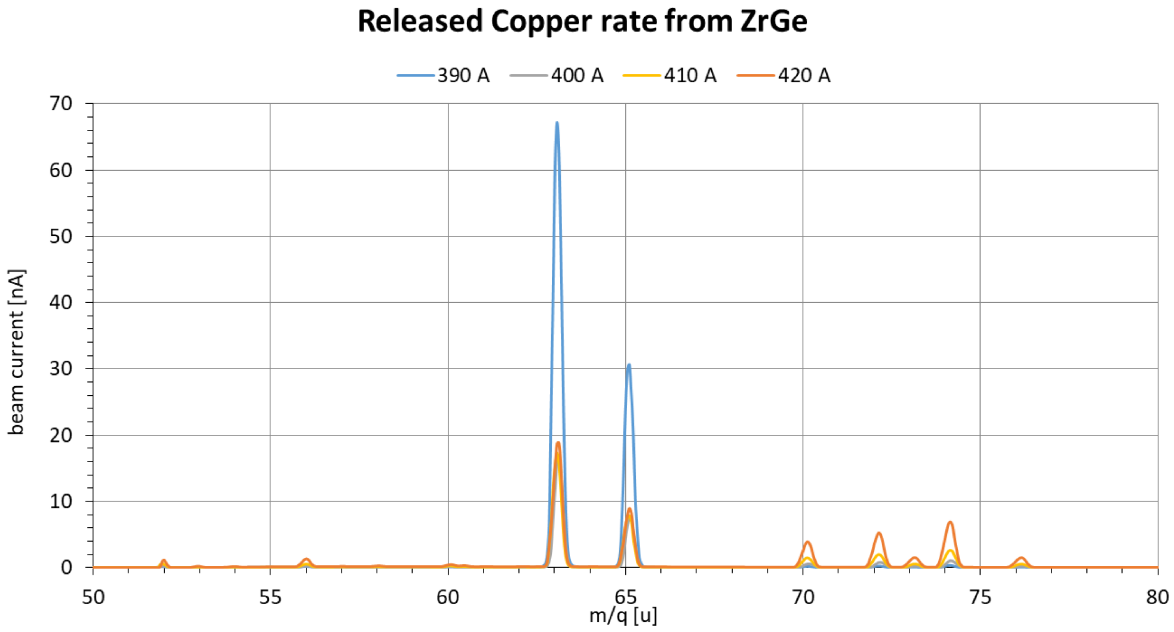

***Figure 4.19**: detail of the Mass Scan performed for different ion source heating current intensities. The peaks at masses 63 and 65 correspond to the stable ^{63}Cu and ^{65}Cu, whereas the peaks at 70, 72, 74 and 76 correspond to respectively ^{70}Ge, ^{72}Ge, ^{73}Ge,^{74}Ge and ^{76}Ge*

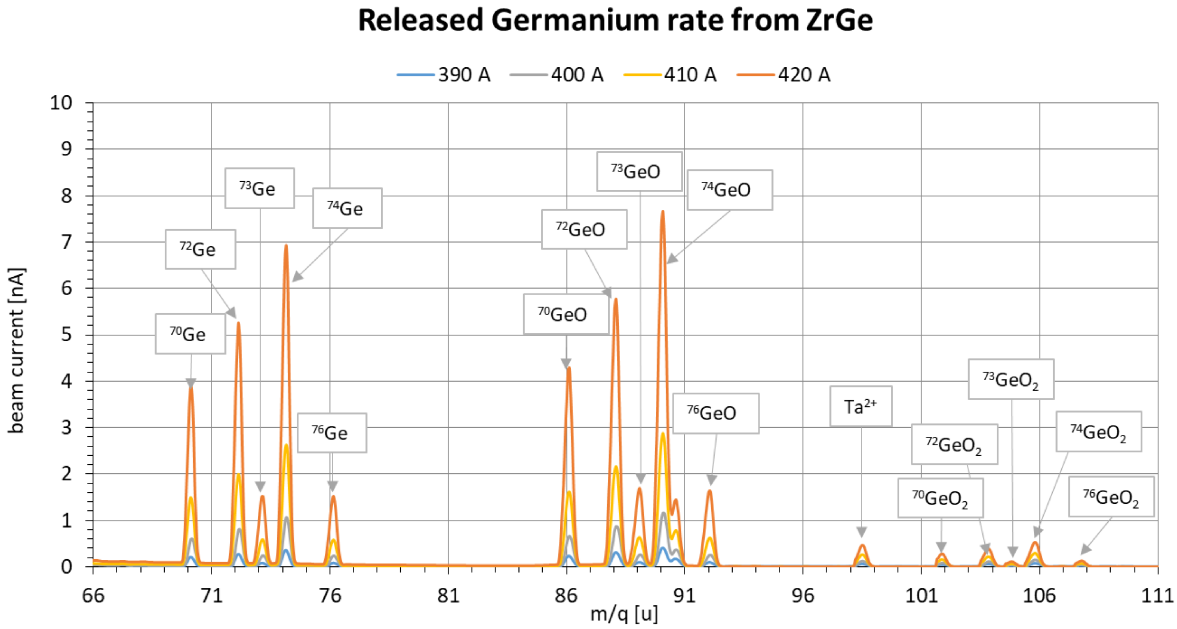

***Figure 4.20**: detail of the Mass Scan performed for different ion source heating current intensities. It is possible to notice that the released Germanium can be released also in the form of incomplete (GeO) and complete (GeO_2) oxide.*

As shown in figure 4.19. the Copper load was efficiently released even when the heating current on the transfer line was 390A, corresponding to approximately 1700°C, indeed, high Cu ion current was detected. For such temperature level, even if the SPES PIS is not working at high efficiency (it requires indeed to operate at temperatures higher than 2000°C [4.38]), a ^{63}Cu ion current of intensity uo to 180 nA was detected, whereas, as shown also in figure 4.20, the beam does not include significant amounts of the Germanium natural isotopes, ^{70}Ge, ^{72}Ge, ^{73}Ge,^{74}Ge and ^{76}Ge. At higher heating currents, namely higher temperatures it is possible to notice more significant presence of Germanium ions, identified as the peaks at mass 70, 72, 73, 74 and 76, whose relative heights are consistent with the natural isotopic abundances (20.52%, 27.45%, 7.76%, 36.52% and 7.75% respectively). The decrease of the released Copper is due to the gradual depleting of the initial load deposed on the ZrGe sample.

Figure 4.21 allows to highlight another interesting occurrence: Germanium isotopes are released not only in the form of atoms, but also as molecules, primarily such as incomplete oxides, or rather monoxides (^{70}GeO, ^{72}GeO, ^{73}GeO,^{74}GeO and ^{76}GeO), that correspond to the peaks at masses 86, 88, 89, 90 and 92, and secondly as fully formed oxides, namely dioxides ($^{70}GeO_2$, $^{72}GeO_2$, $^{73}GeO_2$,$^{74}GeO_2$ and $^{76}GeO_2$), identified as the peaks at masses 102, 104,105,106 and 108. The formation of such molecules might be caused by the unavoidable presence of extremely rarefied air within the vacuum vessel of the ion source. Indeed, atomic and molecular Oxygen (O and O_2) and Carbon Dioxide (CO_2) are commonly found within the beam composition. Since the Oxygen presence within the vacuum vessel is extremely rarefied, the stoichiometric ratio for the fully formation of GeO_2 is not respected, consequently GeO is the most probable molecular form.

As general consideration, according to the test results, ZrGe limiting working temperature should not exceed 1700°C: at such temperature level, the Copper release rate is acceptable, whereas the target degradation rate, identified as the gradual depletion of the Germanium fraction within the target material, is enough low to ensure the survival of the target to long irradiations, as normally foreseen at SPES (generally up to 15 days).

4.6 Discussion and conclusions

The aim of the presented study was to evaluate the possibility of producing ^{64}Cu and ^{67}Cu at SPES facility according to the ISOLPHARM patented method.

Since the ISOL technique, as implemented at LNL, foresees the use of refractory solid production targets, few are the possible target materials adapt for the production of both ^{64}Cu

and ^{67}Cu and able of meeting such requirements. Among those, Zirconium Germanide (ZrGe) was identified as the most promising and first target samples were consequently produced.

According to such material choice, the production of the Copper isotopes of interest was consequently studied through the uncommon reactions ^{nat}Ge(p,X)^{64}Cu and ^{nat}Ge(p,X)^{67}Cu, in the available proton energy range, namely 0 – 70 MeV. Indeed, no experimental data for such reactions were found within the SPES cyclotron energy range.

In order to have preliminary estimations of the possible production yields for the aforementioned copper isotopes, FLUKA and Geant4 Monte Carlo simulations were performed, showing interesting preliminary results. In particular, the reliability of the FLUKA results was further investigated by means of different models for the calculation of the excitation functions of the considered nuclear reactions as in example TALYS. Although al considered codes show that the calculated cross section peaks are expected to be low in the range 0-70MeV, the production of ^{64}Cu and ^{67}Cu is still anyway remarkable, since the beam is dumped within the target, thus the overall integrated cross section is exploited. According to FLUKA ~55 GBq and 1.4 GBq will be the produced activities of respectively ^{64}Cu and ^{67}Cu within the ZrGe target after 5 days of irradiation. The effective reliability of such results will be verified as soon as experimental data on the desired reactions will be available.

Anyway, since the ISOL technique involves not only the in-target production but also the subsequent release, ionization and transport of the nuclide of interest, the effectively collected amounts in the secondary target could be significantly lower. Such drawback can make the ISOL production of copper isotopes less competitive than cyclotron-based techniques, which are able to provide amounts of ^{64}Cu with few hours of irradiation [4.6]. However, on the contrary, current production techniques are not capable to easily provide ^{67}Cu in significant quantities for preclinical studies, thus ISOL could represent a valid alternative to satisfy this need. Anyway, the strength point of this study is the possibility to simultaneously produce both ^{64}Cu and ^{67}Cu with one primary target, and to recover them independently on an appropriate secondary target.

As previously stated, the different processes involved in ISOL affect the amounts of nuclide that will be finally available as radiopharmaceutical precursors. The offline ionization tests performed in this study were indeed aimed to quantify the influence of the ionization, the extraction, the mass separation and recovery on the overall production. It was possible to verify that intense (up to 600 nA) ^{nat}Cu ion beams could be produced using the Plasma Ion Source and the MM technique, and an ionization efficiency factor of ~8% was measured. As in the case of Ag, the presented result could be potentially improved by switching to the resonant laser ionization technique [4.39], that foresees the use of lasers, tuned to the typical wavelengths of

the desired element, and normally ensures a more selective and thus efficient ionization[4.40]. The future performance of tests with a laser ion source would allow to identify the most efficient ionization mechanism for Copper.

In this study the Cu release capabilities of the ZrGe target were qualitatively assessed, with the aim to investigate the optimal working temperature of such material. It was however not possible to estimate quantitatively the release efficiency, but such preliminary tests ensured that Copper volatility is reasonable at 1700°C, the proposed limiting working temperature for ZrGe. Finally, stable Copper ion beams were recovered thanks to the use of a low-cost and low-toxic material: Sodium Chloride. The quantification of the Copper collected on these substrates was performed after their dissolution in nitric acid medium. The amount of recovered Copper was acceptable, but improvements have to be carried out in the chemical extraction of the deposed Cu from the collection target. In example, different deposition substrates could be developed, or different harvesting processes could be evaluated (as in example increasing the solution concentration). For this reason, further studies will be carried out to improve the efficiency of the chemical recovery process.

4.7 References

[4.1] C. Müller, N. P. van der Meulen, M. Benešová, and R. Schibli, "Therapeutic Radiometals Beyond 177Lu and 90Y: Production and Application of Promising α-Particle, β−-Particle, and Auger Electron Emitters," *J. Nucl. Med.*, vol. 58, no. Supplement 2, p. 91S–96S, Sep. 2017.

[4.2] C. J. Anderson and R. Ferdani, "Copper-64 Radiopharmaceuticals for PET Imaging of Cancer: Advances in Preclinical and Clinical Research," *Cancer Biother. Radiopharm.*, vol. 24, no. 4, pp. 379–393, 2009.

[4.3] D. W. McCarthy *et al.*, "Efficient production of high specific activity 64Cu using a biomedical cyclotron," *Nucl. Med. Biol.*, vol. 24, no. 1, pp. 35–43, Jan. 1997.

[4.4] K. Abbas *et al.*, "Cyclotron production of 64Cu by deuteron irradiation of 64Zn," *Appl. Radiat. Isot.*, vol. 64, no. 9, pp. 1001–1005, Sep. 2006.

[4.5] T. Katabuchi *et al.*, "Production of 67Cu via the 68Zn(p,2p)67Cu reaction and recovery of 68Zn target," *J. Radioanal. Nucl. Chem.*, vol. 277, no. 2, p. 467, Mar. 2008.

[4.6] A. Obata *et al.*, "Production of therapeutic quantities of 64Cu using a 12 MeV cyclotron," *Nucl. Med. Biol.*, vol. 30, no. 5, pp. 535–539, May 2003.

[4.7] S. Spellerberg *et al.*, "Target development for diversified irradiations at a medical cyclotron," *Appl. Radiat. Isot.*, vol. 104, pp. 106–112, Oct. 2015.

[4.8] K. Hilgers, T. Stoll, Y. Skakun, H. . Coenen, and S. . Qaim, "Cross-section measurements of the nuclear reactions natZn(d,x)64Cu, 66Zn(d,α)64Cu and 68Zn(p,αn)64Cu for production of 64Cu and technical developments for small-scale production of 67Cu via the 70Zn(p,α)67Cu process," *Appl. Radiat. Isot.*, vol. 59, no. 5–6, pp. 343–351, Nov. 2003.

[4.9] F. Borgna *et al.*, "Early Evaluation of Copper Radioisotope Production at ISOLPHARM," *Molecules*, vol. 23, no. 10, 2018.

[4.10] V. Sabaiduc and others, "BEST 70P Cyclotron Factory Test," in *Proceedings, 6th International Particle Accelerator Conference (IPAC 2015): Richmond, Virginia, USA, May 3-8, 2015*, 2015, p. THPF003.

[4.11] A. J. Koning and D. Rochman, "Modern Nuclear Data Evaluation with the TALYS Code System," *Nucl. Data Sheets*, vol. 113, no. 12, pp. 2841–2934, Dec. 2012.

[4.12] A. Gottberg, "Target materials for exotic ISOL beams," *Nucl. Instruments Methods Phys. Res. Sect. B Beam Interact. with Mater. Atoms*, vol. 376, pp. 8–15, Jun. 2016.

[4.13] C. Sha, L. Zhou, S. Liu, Y. Du, T. Gang, and H. Xu, "Phase equilibria and thermodynamic modeling in the Ge--Zr binary system," *J. Mater. Sci.*, vol. 46, no. 5, pp. 1405–1413, Mar. 2011.

[4.14] G. V Samsonov, *Chemical Properties and Analysis of Refractory Compounds / Khimicheskie Svoistva I Metody Analiza Tugoplavkikh Soedinenii / Химические Свойства И Методы Анализа Тугоплавких Соединений*. Springer US, 2012.

[4.15] E. Parthé and J. T. Norton, "Crystal structures of Zr5Ge3, Ta5Ge3 and Cr5Ge3," *Acta Crystallogr.*, vol. 11, no. 1, pp. 14–17.

[4.16] R. S. Biryukova and O. I. Popova, "Preparation of transition metal germanides," *Sov. Powder Metall. Met. Ceram.*, vol. 23, no. 2, pp. 146–149, Feb. 1984.

[4.17] A. Girotto, "Development of porous refractory targets for nuclear physics and medical applications," Università degli Studi di Padova, 2017.

[4.18] F. Gobbo D'Incà, "Porous ceramic target for the production of radioactive beams for nuclear phisics and medicine.," Università degli Studi di Padova, 2018.

[4.19] A. Monetti *et al.*, "The RIB production target for the SPES project," *Eur. Phys. J. A*, 2015.

[4.20] A. Andrighetto, C. M. Antonucci, S. Cevolani, C. Petrovich, and M. Santana Leitner, "Multifoil UCx target for the SPES project --An update," *Eur. Phys. J. A - Hadron. Nucl.*, vol. 30, no. 3, pp. 591–601, 2006.

[4.21] G. Battistoni *et al.*, "Overview of the FLUKA code," *Ann. Nucl. Energy*, 2015.

[4.22] J. Allison *et al.*, "Recent developments in Geant4," *Nucl. Instruments Methods Phys. Res. Sect. A Accel. Spectrometers, Detect. Assoc. Equip.*, vol. 835, pp. 186–225, Nov. 2016.

[4.23] A. V Ivantchenko, V. N. Ivanchenko, J.-M. Q. Molina, and S. L. Incerti, "Geant4 hadronic physics for space radiation environment," *Int. J. Radiat. Biol.*, vol. 88, no. 1–2, pp. 171–175, 2012.

[4.24] D. H. Wright and M. H. Kelsey, "The Geant4 Bertini Cascade," *Nucl. Instruments Methods Phys. Res. Sect. A Accel. Spectrometers, Detect. Assoc. Equip.*, vol. 804, pp. 175–188, Dec. 2015.

[4.25] G. Folger, V. N. Ivanchenko, and J. P. Wellisch, "The Binary Cascade," *Eur. Phys. J. A - Hadron. Nucl.*, vol. 21, no. 3, pp. 407–417, 2004.

[4.26] Mancusi, D., Boudard, A., Cugnon, J., David, J.-C., Kaitaniemi, P., and Leray, S., "New C++ version of the Liège intranuclear cascade model in Geant4," *SNA + MC 2013 - Joint International Conference on Supercomputing in Nuclear Applications + Monte Carlo*. p. 5209, 2014.

[4.27] V. Ivanchenko *et al.*, "Recent Improvements in Geant4 Electromagnetic Physics Models and Interfaces," in *3th Monte Carlo Conference MC2010*, 2010, vol. 2, pp. 898–903.

[4.28] N. Otuka *et al.*, "Towards a More Complete and Accurate Experimental Nuclear

Reaction Data Library (EXFOR): International Collaboration Between Nuclear Reaction Data Centres (NRDC)," *Nucl. Data Sheets*, vol. 120, pp. 272–276, Jun. 2014.

[4.29] M. Brugger, A. Ferrari, S. Roesler, and P. R. Sala, "Calculation of radionuclide production cross sections with FLUKA and their application in high energy hadron collider studies," in *ND2007*, 2007.

[4.30] D. Rochman *et al.*, "The TENDL library: Hope, reality and future," *EPJ Web Conf.*, vol. 146, p. 02006, Sep. 2017.

[4.31] C. Duchemin, A. Guertin, F. Haddad, N. Michel, and V. Métivier, "Production of medical isotopes from a thorium target irradiated by light charged particles up to 70 MeV," *Phys. Med. Biol.*, vol. 60, no. 3, p. 931, 2015.

[4.32] D. Basile, C. Birattari, M. Bonardi, L. Goetz, E. Sabbioni, and A. Salomone, "Excitation functions and production of arsenic radioisotopes for environmental toxicology and biomedical purposes," *Int. J. Appl. Radiat. Isot.*, vol. 32, no. 6, pp. 403–410, Jun. 1981.

[4.33] B. Crepieux, "Préparation et domaine d'exploitation des mass-marker des cibles ISOLDE," 2006.

[4.34] D. R. Lide, *CRC Handbook of Chemistry and Physics: A Ready-reference Book of Chemical and Physical Data*. CRC-Press, 1995.

[4.35] A. Andrighetto *et al.*, "Spes: An intense source of Neutron-Rich Radioactive Beams at Legnaro," *J. Phys. Conf. Ser.*, vol. 966, no. 1, 2018.

[4.36] F. Borgna, "Pharmaceutical Deveolpment of the ISOL Technique for the Production of Radionuclides and their Applications in Targeted Radionuclide Therapy," University of Padova, 2018.

[4.37] F. Borgna *et al.*, "A preliminary study for the production of high specific activity radionuclides for nuclear medicine obtained with the isotope separation on line technique," *Appl. Radiat. Isot.*, 2017.

[4.38] M. Manzolaro *et al.*, "Ongoing characterization of the forced electron beam induced arc discharge ion source for the selective production of exotic species facility," *Rev. Sci. Instrum.*, vol. 85, no. 2, p. 02B918, 2014.

[4.39] V. N. Fedosseev *et al.*, "ISOLDE RILIS: New beams, new facilities," *Nucl. Instruments Methods Phys. Res. Sect. B Beam Interact. with Mater. Atoms*, vol. 266, no. 19–20, pp. 4378–4382, Oct. 2008.

[4.40] D. Scarpa *et al.*, "ToF diagnostic of Tin resonant laser photoionization in SPES laser offline laboratory," *J. Instrum.*, vol. 11, no. 09, pp. C09001–C09001, Sep. 2016.

Chapter 5

The Titanium based ISOL targets for the production of medical Scandium isotopes

"Dans la nature rien ne se crée, rien ne se perd, tout change."

"In nature nothing is created, nothing is lost, everything changes."

Antoine-Laurent de Lavoisier (French chemist, 1743 – 1794), *Traité élémentaire de chimie.*

5.1 Introduction

Following the increasing interest in theranostic applications, several other radionuclides pair are being studied in addition to ^{64}Cu/^{67}Cu. Among the most promising emerging theranostic pairs, ^{44}Sc/^{47}Sc and ^{43}Sc/^{47}Sc are an extremely interesting case studies, sine chemical properties of Scandium allow the use of the same biomolecules labelled with the PET radionuclide ^{68}Ga, thus their expected bio-distribution is already known. Indeed, Scandium was recently used to obtain the first PET images of human patients, injected with ^{44}Sc labelled radiotracers [5.1 – 5.3]. Among ^{43}Sc and ^{44}Sc, both β^+-emitters, ^{43}Sc is proposed as the most appropriate radionuclide for PET imaging thanks to its physical and chemical properties. Indeed, ^{43}Sc has a half-life of 233 min (^{68}Ga: 68 min; ^{44}Sc: 235 min) and its decay occurs with a high total positron yield of 88.1% (^{68}Ga: 88.9%; ^{44}Sc: 94.3%). Since the emitted positrons have a maximum energy of 1.190 MeV (70.9%) and 0.826 MeV (17.2%), lower than ^{68}Ga (1.899 MeV) and ^{44}Sc (1.474 MeV), imaging adopting such nuclide can have a better image resolution. Furthermore, ^{43}Sc decays emitting an associated low-energy γ ray of 373 keV with 23%

abundance (^{68}Ga: 1077 keV, 3.2% ab.; 44Sc: 1157 keV, 99.9% ab.). This is a desirable feature, because, if any extra γ ray falls within the 511 keV energy window (typically 440–665 keV for modern PET scanners), it may affect the quality of images, as in the case of ^{68}Ga and ^{44}Sc. Moreover, energetic extra γ radiation provides an unwanted additional dose exposure to both patients and hospital personnel. In addition, both ^{43}Sc and ^{44}Sc half-lives are of nearly four hours, thus giving the possibility to transport scandium labelled compound over large distances (more than 500 km) from the production facility [5.4].

The production of ^{43}Sc and ^{44}Sc in quality and quantity suitable for clinical applications is still a challenging issue. Current production routes foresee the employment of medical cyclotrons, and are based on the irradiation of solid targets made with enriched materials. The reactions ^{44}Ca(p,n)^{44}Sc, ^{43}Ca(p,n)^{43}Sc, ^{46}Ti(p,α)^{43}Sc, and ^{42}Ca(d,n)^{43}Sc are thus exploited [5.4]. The most promising therapeutic isotope of Scandium to be paired with the diagnostic ^{43}Sc and ^{44}Sc is ^{47}Sc ($T_{1/2}$ = 3.4 days, E β^-(av) = 162 keV, main Eγ = 159.4 keV, I = 68.3%). It is indeed a very promising low-energy β^- emitter for targeted radiotherapy [5.5, 5.6].

High specific activity ^{47}Sc can be produced in a nuclear reactor irradiating with high energy neutrons (E > 1 MeV) enriched $^{47}TiO_2$ targets via the ^{47}Ti(n, p)^{47}Sc reaction [5.7, 5.8]. As alternative, ^{47}Sc production is possible via a generator system that foresees the irradiation with thermal neutrons of a ^{46}Ca enriched target. Thanks to the ^{46}Ca(n,γ)^{47}Ca reaction ^{47}Ca ($T_{1/2}$ = 4.54 days) is generated and finally after its β^- decay highly pure ^{47}Sc can be milked from the generator [5.9]. Even if thermal neutrons are available in more production facilities, the drawback is the fact that the ^{46}Ca enriched targets are available only at a 30% enrichment level and their cost is prohibitive.

Other alternatives for producing ^{47}Sc are the proton irradiation of ^{nat}Ti [5.10] and γ irradiation of ^{48}Ti exploiting an electron beam [5.11], but the achieved production efficiencies were lower than the former cases. Other methods, recently investigated, are based on the alpha irradiation of ^{44}Ca enriched targets using a cyclotron [5.12], but the low cross section of the ^{44}Ca(α,p)^{47}Sc reaction makes it problematic to obtain the relevant quantities, that are necessary to perform clinical studies. Finally, the ^{47}Sc production via the ^{48}Ca(p,2n)^{47}Sc reaction at medium size cyclotrons (proton energy below 30 MeV) was also studied [5.13], but the side production of the unwanted ^{48}Sc ($T_{1/2}$ = 43.67 h) and ^{46}Sc ($T^{1/2}$ = 83.79 days) decrease the achievable purity.

Considering the difficulties to develop an accelerator-based production of the theranostic pair ^{43}Sc/^{47}Sc, following the conventional techniques, in the framework of ISOLPHARM, a feasibility study was performed in order to verify if the ISOL technology can be used to provide high quality and purity Scandium radionuclides. As for Cu and Ag, such study, includes Monte Carlo simulations for the estimation of the producible amounts and offline ionization tests.

5.2 Titanium Carbide as ISOL target material

As in the case of Copper, the feasibility study of the production of Sc medical isotopes with the ISOLPHARM method foresees the identification of a suitable target material. Indeed such light nuclei are not included in the production spectrum of the SPES UC_x target [5.14], therefore a non-fissile target material including stable nuclei close to the desired products should be considered. Indeed, since at SPES the installed cyclotron is capable of delivering a high intensity proton beam with energy in the range of 35-70 MeV [5.15], the expected products are generated mostly via the light-ion induced fusion reaction.

TENDL-2017 [5.16] and EXFOR [5.17] databases were deeply consulted, and finally Titanium based target were considered as the most suitable for a simultaneous production of both ^{43}Sc and ^{47}Sc. In addition, also ^{44g}Sc could be produced, but the drawback is the unavoidable presence of the long-lived contaminant ^{44m}Sc ($T_{1/2}$ = 58.61 h), that is not eliminated by the Mass Separation step since it shares the same mass number of the more desirable ^{44g}Sc.

Figures 5.1, 5.2 and 5.3 summarizes the data found concerning the reactions ^{nat}Ti(p,X)^{43}Sc, ^{nat}Ti(p,X)^{44m}Sc and ^{nat}Ti(p,X)^{47}Sc [5.18 – 5.22].

Concerning the data published in TENDL-2017 [5.16], the plotted trends were obtained from the weighted average of the single contributes, reported in the database for each stable isotope of Titanium, that are ^{46}Ti (nat. abundance 20.52%), ^{47}Ti (nat. abundance 27.45%), ^{48}Ti (nat. abundance 7.76%), ^{49}Ti (nat. abundance 36.52%) and ^{50}Ti (nat. abundance 7.75%), using as weight the respective natural abundances.

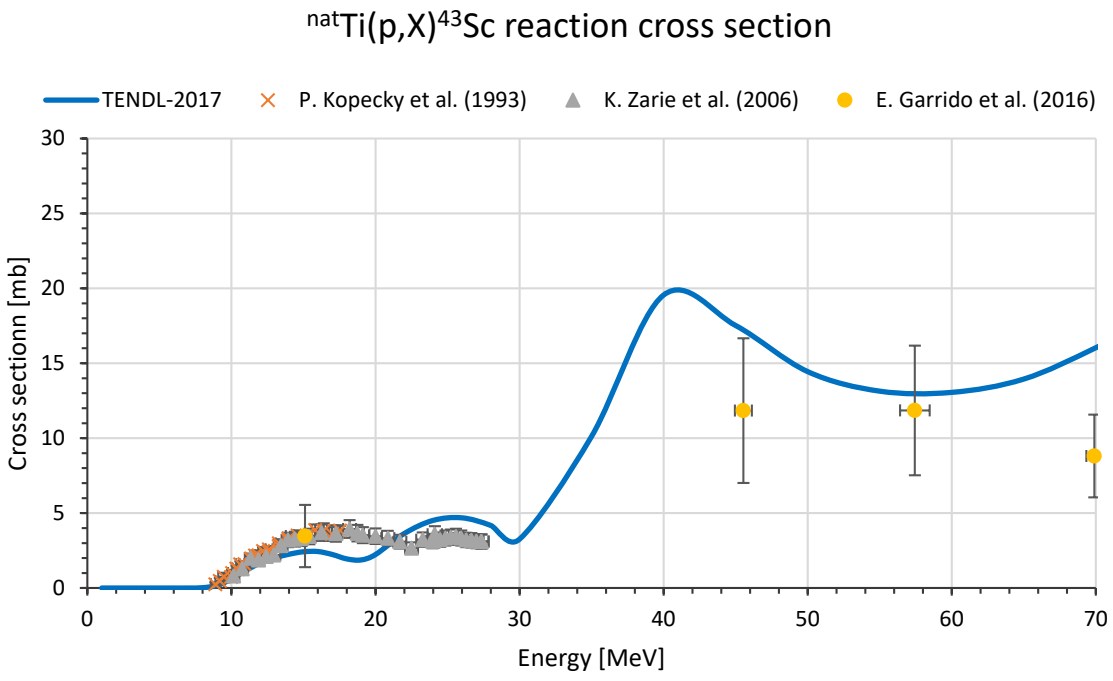

Figure 5.1: *cross section data for the ^{nat}Ti(p,X)^{43}Sc reaction taken form TENDL-2017* [16] *and from experimental studies included in EXFOR* [20]–[22]

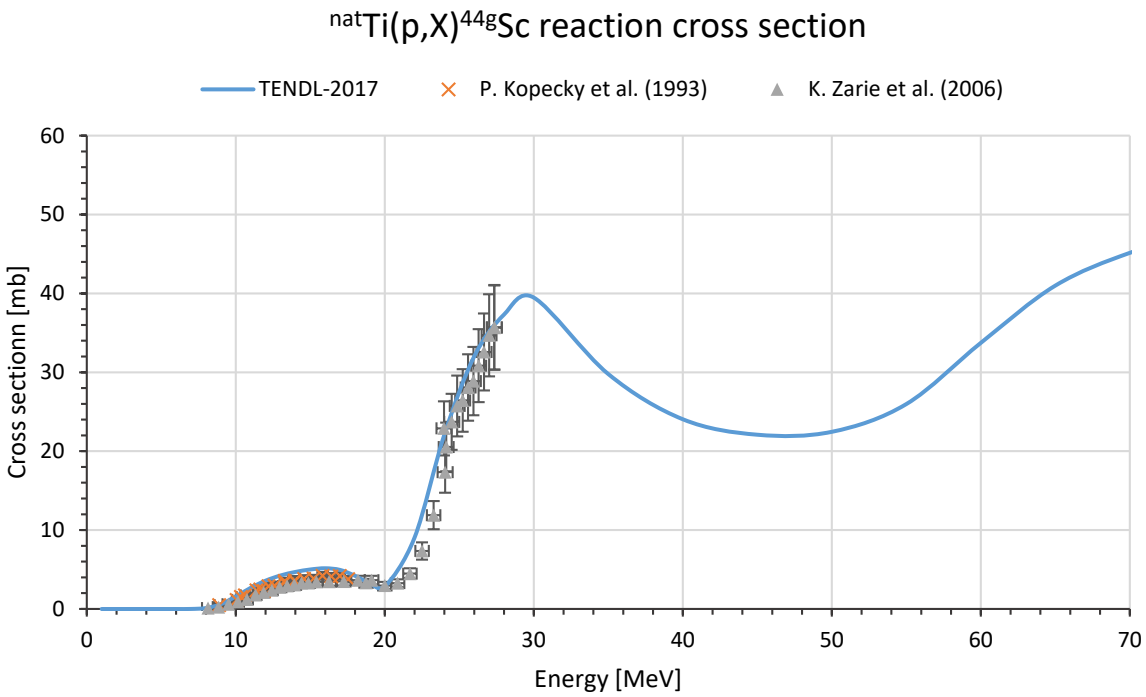

Figure 5.2: *cross section data for the $^{nat}Ti(p,X)^{44g}Sc$ reaction taken form TENDL-2017* [16] *and from experimental studies included in EXFOR* [20], [21]

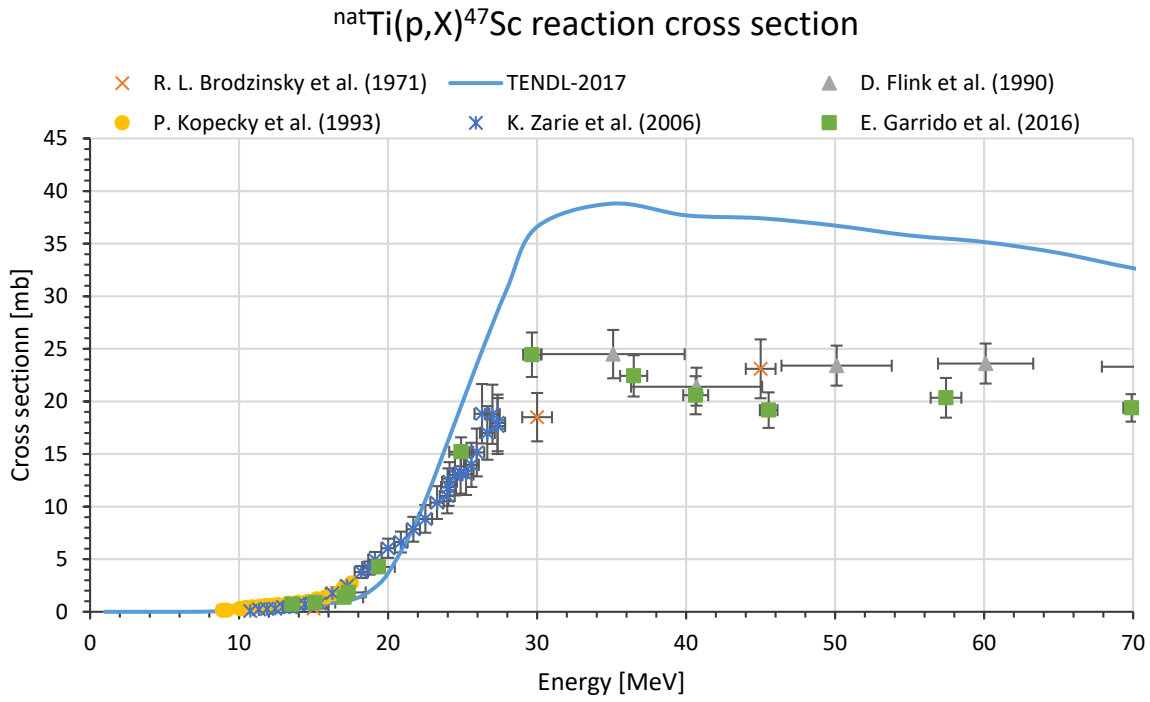

Figure 5.3: *cross section data for the $^{nat}Ti(p,X)^{47}Sc$ reaction taken form TENDL-2017* [16] *and from experimental studies included in EXFOR* [18]–[22]

Considering the need to operate ISOL targets at the highest acceptable temperature (above 2000°C) to boost the nuclides release, and the requirement to use only solid materials as targets at SPES, Titanium Carbide was identified as a promising candidate for this feasibility study.

5.2.1 The Titanium carbide target material

Carbides are the most interesting materials for the ISOL target production due to their capability of efficiently releasing short-lived isotopes. Titanium Carbide was indeed already used and tested as a target material at CERN-ISOLDE [5.23], and its release properties were characterized [5.24].

Titanium Carbide (TiC) is an interstitial carbide of group IV, characterized by a high hardness, strength, stiffness and wear resistance, that is therefore industrially used as a secondary carbide in cemented tungsten carbide cutting and grinding tools and for highly resistant coatings.

As indicated in the Ti-C phase diagram in Figure 5.4 [5.25], the only possible stable compound involving Titanium and Carbon is the monocarbide TiC. In addition, its refractoriness is highlighted by the melting point of 3065.7°C, at atmospheric pressure at stoichiometric composition.

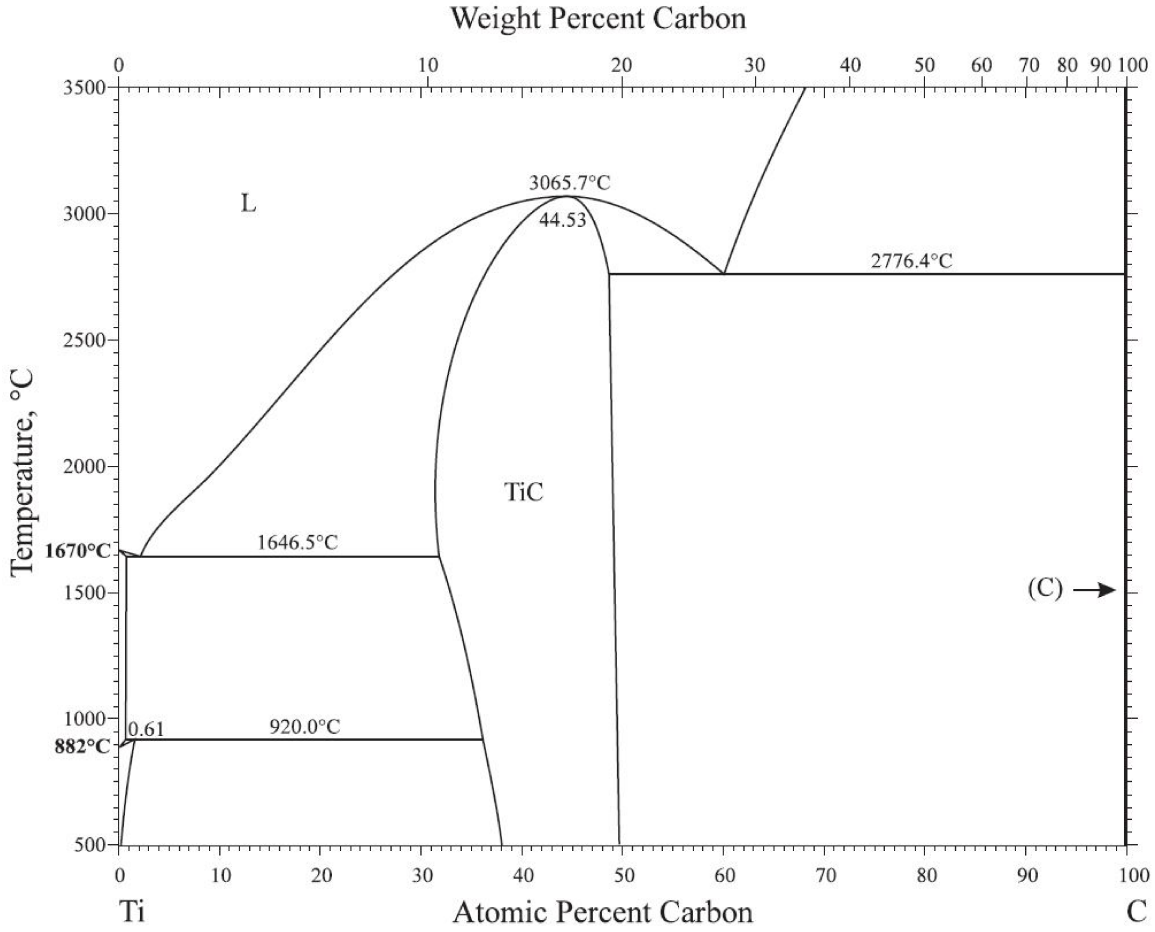

Figure 5.4: *the Ti-C system phase diagram* [5.25]

Additional developments aimed to increase the capability of Titanium Carbide to rapidly release the produced nuclides are being investigated. In particular its synthesis as nanomaterial was studied at CERN [26], and the possibility to produce it with the additive manufacturing technologies was investigated at INFN-LNL (figure 5.5) [5.27]. Such studies are both aimed to

increase the porosity of the material, without compromising excessively its mechanical resistance and thermal properties.

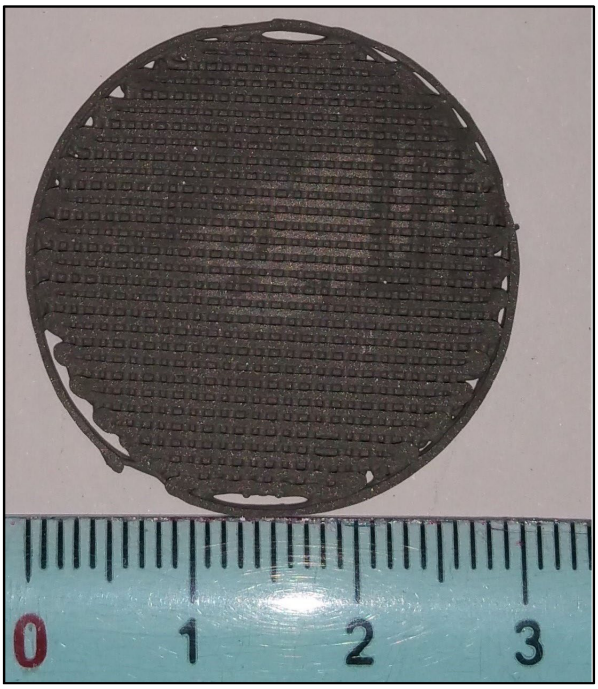

Figure 5.5: *a sample of TiC target disk obtained with additive manufacturing*

5.2.2 Yields from a TiC target

Once the proper target material was identified, the next step was to estimate the expected in-target yields from TiC of the desired nuclides (figure 5.6).

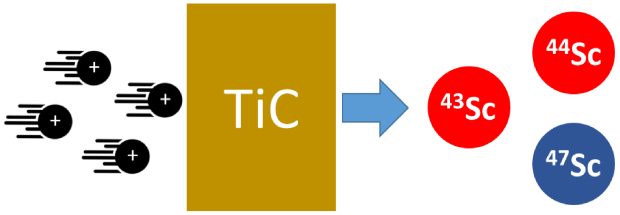

Figure 5.6*: possible medical radionuclides from the TiC target*

As highlighted in the analysis of the cross sections for the reactions involved, in figures 5.1, 5.2 and 5.3, generally, the higher is the proton energy, the higher are the cross sections. Anyway, the energy threshold to activate the desired reactions is generally low, around 10 MeV, whereas the maximum peak is normally reached at around 30-40 MeV, thereafter no appreciable increase is achieved. For these reasons, a proton beam with energy of 40 MeV should be sufficient to produce decent amounts of the desired nuclides. Thus for the estimations of the effective in-target yields a proton beam of 40 MeV energy and 200 μA intensity was considered, since also for the TiC target a multi-foil target architecture could be proposed [5.28].

For the preliminary investigations of the expected in-target yields of ^{43}Sc, ^{44}Sc and ^{47}Sc the Monte Carlo code FLUKA [5.29] (version 2011.2x.2)was employed. As in the case of the Zirconium Germanide target, a simplified 4 cm diameter cylindrical geometry was considered for the Titanium Carbide target, and a hypothesized material density of 4 g/cm^3 was assumed, supposing the realization of an averagely porous material. Concerning the target thickness, a value of 5cm was set in order to ensure the dumping of the proton beam within the production target. For the 40 MeV 200 μA (1.248E+15 p/s) proton beam a Gaussian profile was used with rms of 0.5 cm in both transverse axes. Figure 5.7 summarizes the so-calculated yields.

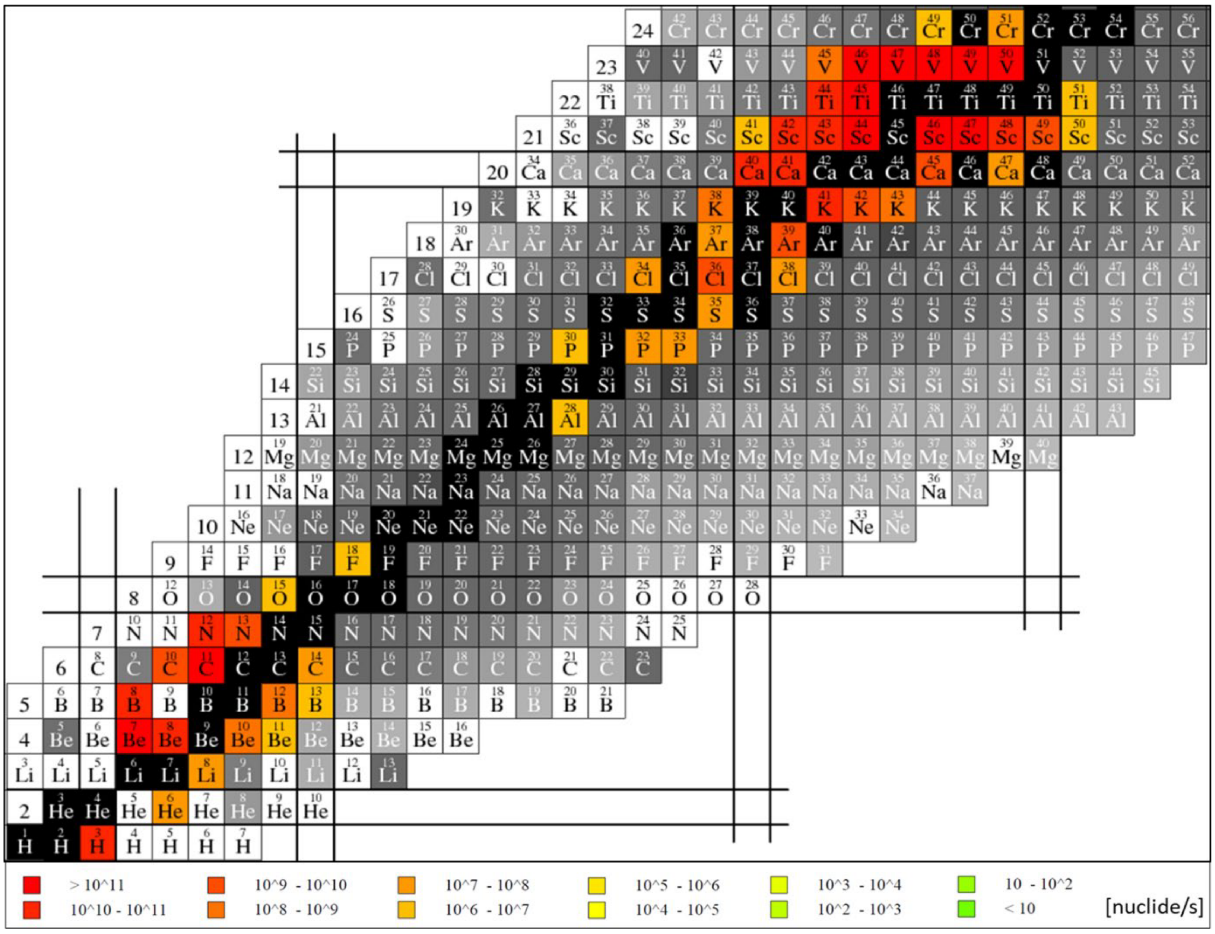

***Figure 5.7**: estimated in-target yields according to FLUKA*

As shown in figure 5.7, the expected nuclide production ranges from Aluminum to Vanadium if stable Titanium is used as target nucleus, whereas the proton induced reactions on Carbon generate products from Helium to Nitrogen.

The excitation functions considered by FLUKA are based on the PEANUT nuclear interaction model [5.30]. In order to increase the reliability of the results, other simulations were launched considering different models for the calculation of the cross sections. For such additional studies, the Monte Carlo toolkit Geant4 (version 4.10.04.p02) [5.31] was used, and different Physics Lists, that correspond to different nuclear interaction models, were considered.

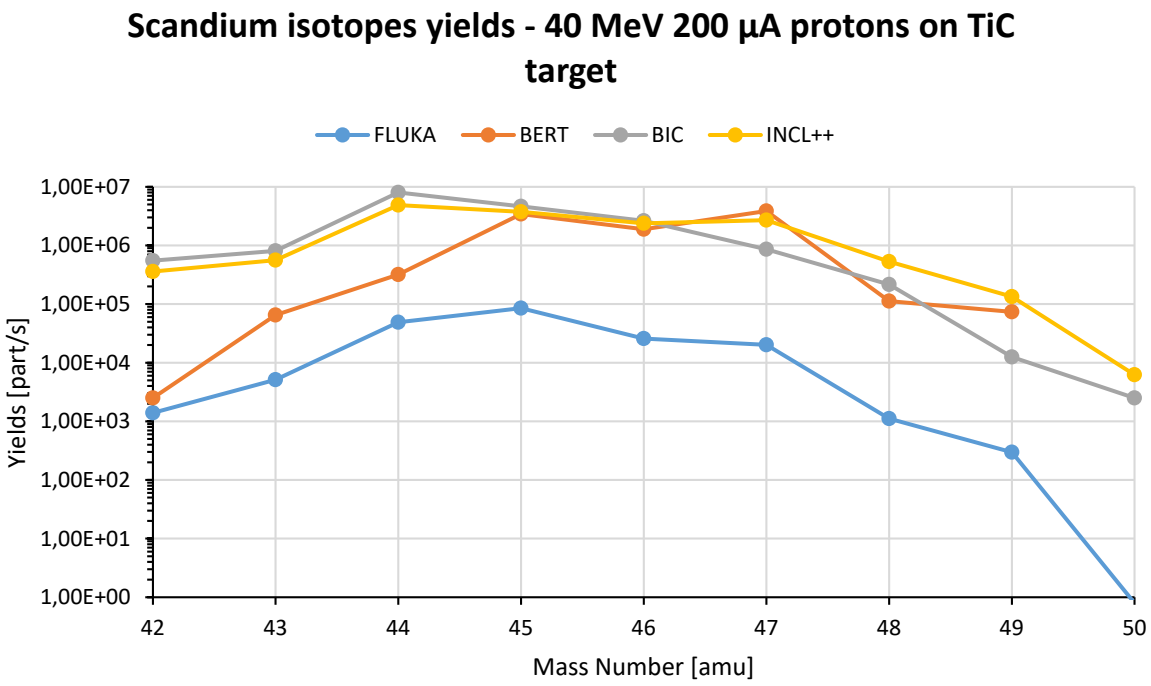

Figure 5.8: *Scandium isotopes yields according to different models for a 40 MeV 200 µA proton beam on a TiC target*

The comparison between the various nuclear models used in the simulations is summarized in figure 5.8. In particular, such study was focussed on the yields for the Scandium isotopes.

In addition to the FLUKA-PEANUT results, as in the case of the feasibility study for Copper, the nuclear interaction models considered with Geant4 were the Bertini cascade model [5.32, 5.33], the Binary Cascade model (BIC) [5.32, 5.34] and the Liège intranuclear cascade model (INCL++) [5.35].

Regarding the implementation in Geant4, the activated Physics Lists were FTFP_BERT, QGSP_BIC and QGSP_INCLXX for respectively the Bertini cascade, the BIC model, and INCL++ cascade. Additionally, the reliability of the results at low energies was increased by activating the electromagnetic option EMZ [5.36].

As a general consideration, the set of results produced by the various models shows, in some cases, orders of magnitude of difference. This is, for example, the case of the ^{43}Sc yields, were according to the Bertini cascade model approximately 6.5E+04 particles/s are produced, the BIC and INCL++ models indicate a production of 5.6E+05 particles/s whereas FLUKA suggests the generation of 5E+03 particles/s. It is possible also to highlight also that the differences between the models increases at higher mass numbers.

Anyway, for the subsequent preliminary evaluation of the in-target produced activities, the FLUKA results were taken into account, because the comparison highlighted it as the most conservative model.

5.2.3 Expected in-target production of ^{43}Sc and ^{47}Sc

Since the MC code FLUKA was taken as for the further evaluations of the presented feasibility study, it was also used to simulate the in-target produced activities at different irradiation times. For the performance of such simulations, the radioactive decays were activated, and timepoints of 0.5, 1, 2, 3, 4, 5 and 6 days were considered, in accordance with the maximum expected irradiation time for the SPES targets, namely 15 days. A primary proton beam of 40 MeV energy and 200 μA intensity was considered, as in the case of the yields simulations.

Table 5.1 summarizes the calculated activities for the Scandium isotopes of interest, ^{43}Sc and ^{47}Sc, together with ^{44}Sc; showing promising results. Indeed, for ^{43}Sc the expected produced activity after 5 days of irradiation was 64.6 GBq, while for ^{47}Sc was 163 GBq. Concerning ^{44}Sc, a high production of such isotope was highlighted, however, the calculated results are the sum of the rates for the two isomers ^{44m}Sc and ^{44g}Sc, that cannot be separated neither with the ISOLPHARM method, thus the produced fraction of ^{44g}Sc should be carefully evaluated.

Table 5.1: *the expected in-target activity for ^{43}Sc and ^{47}Sc at different irradiation timepoints*

TiC target (200 μA 40 MeV PPB)									
	^{43}Sc prodcution ($t_{1/2}$: 3.89 h)			^{44}Sc prodcution ($t_{1/2}$: 3.97 h)			^{47}Sc prodcution ($t_{1/2}$: 3.35 d)		
Time	Activity		Nuclei	Activity		Nuclei	Activity		Nuclei
[days]	[Bq]	[Ci]	[#]	[Bq]	[Ci]	[#]	[Bq]	[Ci]	[#]
0.5	5.70E+10	1.54	1.15E+15	2.64E+11	7.14	5.37E+15	2.48E+10	0.67	1.04E+16
1	6.37E+10	1.72	1.29E+15	3.25E+11	8.78	6.61E+15	4.72E+10	1.28	1.97E+16
1.5	6.45E+10	1.74	1.30E+15	3.57E+11	9.65	7.26E+15	6.74E+10	1.82	2.81E+16
2	6.46E+10	1.75	1.30E+15	3.83E+11	10.34	7.79E+15	8.56E+10	2.31	3.57E+16
3	6.46E+10	1.75	1.31E+15	4.24E+11	11.45	8.62E+15	1.17E+11	3.16	4.87E+16
4	6.46E+10	1.75	1.31E+15	4.55E+11	12.28	9.25E+15	1.42E+11	3.84	5.93E+16
5	6.46E+10	1.75	1.31E+15	4.78E+11	12.91	9.72E+15	1.63E+11	4.40	6.78E+16
6	6.46E+10	1.75	1.31E+15	4.95E+11	13.38	1.01E+16	1.79E+11	4.85	7.48E+16

5.3 Titanium Boride as alternative target material

As already introduced, TiC as ISOL target material was already tested and several ongoing developments aimed to increase its performances in terms of release are being implemented. Recent studies showed that TiC is capable of releasing most in-target produced elements even at low temperatures as in example 1200°C and various microstructures were tested [5.24]. However, in the same studies several TiC microstructures were testes at different temperatures [5.24], highlighting difficulties in the released Scandium [5.23, 5.37], as shown in figure 5.9a [5.24]. A small released fraction (20 %) was seen for Sc in TiC-3C at higher temperatures (1900 ◦ C) [5.24], whereas, in case of pure metallic Ti targets [5.38], the released amounts of Sc were

fairly high, as shown in figure 5.9b [5.24]. The explanation of such phenomenon may be the eventual reaction of the generated Sc with the carbon based target material, and the subsequent formation of the refractory Scandium Carbide [5.24].

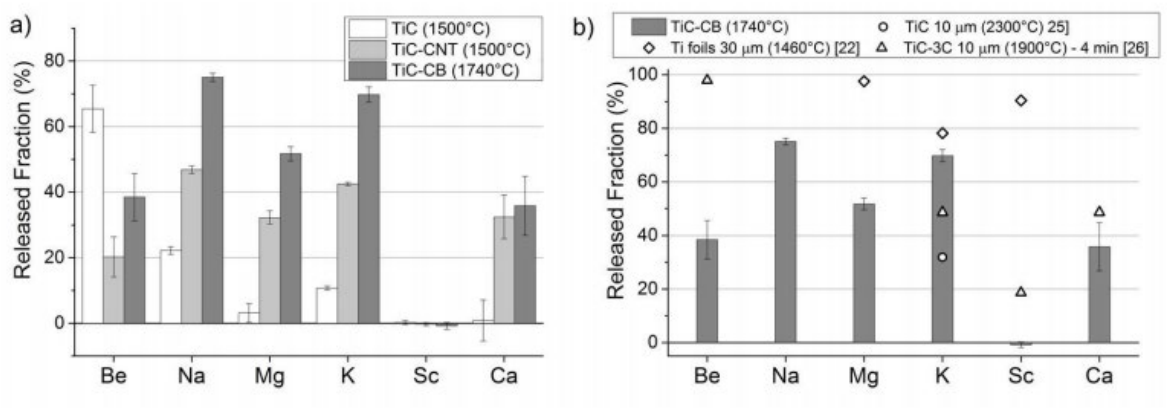

Figure 5.9: *Released fraction for Be, Na, Mg, K, Sc and Ca for three different TiC microstructures at 1500 (TiC and TiC-CNT) and 1740 ◦C (TiC-CB) (a) and comparison of TiC-CB release fraction with literature values* [5.23, 5.37]*, including metallic Ti (b)* [5.24].

Provided that the high temperature chemistry of the Sc-C system in high vacuum is not yet totally known, the issue of the eventual formation of the refractory Scandium Carbide can be avoided by switching to a non-Carbon-based target material. Thus, investigating among the other Titanium binary compounds, Titanium Boride (TiB_2) was identified as a promising candidate.

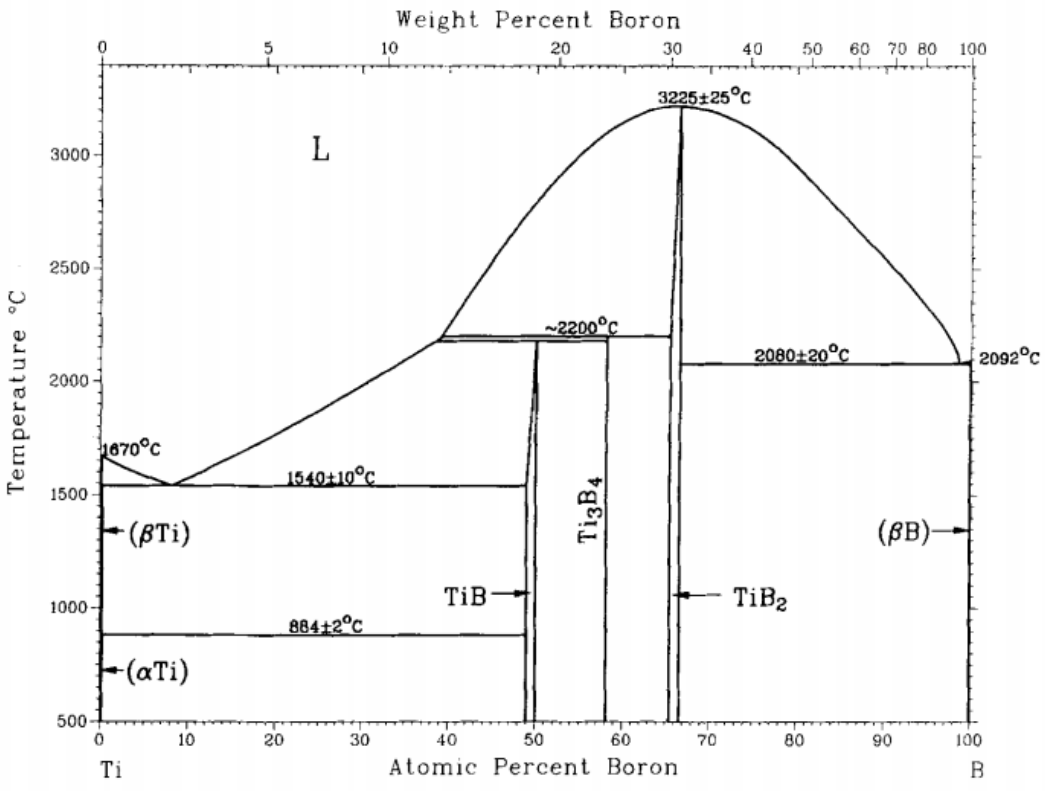

Figure 5.10: *the Ti-B system phase diagram* [5.39]

Indeed, as suggested by the Ti-B phase diagram [5.39] in figure 5.10, TiB_2 is a highly refractory compound, thus suitable for the operation as solid ISOL target material.

5.3.1 Yields from a TiB_2 target

Once TiB_2 was identified as possible target material the following step was to estimate the possible yields with Monte Carlo simulations. Indeed, the presence of a lesser amount of Ti in the target composition could potentially lead to a non-negligible decrease in terms of Scandium isotopes production.

As in the case of TiC, the Monte Carlo code FLUKA [5.29] (version 2011.2x.2) was employed, and the same settings were implemented, with the only obvious exception of the target material. The so-obtained yields were consequently compared with those of TiC, as shown in figure 5.11. As expected, the Sc yields from a TiB_2 targets are slightly lower than those from TiC, anyway, such differences are negligible. Consequently, if Titanium Boride target shows better release capabilities of Scandium isotopes than its carbide counterpart, it can be employed as target material without the drawback of a decreased amount of recoverable nuclides of interest.

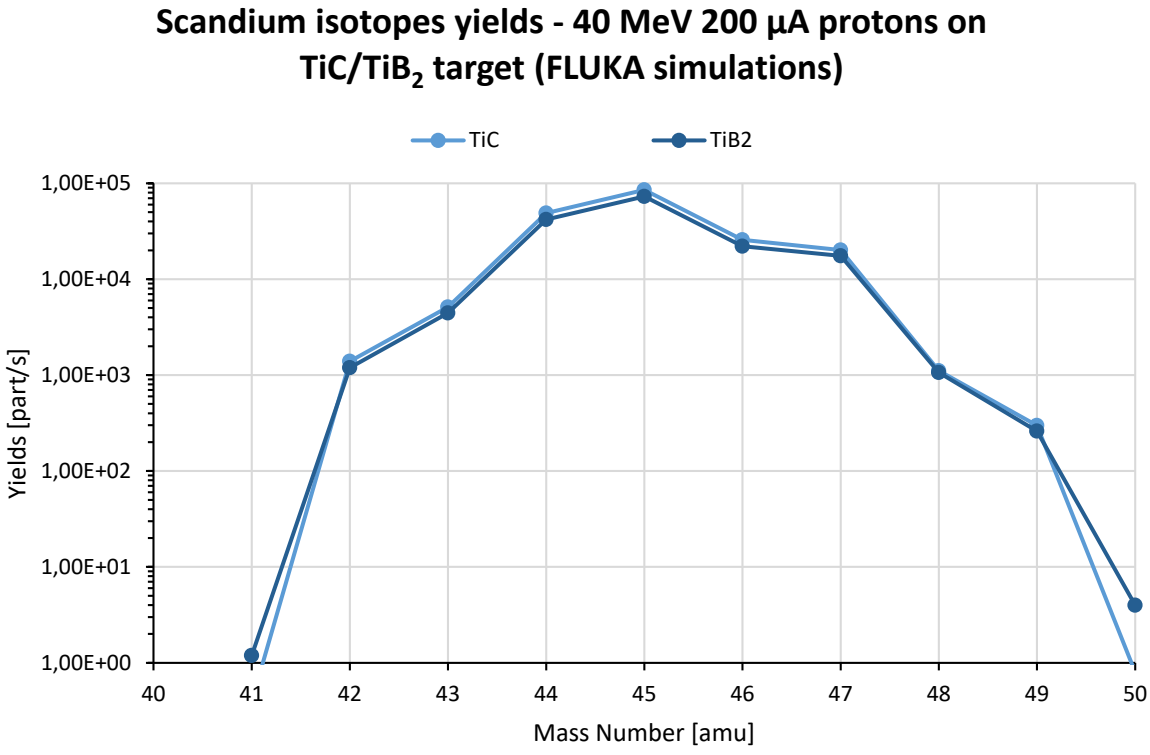

Figure 5.8: *Scandium isotopes yields according to FLUKA for a 40 MeV 200 µA proton beam on a TiC target and on a TiB_2 target. It is possible to highlight that the production yields for the two different target materials ara comparable*

5.4 Early offline ionization tests of stable scandium

Once the best target material candidates were found and the evaluation of the expected in target yields and produced activities was performed, the subsequent crucial step was the investigation of the feasibility of the ionization extraction and mass separation of the Scandium isotopes with the SPES technologies. Indeed, since only a fraction of the amount of in-target produced Scandium nuclides will be ionized and extracted into a beam, in order to better estimate the recoverable amounts of nuclei of interest, the efficiency of the ionization process has to be carefully evaluated. Thus, tests with stable Scandium beams were performed with the SPES Front End prototype in offline modality, as previously done in the cases of Strontium, Yttrium, Iodine, Silver and Copper [5.40, 5.41]. The use of stable isotopes of Scandium (^{45}Sc, natural abundance 100%) for the tests purposes allows to obtain results relevant also for their radioactive counterparts, since the ionization efficiency is related only to the chemical properties of the element of interest.

As introduced in chapter 3 and 4, the experimental apparatus used for the ionization tests is the offline prototype of the SPES Front End, a linear accelerator made of six main functional subsystems. As a recap, such components are: the Target - Ion Source (TIS) unit, the first beam optics subsystem, including four steers, the first triplets, and the first diagnostic box, the Wien filter (WF), namely the electromagnetic mass separator, the second diagnostic box including the slits, the second beam optic subsystem, namely the second triplets and the secondary target station for the collection of the beam. The beamline pressure levels normally range between 10^{-5} and 10^{-6} mbar.

Being Scandium first ionization potential 6.56 eV [5.42], the SPES Plasma Ions Source (PIS) was used, which is capable to ionize a wide set of elements, also the most electronegative [5.43]. The following parameters were used for the performance of the tests:

- The ion source and transfer line were heated by joule effect with a current intensity of 415 A, thus reaching a temperature level generally above 2000°C
- The extraction electrode was positioned at 50% of its maximum stroke, and potential drop of 25 kV was applied between the latter and the TIS unit
- Concerning the first beam optics subassembly, the deflectors S1, S2, S3 and S4 were set at respectively 230 V, 120 V, 25 V and 20 V, whereas the three quadrupoles Q1, Q2 and Q3 forming the first triplet were set respectively at 875, 695 and 1398 V.
- The Wien Filter settings were studied in order to allow the selection of only ^{45}Sc, the only stable isotope of Scandium. A constant electric field of 103.16 kV/m was set into the WF by means of two couple of electrodes, respectively at 590 V (pre-electrodes) and 2579 V

(electrodes). The magnetic field was adjusted by means of the WF coil current, set at 94 A, in order that only mass 45 atoms are not diverted

- The slits were positioned leaving an aperture with 12 mm width, in order that all diverted particles are dumped. Such aperture was selected with the aim that the eventual presence of an intense mass 44 amu beam current would not affect the reliability of the measurement. Indeed, mass 44 correspond to CO_2, that is normally found within the extracted particles, when the SPES plasma ion source is used [5.43].
- The second Faraday Cup (FC2) was left into the beam line, in order to measure constantly the beam current.
- The subsequent triplets were left off, since the beam was dumped onto the second Faraday cup.

Concerning the introduction of Scandium in the TIS unit, several methods were considered. Firstly, the Mass Marker (MM) technique was used [5.44], as in the case of Silver and Copper [41]: 40 µL of Scandium standard solution ($Sc(NO_3)_3$ 1 g/L, Fluka Analytics) were deposed on a thin tantalum foil (the Mass Marker – MM), that was lately accurately folded and inserted inside a small tubular oven. Such oven was stepwise heated by Joule effect in order to allow the atomization of the substrate previously deposed on the foil, and the migration of the neutrals towards the ion source through the transfer line (figure 5.9).

Figure 5.9: *The SPES PIS with the oven loaded with $Sc(NO_3)_3$*

Adopting such method, very low Sc current was reported even for high intensity of the oven heating current (2 nA), thus suggesting that very few Scandium nuclei were reaching the ion source. One possible explanation was the eventual presence of cold-spots along the oven, where the atomized scandium might stick, since it is a high boiling point element (2836°C in atmosphere). Thus, as in the case of Yttrium, whose ionization had similar issues, the second method explored was the direct insertion of the MM within the transfer line, without the use of the oven system. The MM sample was consequently heated simultaneously with the ion source. Even in such case a very low Sc ion current was reported (10 nA), but after the test the sample was removed from the ion source. Consequently, it was possible to notice the presence of a whitish stain in place of the former $Sc(NO_3)_3$ deposition, thus suggesting that the Scandium Nitrate transmutation into Sc_2O_3 had occurred.

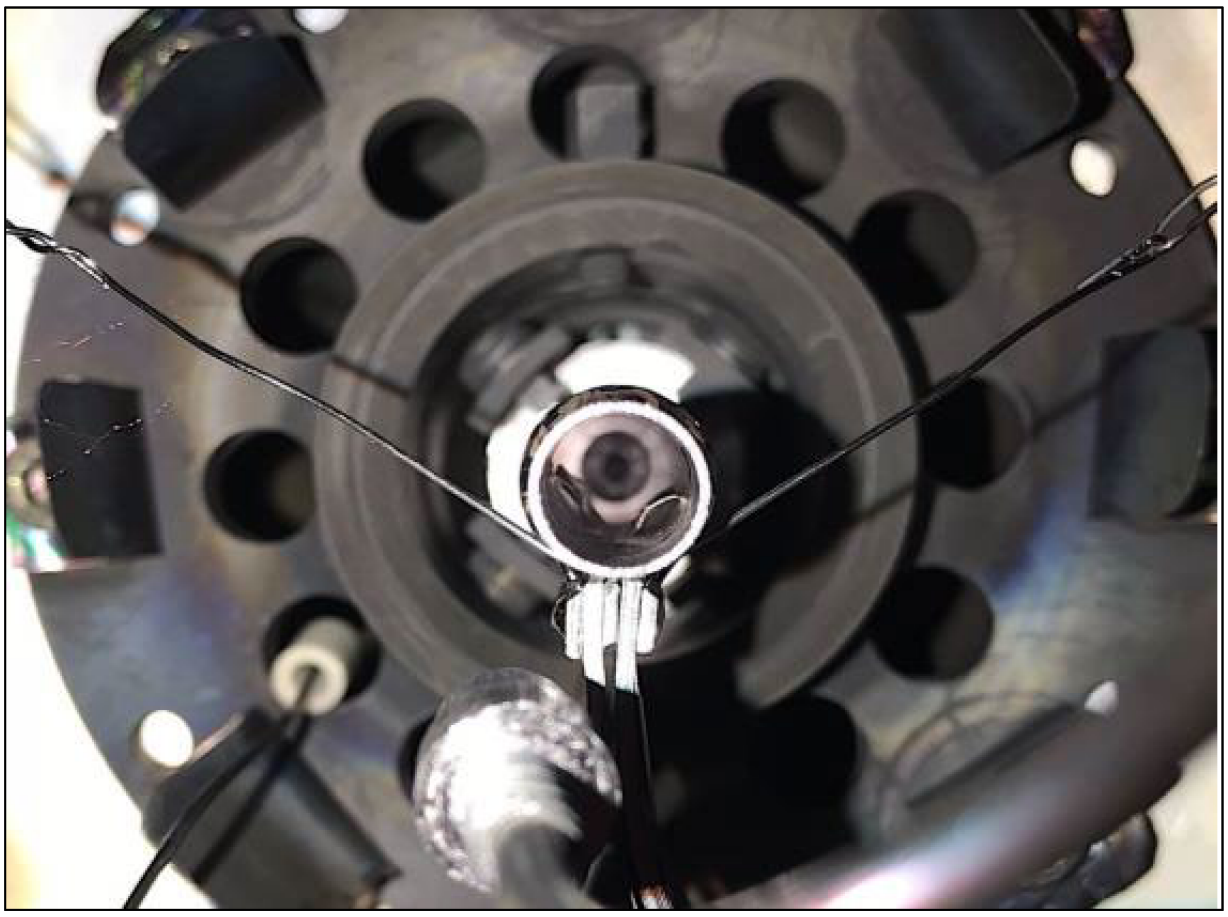

Figure 5.10: *The MM loaded with $Sc(NO_3)_3$ directly inserted in the SPES PIS transfer line*

In order to avoid such issue, a new Scandium chemical form not including Oxygen was considered, namely Scandium Chloride ($ScCl_3$). The sample loaded with 40 μL of $ScCl_3$ aqueous solution (1 g/L) was again placed directly in the transfer line, and finally a mass 45 ion current up to 40 nA of was detected.

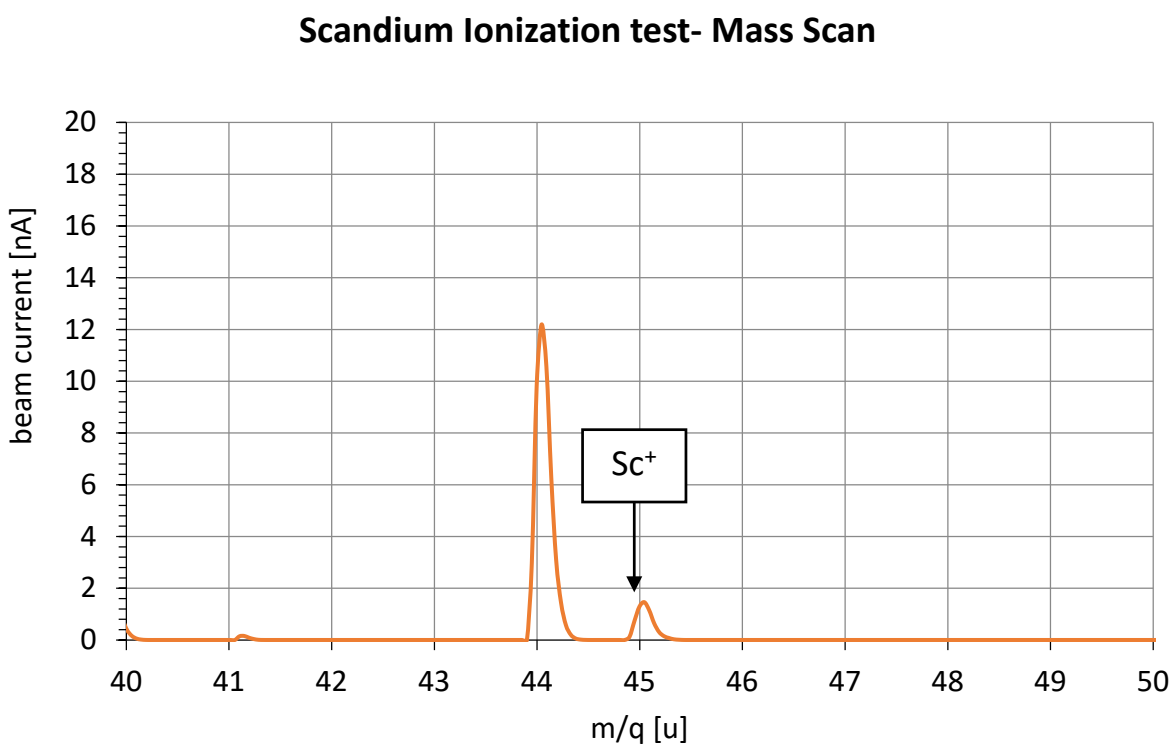

Figure 5.11: *mass scan performed during the Scandium ionization tests. Mass 45 corresponds to the stable isotope of Scandium ^{45}Sc and mass 44 was identified as CO_2*

The effective presence of Scandium within the extracted beam was verified by means of the analysis of the ion masses transported along the beam line. A typical mass scan is reported in figure 5.11.

Scandium was clearly identified thanks to the presence of a peak at mass 45, corresponding to the only stable isotope of Sc, ^{45}Sc. The other peak, at mass number 44, as expected, corresponds to the CO_2 molecular ion, that is originated both by the presence of rarefied air inside the vacuum chamber, and both by the fact that the plasma ion source includes graphite components, that undergo heating. However, since these impurities don't share the same mass number of the isotope of interest, they are not affecting the final result of the test, since they are deflected by the mass separator and dumped at the slits position, and tend to disappear gradually after a long permanence in vacuum and a long heating.

Provided that the direct insertion of the Mass Marker does not decouple the heating of the ion source with the heating of the MM sample as in the case of the oven system, the measurement of the ionization efficiency was still possible, but the so-obtained results might not be fully reliable, since part if the loaded charge might have escaped prior that the ion source was capable to operate efficiently. Anyway, since Scandium proved to suffer of bad volatility, the escaped amount during the ion source temperature increase should have been negligible.

Table 5.2: *the results of the three ionization tests*

Scandium Ionization Efficency tests			
Test number	**Loaded charge**	**Measured charge**	**Efficiency**
[#]	[C]	[C]	[%]
1	8.59E-02	7.24E-05	0.32
2	8.59E-02	6.91E-05	0.30
3	8.59E-02	3.21E-05	0.14

The tests with the use of the MM sample, loaded with $ScCl_3$ were performed three times and the results are summarized in table 5.2. As already highlighted, the problematic atomization of Scandium led to low ionization efficiency values, generally around 0.3%.

In addition to the ionization of Scandium, also very preliminary deposition tests were performed, inserting a NaCl substrate in the secondary target station.

For the performances of such tests, the MM load was increased up to 200 µL of $ScCl_3$ (1 g/L) and the second triplets QT1, QT2 and QT3 were turned on and set at respectively at 1760 V, 850 V and 1775 V.

Figure 5.12 represent a collection target after the performance of such tests: it is possible to identify a pale spot in the center of the NaCl substrate, corresponding to the collection of mass Scandium ions. The quantification of such collection via substrate analysis was however not possible, since the collected amount of Sc was not sufficient for the performance of such chemical measurements, as in the case of Silver and Copper. Thus, either longer irradiation durations are suggested, or a larger amount of Sc should be introduced in the MM sample.

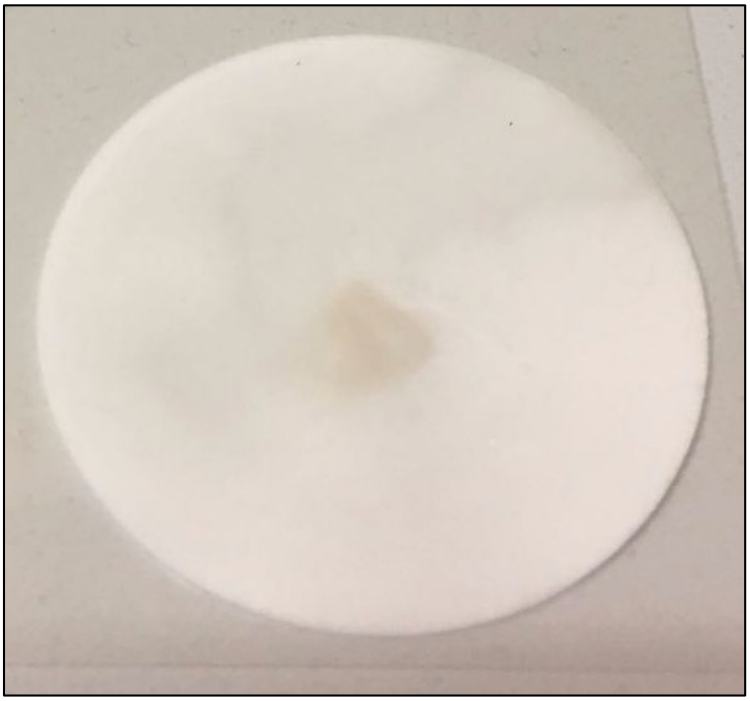

Figure 5.12: *NaCl collection target after the performance of the Sc deposition tests. The pale spot in the center correspond to the stable Sc collection.*

5.5 Discussion and conclusions

The presented study was aimed to evaluate the feasibility of the production of the theranostic pair ^{43}Sc and ^{47}Sc at SPES facility according to the ISOLPHARM patented method.

Concerning the target material, several studies of the involved nuclear reactions suggested the use of Titanium based targets for the production of Sc radioisotopes. Among those, Titanium carbide was firstly proposed, being a material familiar to ISOL applications. However, as studies performed at ISOLDE suggested, the employment of TiC for the production of Scandium beams might not be the best solution, since the presence of Carbon within the target lattice could lead to the formation of the refractory Scandium Carbide compound, that is expected to affect significantly the release. Together with the performance of improvements on the microstructure of TiC targets (nanostructured materials, 3D printing), in this study, TiB_2 was proposed as alternative material for ISOL targets, and its calculated Sc isotope yields were compared to the former one, showing comparable results. Consequently, in order to select the most suitable target material among the two options, dedicated release tests should be performed as soon as samples of the Ti compounds are available. In addition, the lesser known high temperature chemistry of Sc should be further investigated, to understand if there are temperature levels in which molecular break-up of Scandium carbide may occur.

In order to have preliminary estimations of the possible production yields for ^{43}Sc and ^{47}Sc, FLUKA and Geant4 Monte Carlo simulations were performed, showing interesting preliminary results. According to FLUKA ~64.6 GBq and 163 GBq will be the produced activities of respectively ^{43}Sc and ^{47}Sc within the TiC target after 5 days of irradiation with a 200 μA 40 MeV proton beam. Also significant amounts of ^{44}Sc can be produced, but the drawback is that the non-eliminable long lived metastable isomer is produced along with the desirable ground state nuclide.

In addition to the evaluation of the in-target yields, such study was aimed also to preliminary evaluate the efficiencies involved in the Sc ionization and deposition processes.

Several issues were found concerning the offline ionization tests: Scandium suffered indeed of bad volatility, thus various techniques for the insertion of the neutrals within the offline Front End were used. Reasonable Sc ion currents were extracted only in the case of direct insertion of the Mass Marker loaded with $ScCl_3$ within the SPES PIS transfer line. With such technique, an ionization efficiency factor of ~0.3% was measured, suggesting thus the evident need of improvements. Anyway, the PIS adopted for the offline tests and the online version are slightly different, since the transfer line temperature profile was optimized in the latter, to avoid cold spots, where probably part of the released Sc could stick. As in the case of Ag and Cu, improvements could be achieved by switching to the resonant laser ionization technique [5.44].

In addition, for refractory and high boiling point elements, other techniques could be used to boost the release, as in example the employment of molecular beams. Such technique consists in the introduction within the target of extraneous chemical elements, often in the form of gasses. The high temperature of the targets catalyzes the formation of molecular compounds with the chemical species present in the target. In such way, refractory elements could be potentially released towards the ion source in the form of highly volatile molecules [5.45, 5.46].

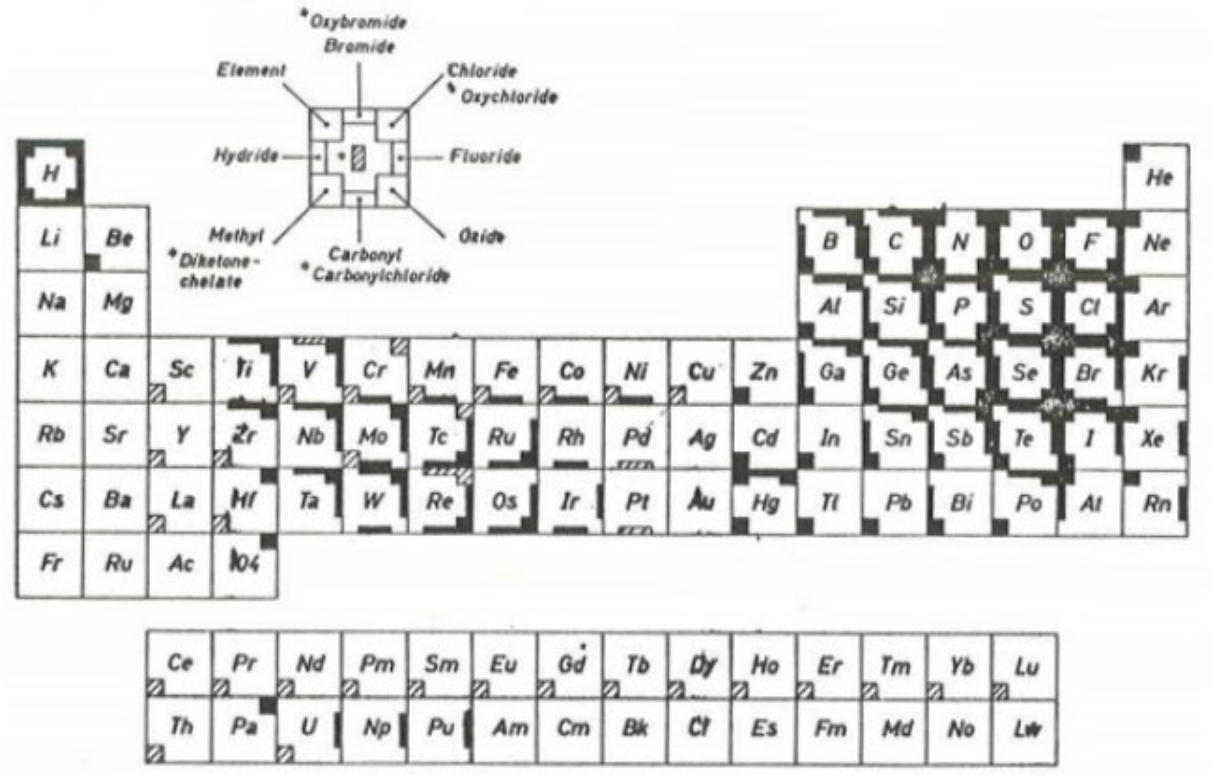

Figure 5.13: *Periodic table with suggestions on how refractory elements can be extracted by formation of molecules* [5.46]

As highlighted in figure 5.13 the release of Scandium could be boosted by the injection of methyl gases such as the gaseous Carbon tetrafluoride (CF_4), thus promoting the formation of the volatile molecule ScF_3, that could be easily ionized and extracted as a beam, as already done at ISOLDE [5.38]. Ongoing developments are being performed to equip the SPES offline Front End with the capability to inject CF_4 within the ion source.

Finally, a very preliminary test for the recovery of stable Scandium was performed, but, because of the low ionization efficiency, too small amounts of Sc were collected, thus hindering the quantification of the collection efficiency. Once the ionization process has been improved, such tests should be repeated.

5.6 References

[5.1] F. Rösch and R. P. Baum, "Generator-based PET radiopharmaceuticals for molecular imaging of tumours: on the way to THERANOSTICS," *Dalt. Trans.*, vol. 40, no. 23, pp. 6104–6111, 2011.

[5.2] A. Singh *et al.*, "Scandium-44 DOTATOC PET/CT: First in-human molecular imaging of neuroendocrine tumors and possible perspectives for Theranostics," *J. Nucl. Med.*, vol. 56, no. supplement 3, pp. 267–267, May 2015.

[5.3] N. P. van der Meulen *et al.*, "Cyclotron production of 44Sc: From bench to bedside," *Nucl. Med. Biol.*, vol. 42, no. 9, pp. 745–751, Sep. 2015.

[5.4] T. S. Carzaniga *et al.*, "Measurement of 43Sc and 44Sc production cross-section with an 18 MeV medical PET cyclotron," *Appl. Radiat. Isot.*, vol. 129, pp. 96–102, Nov. 2017.

[5.5] K. L. Kolsky, V. Joshi, L. F. Mausner, and S. C. Srivastava, "Radiochemical purification of no-carrier-added scandium-47 for radioimmunotherapy," *Appl. Radiat. Isot.*, vol. 49, no. 12, pp. 1541–1549, Dec. 1998.

[5.6] A. Majkowska, M. Neves, I. Antunes, and A. Bilewicz, "Complexes of low energy beta emitters 47Sc and 177Lu with zoledronic acid for bone pain therapy," *Appl. Radiat. Isot.*, vol. 67, no. 1, pp. 11–13, Jan. 2009.

[5.7] S. C. Srivastava, "Paving the Way to Personalized Medicine: Production of Some Promising Theragnostic Radionuclides at Brookhaven National Laboratory," *Semin. Nucl. Med.*, vol. 42, no. 3, pp. 151–163, May 2012.

[5.8] L. F. Mausner, K. L. Kolsky, V. Joshi, and S. C. Srivastava, "Radionuclide development at BNL for nuclear medicine therapy," *Appl. Radiat. Isot.*, vol. 49, no. 4, pp. 285–294, Apr. 1998.

[5.9] C. Müller *et al.*, "Promising Prospects for 44Sc-/47Sc-Based Theragnostics: Application of 47Sc for Radionuclide Tumor Therapy in Mice," *J. Nucl. Med.*, p. jnumed.114.141614, Oct. 2014.

[5.10] M. U. Khandaker *et al.*, "Investigations of the natTi(p,x)43,44m,44g,46,47,48Sc,48V nuclear processes up to 40 MeV," *Appl. Radiat. Isot.*, vol. 67, no. 7–8, pp. 1348–1354, Jul. 2009.

[5.11] M. Yagi and K. Kondo, "Preparation of carrier-free 47Sc by the 48Ti (γ,p) reaction," *Int. J. Appl. Radiat. Isot.*, vol. 28, no. 5, pp. 463–468, May 1977.

[5.12] K. Minegishi, K. Nagatsu, M. Fukada, H. Suzuki, T. Ohya, and M.-R. Zhang, "Production of scandium-43 and -47 from a powdery calcium oxide target via the nat/44Ca(α,x)-channel," *Appl. Radiat. Isot.*, vol. 116, pp. 8–12, Oct. 2016.

[5.13] R. Misiak, R. Walczak, B. W\kas, M. Bartyzel, J. W. Mietelski, and A. Bilewicz, "47Sc

production development by cyclotron irradiation of 48Ca," *J. Radioanal. Nucl. Chem.*, vol. 313, no. 2, pp. 429–434, 2017.

[5.14] A. Monetti *et al.*, "The RIB production target for the SPES project," *Eur. Phys. J. A*, 2015.

[5.15] V. Sabaiduc and others, "BEST 70P Cyclotron Factory Test," in *Proceedings, 6th International Particle Accelerator Conference (IPAC 2015): Richmond, Virginia, USA, May 3-8, 2015*, 2015, p. THPF003.

[5.16] D. Rochman *et al.*, "The TENDL library: Hope, reality and future," *EPJ Web Conf.*, vol. 146, p. 02006, Sep. 2017.

[5.17] N. Otuka *et al.*, "Towards a More Complete and Accurate Experimental Nuclear Reaction Data Library (EXFOR): International Collaboration Between Nuclear Reaction Data Centres (NRDC)," *Nucl. Data Sheets*, vol. 120, pp. 272–276, Jun. 2014.

[5.18] L. A. McVey, R. L. Brodzinski, and T. M. Tanner, "In situ neutron activation analysis of and the neutron capture cross-section for90Sr+," *J. Radioanal. Chem.*, vol. 76, no. 1, pp. 131–137, Mar. 1983.

[5.19] D. Fink *et al.*, "Production of 41Ca and K, Sc and V short-lived isotopes by the irradiation of Ti with 35 to 150 MeV protons: applications to solar cosmic ray studies," *Nucl. Instruments Methods Phys. Res. Sect. B Beam Interact. with Mater. Atoms*, vol. 52, no. 3–4, pp. 601–607, Dec. 1990.

[5.20] P. Kopecky, F. Szelecsényi, T. Molnár, P. Mikecz, and F. Tárkányi, "Excitation functions of (p, xn) reactions on natTi: Monitoring of bombarding proton beams," *Appl. Radiat. Isot.*, vol. 44, no. 4, pp. 687–692, Apr. 1993.

[5.21] K. Zarie, N. Al-Hammad, and A. Azzam, "Experimental study of excitation functions of some proton induced reactions on natTi for beam monitoring purposes," *Radiochimica Acta*, vol. 94. p. 795, 2006.

[5.22] E. Garrido, C. Duchemin, A. Guertin, F. Haddad, N. Michel, and V. Métivier, "New excitation functions for proton induced reactions on natural titanium, nickel and copper up to 70 MeV," *Nucl. Instruments Methods Phys. Res. Sect. B Beam Interact. with Mater. Atoms*, vol. 383, pp. 191–212, Sep. 2016.

[5.23] P. Hoff, O. C. Jonsson, E. Kugler, and H. L. Ravn, "Release of nuclear reaction products from refractory compounds," *Nucl. Instruments Methods Phys. Res.*, vol. 221, no. 2, pp. 313–329, Apr. 1984.

[5.24] J. P. Fernandes Pinto Ramos, "Titanium carbide-carbon porous nanocomposite materials for radioactive ion beam production processing, sintering and isotope release properties," p. 232, 2017.

[5.25] H. Okamoto, "C-Ti (Carbon-Titanium)," *J. Phase Equilibria Diffus.*, vol. 19, no. 1, p. 89, 1998.

[5.26] J. P. Ramos *et al.*, "Target nanomaterials at CERN-ISOLDE: synthesis and release data," *Nucl. Instruments Methods Phys. Res. Sect. B Beam Interact. with Mater. Atoms*, vol. 376, pp. 81–85, Jun. 2016.

[5.27] A. Girotto, "Development of porous refractory targets for nuclear physics and medical applications," Università degli Studi di Padova, 2017.

[5.28] A. Andrighetto, C. M. Antonucci, S. Cevolani, C. Petrovich, and M. Santana Leitner, "Multifoil UCx target for the SPES project --An update," *Eur. Phys. J. A - Hadron. Nucl.*, vol. 30, no. 3, pp. 591–601, 2006.

[5.29] G. Battistoni *et al.*, "Overview of the FLUKA code," *Ann. Nucl. Energy*, 2015.

[5.30] G. Battistoni, F. Cerutti, A. Ferrari, J. Ranft, S. Roesler, and P. R. Sala, "Hadron production simulation by FLUKA," *J. Phys. Conf. Ser.*, vol. 408, no. 1, p. 12051, 2013.

[5.31] J. Allison *et al.*, "Recent developments in Geant4," *Nucl. Instruments Methods Phys. Res. Sect. A Accel. Spectrometers, Detect. Assoc. Equip.*, vol. 835, pp. 186–225, Nov. 2016.

[5.32] A. V Ivantchenko, V. N. Ivanchenko, J.-M. Q. Molina, and S. L. Incerti, "Geant4 hadronic physics for space radiation environment," *Int. J. Radiat. Biol.*, vol. 88, no. 1–2, pp. 171–175, 2012.

[5.33] D. H. Wright and M. H. Kelsey, "The Geant4 Bertini Cascade," *Nucl. Instruments Methods Phys. Res. Sect. A Accel. Spectrometers, Detect. Assoc. Equip.*, vol. 804, pp. 175–188, Dec. 2015.

[5.34] G. Folger, V. N. Ivanchenko, and J. P. Wellisch, "The Binary Cascade," *Eur. Phys. J. A - Hadron. Nucl.*, vol. 21, no. 3, pp. 407–417, 2004.

[5.35] Mancusi, D., Boudard, A., Cugnon, J., David, J.-C., Kaitaniemi, P., and Leray, S., "New C++ version of the Liège intranuclear cascade model in Geant4," *SNA + MC 2013 - Joint International Conference on Supercomputing in Nuclear Applications + Monte Carlo*. p. 5209, 2014.

[5.36] V. Ivanchenko *et al.*, "Recent Improvements in Geant4 Electromagnetic Physics Models and Interfaces," in *3th Monte Carlo Conference MC2010*, 2010, vol. 2, pp. 898–903.

[5.37] L. C. Carraz, I. R. Haldorsen, H. L. Ravn, M. Skarestad, and L. Westgaard, "Fast release of nuclear reaction products from refractory matrices," *Nucl. Instruments Methods*, vol. 148, no. 2, pp. 217–230, Jan. 1978.

[5.38] T. Bjørnstad *et al.*, "Recent development of high-temperature metal targets for ISOLDE," *Nucl. Instruments Methods Phys. Res. Sect. B Beam Interact. with Mater.*

Atoms, vol. 26, no. 1–3, pp. 174–182, May 1987.

[5.39] J. L. Murray, P. K. Liao, and K. E. Spear, "The B−Ti (Boron-Titanium) system," *Bull. Alloy Phase Diagrams*, vol. 7, no. 6, pp. 550–555, 1986.

[5.40] F. Borgna *et al.*, "A preliminary study for the production of high specific activity radionuclides for nuclear medicine obtained with the isotope separation on line technique," *Appl. Radiat. Isot.*, 2017.

[5.41] F. Borgna *et al.*, "Early Evaluation of Copper Radioisotope Production at ISOLPHARM," *Molecules*, vol. 23, no. 10, 2018.

[5.42] D. R. Lide, *CRC Handbook of Chemistry and Physics: A Ready-reference Book of Chemical and Physical Data*. CRC-Press, 1995.

[5.43] A. Andrighetto *et al.*, "Spes: An intense source of Neutron-Rich Radioactive Beams at Legnaro," *J. Phys. Conf. Ser.*, vol. 966, no. 1, 2018.

[5.44] V. N. Fedosseev *et al.*, "ISOLDE RILIS: New beams, new facilities," *Nucl. Instruments Methods Phys. Res. Sect. B Beam Interact. with Mater. Atoms*, vol. 266, no. 19–20, pp. 4378–4382, Oct. 2008.

[5.45] C. Seiffert, "Production of radioactive molecular beams for CERN-ISOLDE," Technische Universität, Darmstadt, 2015.

[5.46] K. Baechmann, "CHEMICAL PROBLEMS OF THE ON-LINE SEPARATION OF SHORT-LIVED NUCLIDES.," *Forschungsbericht K70-28*, vol. BMBK-FB-L7, 1970.

Chapter 6

The Gadolinium based ISOL target for the production of Terbium medical isotopes

"Gewöhnlich wird eine Entdeckung nicht auf den einfachsten, sondern auf einem komplizierten Wege gemacht; die einfachen Fälle zeigen sich erst später"

"Usually, a discovery is not made in the easiest but on a complicated way; the simple cases show up only later"

Otto Hahn (German chemist, 1879 – 1968), *Vom Radiothor zur Uranspaltung. Eine wissenschaftliche Selbstbiographie.*

6.1 Introduction

In recent years, several radiolanthanides have been studied for their potential use in nuclear medicine. Among those, a unique quadruplet of Terbium radionuclides, namely ^{149}Tb, ^{152}Tb, ^{155}Tb and ^{161}Tb were employed for labelling a set of new tumour-targeting radiopharmaceuticals, that were used for a preclinical study, showing promising results [6.1]. In such study, the reported excellent results were obtained with a folate-based targeting agent containing a DOTA chelator for the radiometal complexation.

What makes the aforementioned four radionuclides extremely interesting is the fact that each of the different isotopes has decay properties suitable for one of the three major modalities of nuclear medicine, namely PET, SPECT and Target Radionuclide Therapy, and they belong to the same element, thus they share the same chemical behaviour. According to such

characteristics, thus, it is possible to design appropriate theranostics procedures with Terbium radionuclides.

^{152}Tb ($T_{1/2}$ = 17.5 h) decays with the emission of β^+ particles, with average energy of 1140 keV (20.3% intensity), and co-emission of γ-rays at energies of 271 keV (9.53% intensity), 344 keV (63.5% intensity), 586 keV (9.21% intensity) and 779 keV (5.54% intensity). Such decay properties, together with the absence of co-emission of therapeutic particles, make this nuclide suitable for PET applications, in particular for pre-therapeutic imaging [6.2].

Among the listed Terbium radioisotope ^{155}Tb ($T_{1/2}$ = 5.32 days) is the most suitable for SPECT imaging. It decays indeed by electron capture, thus co-emitting γ-rays with energy 87 keV (32% intensity) and 105 keV (25% intensity), and preclinical tests with human tumours xenografted into mice showed the achievement of high quality, high resolution tomographic images [6.3].

Following the principles of theranostics the same compounds labelled with the aforementioned diagnostic nuclides could be employed with the therapeutic ^{149}Tb and ^{161}Tb.

^{149}Tb ($T_{1/2}$ = 4.12 h) is among the most interesting therapeutic alpha emitting nuclides. It decays by emission of short-range α-particles (Eα = 3.967 MeV), and was recently used for preclinical studies, where it showed remarkable therapeutic potential [6.4].

Finally, ^{161}Tb ($T_{1/2}$ = 6.91 days) is an interesting β^- emitter with average β^- particle energy of 0.15 MeV, and thus very similar to the already used ^{177}Lu ($T_{1/2}$ = 6.65 days, β^- average energy 0.14 MeV) [6.5]. In addition, such nuclide emits a few photons of 75-keV energy (10% intensity), that can be used for gamma camera imaging thus performing the follow-up of the therapy. Furthermore, to one beta particle per decay, 2.24 Auger and conversion electrons are also emitted on average with energies mostly up to 50 keV (some electrons up to 300 keV are also emitted but with ~2% intensity). In particular, such particles contribute to 27% of the beta energy but provide much higher local dose density due to their shorter range in tissue (0.5–30 μm) [6.5]. With this yield of conversion and Auger electrons, ^{161}Tb is comparable to radionuclides such as ^{67}Ga and ^{111}In [6.6].

Concerning ^{149}Tb and ^{161}Tb, recent studies suggest the possibility that cocktails of these two isotopes might optimize the efficacy of the treatment, but a further systematic investigation is required [6.7].

Provided that the presented Terbium radioisotopes are extremely promising, their large scale production is still a challenging issue. Indeed, with the exception of ^{161}Tb, medical Tb radionuclides are not yet generally available at radionuclidic purity suitable for medical use with conventional production techniques.

Concerning ^{161}Tb, it can be produced in non-carrier-added form by neutron irradiation of highly enriched ^{160}Gd targets in the quantity and quality required for the preparation of ^{161}Tb-labeled

therapeutic agents.[6.5] Such production routine foresees its accumulation in the target from the β^- decay of the short-lived intermediate ^{161}Gd ($T_{1/2}$ = 3.66 min) via the ^{160}Gd(n,γ)^{161}Gd→^{161}Tb nuclear reaction and its subsequent chemical separation from the target material.

On the other hand, for the other medical Terbium radionuclides, several studies are ongoing investigating various possible nuclear reactions, mostly using accelerator-based techniques.

In example, an early study demonstrated the photonuclear production of ^{155}Tb via the reaction ^{156}Dy(γ,n)^{155}Dy→^{155}Tb, using bremsstrahlung radiation with energy up to 25 MeV at an electron accelerator [6.8]. Although a very high radionuclidic purity could be obtained (> 99.9%), the corresponding yields were relatively small, due to the limited intensity of the electron beam.

Other studies explored the use of ^{12}C beams for the production of ^{149}Tb and ^{152}Tb. In particular the reactions ^{nat}Nd(^{12}C,xn)^{152}Dy→^{152}Tb [6.9] and ^{nat}Nd(^{12}C,xn)^{149}Dy→^{149}Tb [6.10] were considered, leading to the production of relevant yields but with the non-negligible drawback of the unavoidable formation of other Tb isotopes that decrease significantly the achievable specific activity.

Other studies considered several other reactions, with the aim to evaluate the feasibility of the production of Terbium medically relevant nuclides using a cyclotron. In example, production cross sections for the direct formation of ^{149}Tb, ^{152}Tb ,^{155}Tb in a ^{nat}Gd target impinged by protons with energy up to 66 MeV were measured. Such energy is indeed coherent with the availability of the new generation of commercial 70 MeV cyclotrons, which can also deliver beams of high intensity (several hundred μA) [6.11]. However, both the existence of seven stable Gd isotopes, that leads to the opening of many reaction channels, and the fact that a relatively large number of Tb radionuclides close to the desires ones have half-lives of several hours to a few days, compromise the achievable radionuclidic purity. In addition, ^{149}Tb is quite far from the stability valley of the nuclide chart, thus the energy required to produce it has to be high enough, activating consequently many reaction channels that lead to the formation of various Tb isotopes with higher mass number.

Other studies evaluated the possibility to irradiate with protons isotopically enriched Gadolinium targets, such as ^{152}Gd and ^{155}Gd, and the cross sections for the reactions ^{152}Gd(p,4n)^{149}Tb and ^{155}Gd(p,4n)^{152}Tb were measured, showing interesting yields, but again the side production of other Tb radionuclides affects significantly the radionuclidic purity [6.7]. In addition, the indirect formation of ^{155}Tb via the decay of its precursor ^{155}Dy ($T_{1/2}$ = 9.9 h) in proton irradiated natural Terbium (^{159}Tb) target was evaluated. As a general result of such

studies, even if high Tb yields were reached, the achieved radionuclidic purity was generally not acceptable.

In addition to the conventional approaches, non-carrier-added Terbium radionuclides were successfully collected at the ISOLDE facility at CERN, where they were produced in proton-induced spallation reactions on a Tantalum target [6.2, 6.9, 6.12]. Indeed, the use of electromagnetic isotope separation, as foreseen by the ISOL technique, ensure a radionuclidic purity close to the maximum value. Since the production performed at ISOLDE ensured the most promising results, a dedicated facility for medical isotope production was built at CERN, namely MEDICIS [6.13]. Anyway the drawback is that the achievements of such facility are difficult to replicate elsewhere since only few research centers have the availability of GeV proton beams.

As a consequence, provided that it was demonstrated that the ISOL technique is the most suitable option for the production of ^{149}Tb, ^{152}Tb and ^{155}Tb, ISOLPHARM could have the capability to expand the availability of such radionuclides, once running. Furthermore, since the proton beam driver at SPES-ISOLPHARM is a commercial 70 MeV cyclotron [6.14], once a suitable production target is identified, the ISOLPHARM facility could be replicated more easily.

The following chapter summarizes the feasibility study performed in order to identify a suitable target for the production of ^{149}Tb, ^{152}Tb and ^{155}Tb at ISOLPHARM.

6.2 Gadolinium-based possible ISOL target materials

As highlighted in the previously presented studies, the production of ^{149}Tb, ^{152}Tb and ^{155}Tb according to the conventional techniques is extremely difficult, and only the ISOL based method adopted at CERN-ISOLDE proved to be reasonably efficient in terms of both achievable amounts and radionuclidic purity [6.7]. Thus, since also the ISOLPHARM method foresees the employment of the SPES ISOL technologies, comparable production of Terbium radionuclides could potentially be achieved, if a suitable production target material is identified. Indeed, both the maximum primary beam energy available at SPES is far below the GeVs protons available at CERN, and Terbium nuclides are not in the production spectrum of the SPES UC_x target [6.15]. As a consequence, neither the Tantalum spallation target proposed at MEDICIS [6.16], nor the SPES UC_x target are suitable, therefore a non-fissile target material including stable nuclei close to the desired products should be considered.

According to recent studies, aimed to evaluate the feasibility of the production of radioactive Terbium medical nuclides, Gadolinium targets proved to be capable of high production rates of

^{149}Tb, ^{152}Tb and ^{155}Tb with proton energies in the range of 35-70 MeV, thus the same available at SPES [6.14]. In addition, TENDL-2017 [6.17] and EXFOR [6.18] databases were consulted to verify the feasibility of the simultaneous production of Terbium medical nuclides from a Gd target, and identify the most desirable energy range according to the nuclear cross section trends. Figures 6.1, 6.2 and 6.3 summarize the data found concerning the reactions ^{nat}Gd(p,xn)^{149}Tb, ^{nat}Gd(p,xn)^{152}Tb and ^{nat}Gd(p,xn)^{155}Tb [6.19, 6.20].

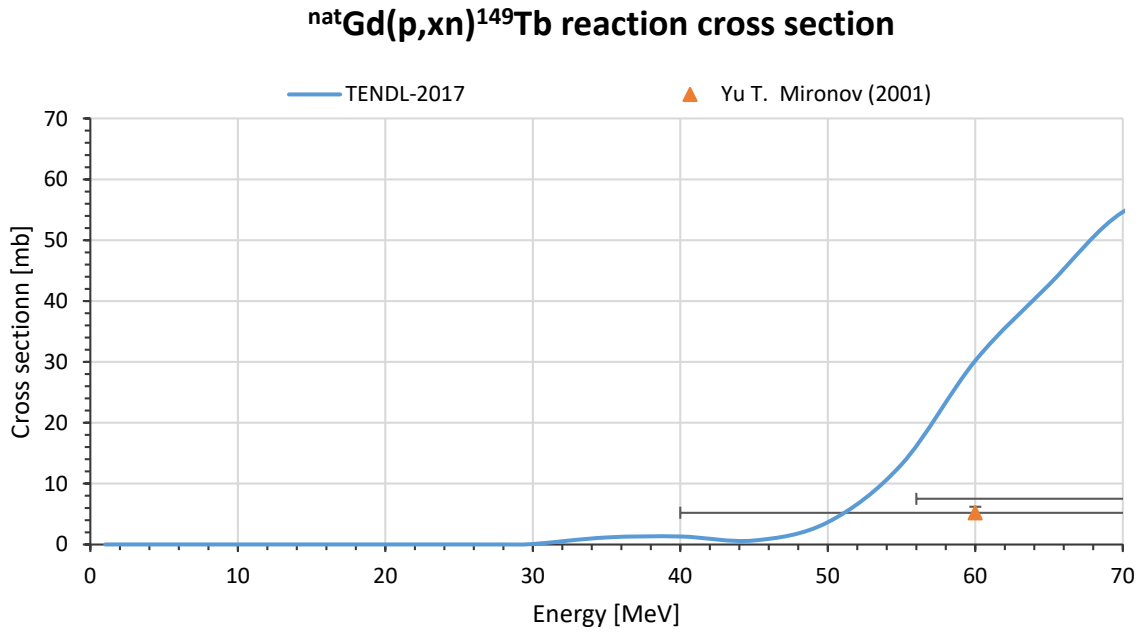

Figure 6.1: *cross section data for the ^{nat}Gd(p,xn)^{149}Tb reaction taken form TENDL-2017* [6.17] *and from experimental studies included in EXFOR* [6.19]

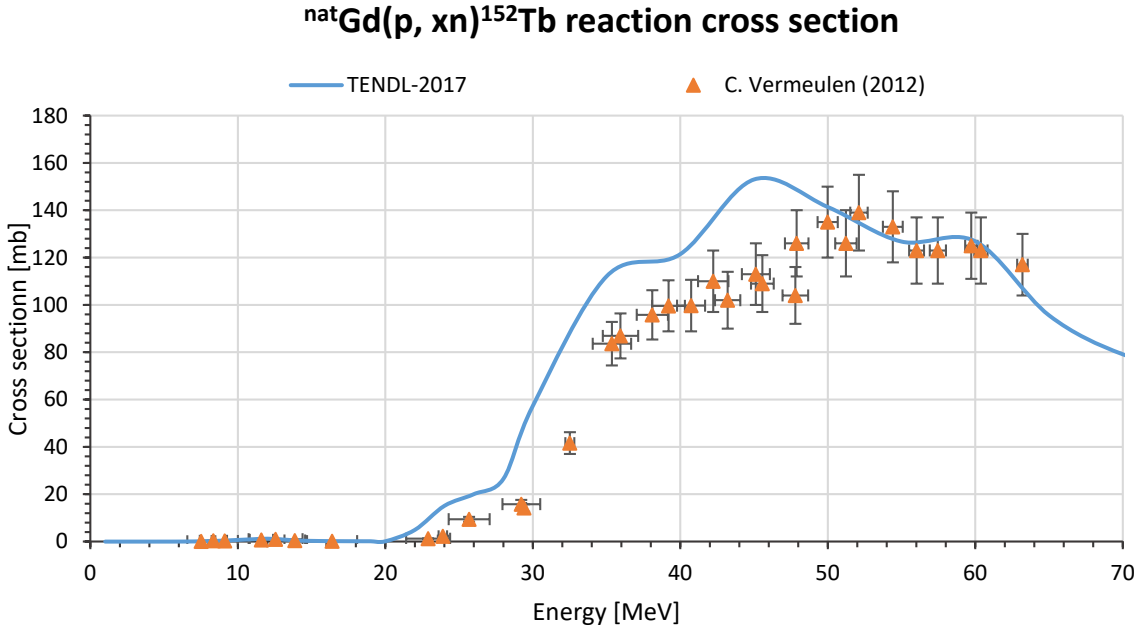

Figure 6.2: *cross section data for the ^{nat}Gd(p,xn)^{152}Tb reaction taken form TENDL-2017* [6.17] *and from experimental studies included in EXFOR* [6.20]

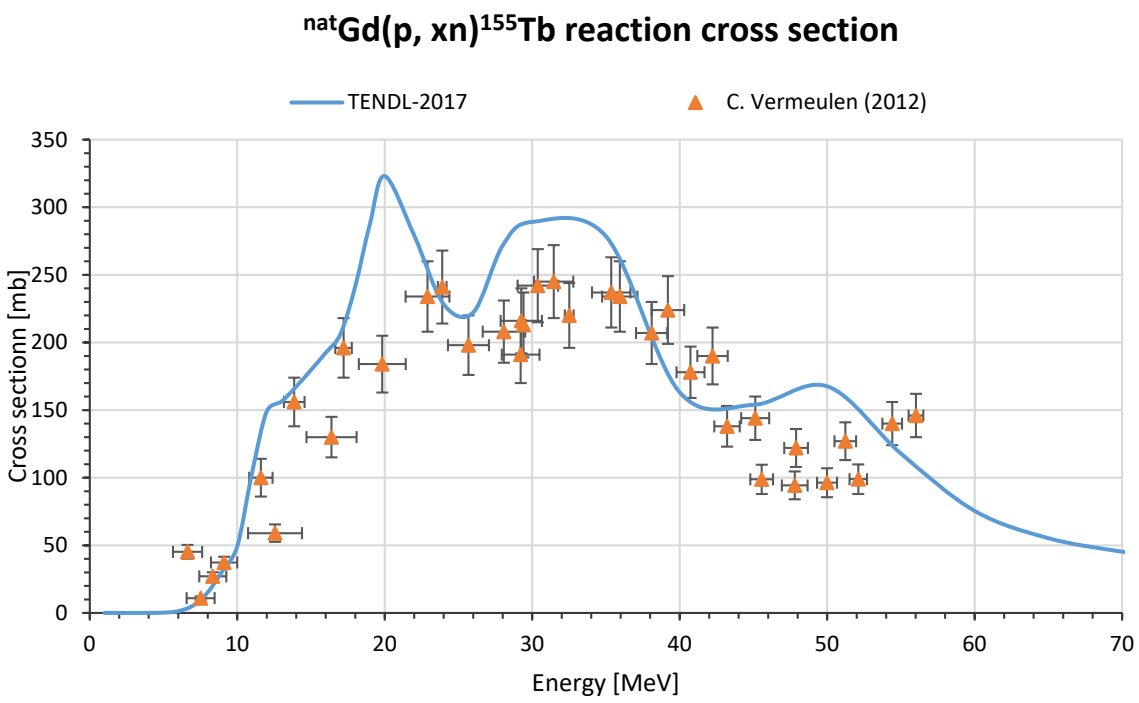

Figure 6.3: *cross section data for the $^{nat}Gd(p,xn)^{155}Tb$ reaction taken form TENDL-2017* [6.17] *and from experimental studies included in EXFOR* [6.20]

Concerning the data published in TENDL-2017 [6.17], the plotted trends were obtained from the weighted average of the single contributes, reported in the database for each of the seven stable isotopes of Gadolinium, that are ^{152}Gd (nat. abundance 0.20%), ^{154}Gd (nat. abundance 2.18%), ^{155}Gd (nat. abundance 14.80%), ^{156}Gd (nat. abundance 20.47%), ^{157}Gd (nat. abundance 15.65%), ^{158}Gd (nat. abundance 24.84%) and ^{160}Gd (nat. abundance 21.86%), using as weight the respective natural abundances.

According to the presented plots, whereas the cross sections of the nuclear reactions generating ^{152}Tb and ^{155}Tb are high even at energies around 30-40 MeV, the production of ^{149}Tb could be reasonable only if the incident protons have high energy, close to 70 MeV.

Concerning the material, Gadolinium cannot be used as ISOL target material as a pure metal, because of its low melting point, at 1312°C. Thus, a refractory Gd-based compound has to be identified.

Although little information was found about Gadolinium refractory binary compounds, such element belongs to the so-called “Rare Earths” metals, that share similar properties [6.21].

As found in the literature, many binary or ternary compounds involving a Rare Earth metal are possible [6.22], and Borides [6.23] and Carbides [6.24] are among the most refractory, thus suitable for the application as ISOL target material.

6.2.1 Gadolinium Carbide as target material

Since its early operation, the ISOLDE facility at CERN, operated successfully irradiating porous Carbides pellets as a target [6.25]. The results were promising, and showed that the release of many elements was rapid, with release half-times (i.e. 50% released) of about 1 min for the most volatile elements at temperatures as low as 1600°C. Furthermore, on-line tests at higher temperatures revealed release half-times of some seconds.

In addition, the use of Rare Earth carbides as target material for ISOL applications is not new. Indeed, other lanthanide carbides were already developed, such as the lanthanum carbide [6.26, 6.27], and the preparation method of several other compounds was developed at the IRIS facility, in St. Petersburg Nuclear Physics Institute in Russia [6.28]. In the latter study, in particular, also the preparation method of Gadolinium Carbide was presented, highlighting also that, as most Rare Earths binary compounds, it is composed of two phases, the effective GdC_2 and graphite, thus it is normally indicated as GdC_x.

Gadolinium carbide, GdC_2, is a tetragonal material with less than 5% of Gd_2C_3. It's a material which decomposes by presence of water and in some gas as methane 63,30%, acetylene 12,65%, ethylene 8,40% and hydrogen 6,90% (in volume percentage). It can also turn into Gd_2O_3 in air atmosphere by oxidation [6.29].

At LNL-INFN, first samples of GdC_x (figure 6.4) were synthetized exploiting the reaction:

$$Gd_2O_3 + 11C \rightarrow 2GdC_2 + 4C + 3CO \tag{6.1}$$

Such reaction was performed in a vacuum furnace following similar procedures to those developed for UC_x and LaC_x. In particular, the preparation steps were:

- Mixing of the precursors powders by means either of a planetary ball mill or of an agate mortar. The addition of a small quantity of a phenolic resin binder, usually 2% wt., is foreseen in order to prevent the damaging or the loss of powder of the green pellets during handling.
- Uniaxial cold pressing of the mixed powders into pellets, using a hydraulic press with a specifically designed die
- After extraction of the pressed pellet from the die, its thermal treatment is carried out in a high vacuum furnace developed to reach very high temperatures (~ 1800°C).

After synthesis, the samples were extracted from the furnace, and analysed. In particular, it was possible to notice that the GdC_x samples suffered of high corrosion rates in air, since the presence of Oxygen and humidity in atmospheric air caused the formation of Gadolinium oxide. Thus, the produced samples had to be kept in inert atmosphere.

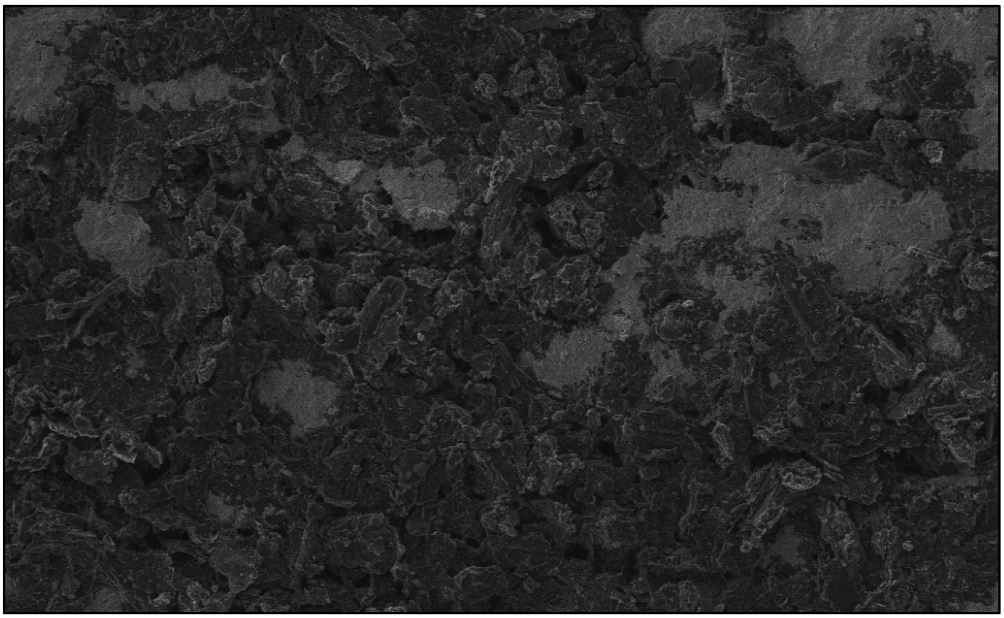

Figure 6.4: *SEM images of GdC_x sample obtained at LNL. The different grayscale allows to notice the presence of two phases, GdC_2 and C.*

6.2.2 Gadolinium Boride as target material

Provided that GdC_x handling in atmospheric air may be problematic for the fast corrosion of the target material, other gadolinium-based compounds were considered. Among those, Gadolinium Boride (GdB_4) resulted as the most promising as ISOL target, thanks to its refractoriness and well established synthesis procedure [6.30].

Thus, it was possible to purchase commercially available GdB_4 powder (Sigma Aldrich®) and test the feasibility of the sintering of samples. The first GdB_4 disks were consequently created (figure 6.5), following the same procedure presented for GdC_x. Since its major chemical stability was verified, Gadolinium boride was consequently chosen as ISOL target material.

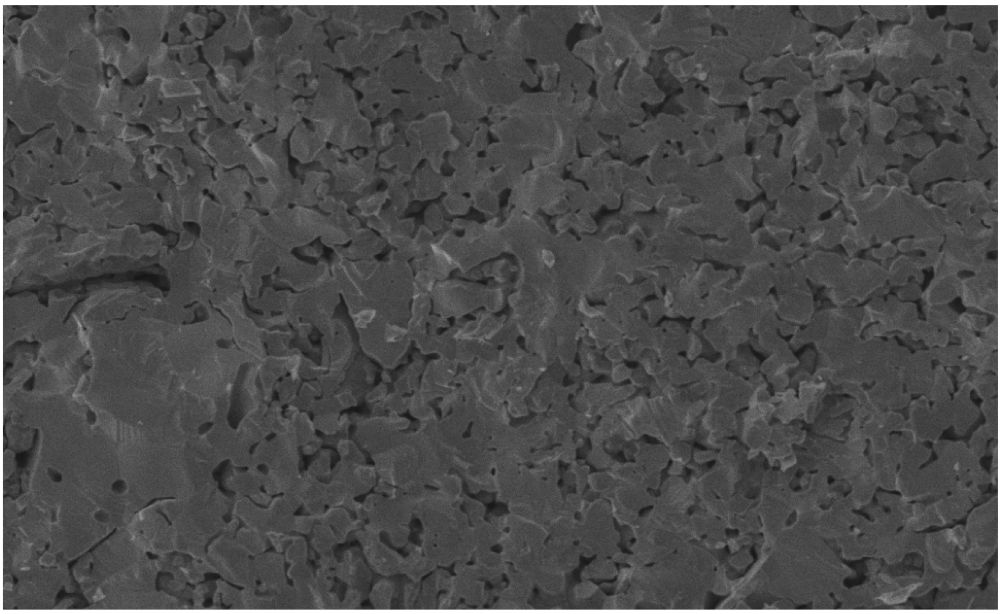

Figure 6.5: *SEM images of GdB_4 sample obtained at LNL.*

6.2.3 Yields from a GdB_4 target

After the identification of a suitable ISOL target material, the next step was to estimate the expected in-target yields from GdB_4 of the desired nuclides (figure 6.6).

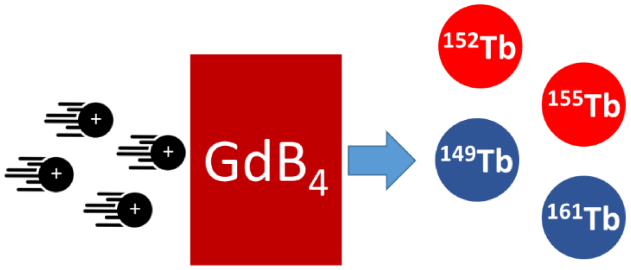

***Figure 6.6**: possible medical radionuclides from the GdB_4 target*

The analysis of the cross sections for the reactions involved, in figures 6.1, 6.2 and 6.3, highlighted the necessity to employ high proton energies, if the production of reasonable amounts of ^{149}Tb is searched. Thus, of 70 MeV energy and 100 μA intensity was considered for the estimations of the effective in-target yields a proton beam, and also for the GdB_4 target a multi-foil target architecture is proposed [6.31].

Also in this case, the preliminary investigations of the expected in-target yields of the desired Terbium nuclides were performed with the Monte Carlo code FLUKA [6.32] (version 2011.2x.2). Concerning the simulation settings, the same simplifications adopted for Zirconium Germanide and Titanium Carbide targets were used, thus a simplified 4 cm diameter cylindrical target with material density of 4 g/cm^{3}was considered, and a 70 MeV 100 μA (6.242E+14 p/s) proton beam was simulated. Figure 6.7 summarizes the so-calculated yields.

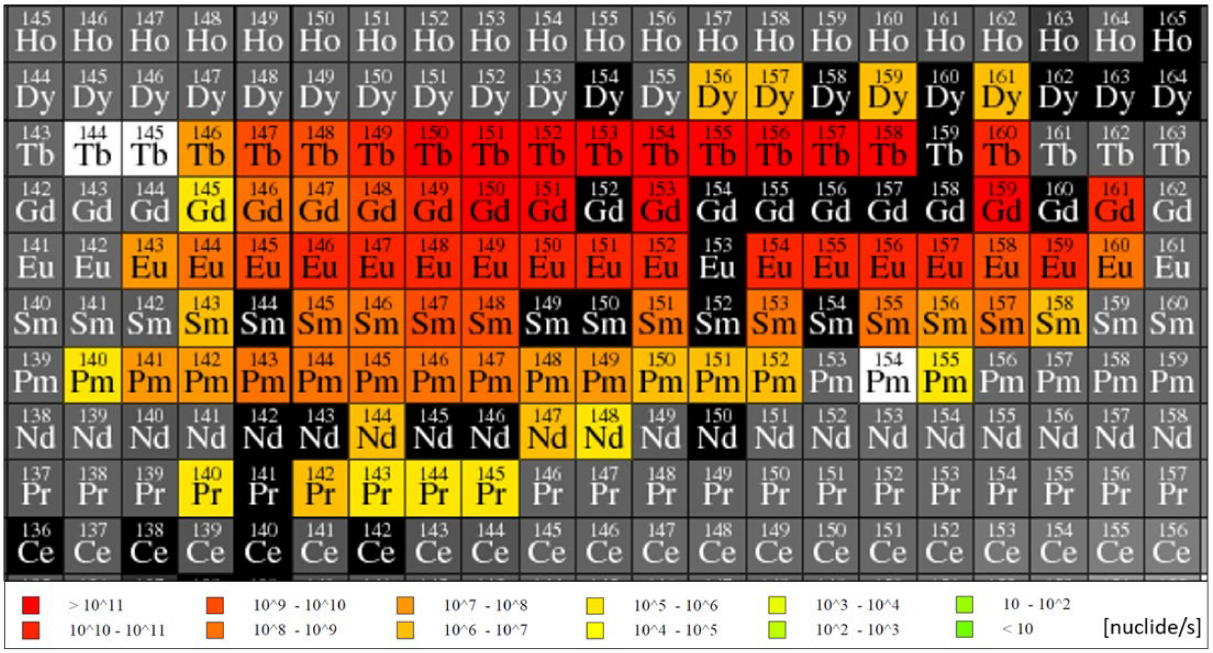

***Figure 6.7**: the relevant part of the estimated in-target yields according to FLUKA*

As shown in figure 6.7, the expected nuclide production ranges from Praseodymium to Dysprosium if stable Gadolinium is used as target nucleus, whereas the products generated by the interaction of protons with Boron, not displayed in figure 6.7, vary from Helium to Carbon. The excitation functions considered by FLUKA are based on its typical models, namely the PEANUT nuclear interaction model [6.33]. For the sake of increasing the reliability of the FLUKA results, other simulations were launched considering different models for the calculation of the excitation functions. For such additional studies, the Monte Carlo toolkit Geant4 (version 4.10.04.p02) [6.34] was used, and different Physics Lists, that correspond to different nuclear interaction models, were considered.

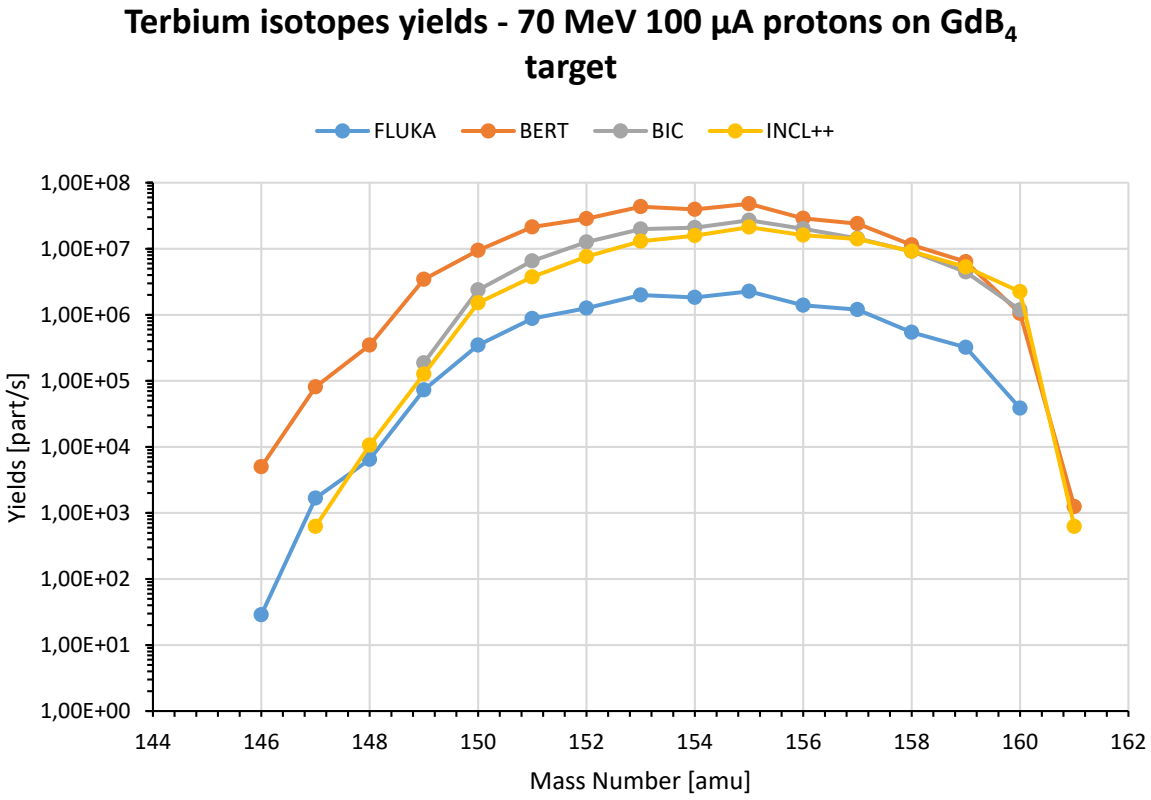

Figure 6.8: *terbium isotopes yields according to different models for a 70 MeV 100 µA proton beam on a GdB_4 target*

The comparison between the various nuclear models used in the simulations for the production of Terbium isotopes is summarized in figure 6.8.

In addition to the FLUKA-PEANUT results, as in the case of the feasibility studies for Copper and Scandium, the additional nuclear interaction models considered implemented with Geant4 were the Bertini cascade model [6.35, 6.36], the Binary Cascade model (BIC) [6.35, 6.37] and the Liège intranuclear cascade model (INCL++) [6.38].

Thus, in Geant4, the activated Physics Lists were FTFP_BERT, QGSP_BIC and QGSP_INCLXX for respectively the Bertini cascade, the BIC model, and INCL++ cascade.

Additionally, the reliability of the results at low energies was increased by activating the electromagnetic option EMZ [6.39].

As a general consideration, the set of results produced by the various models shows, in some cases, orders of magnitude of difference, in other cases a very good accordance. For example, in the case of the ^{149}Tb, most models provide as result a yield of 1E+05 particles/s, whereas, in the case of ^{152}Tb according to the Bertini cascade model approximately 2.9E+07 particles/s are produced, the BIC and INCL++ models indicate a production of approximately 1E+07 particles/s and finally FLUKA suggests the generation of 1.26E+06 particles/s. It is possible also to highlight also that the differences between the models increases at higher mass numbers. In addition, BERT and INCL++ reasonably indicate also the generation of ^{161}Tb, not indicated by the other models. Indeed, such isotope may be generated by the presence of ^{160}Gd (natural abundance 21.86%) by the reaction ^{160}Gd(p,γ)^{161}Tb, but, according to TENDL-2017 [6.17], the cross section is extremely low in the considered proton energy range, thus the ^{161}Tb production is extremely low (figure 6.9).

Anyway, for the subsequent preliminary evaluation of the in-target produced activities, the FLUKA results were taken into account, because the comparison highlighted it as the most conservative model.

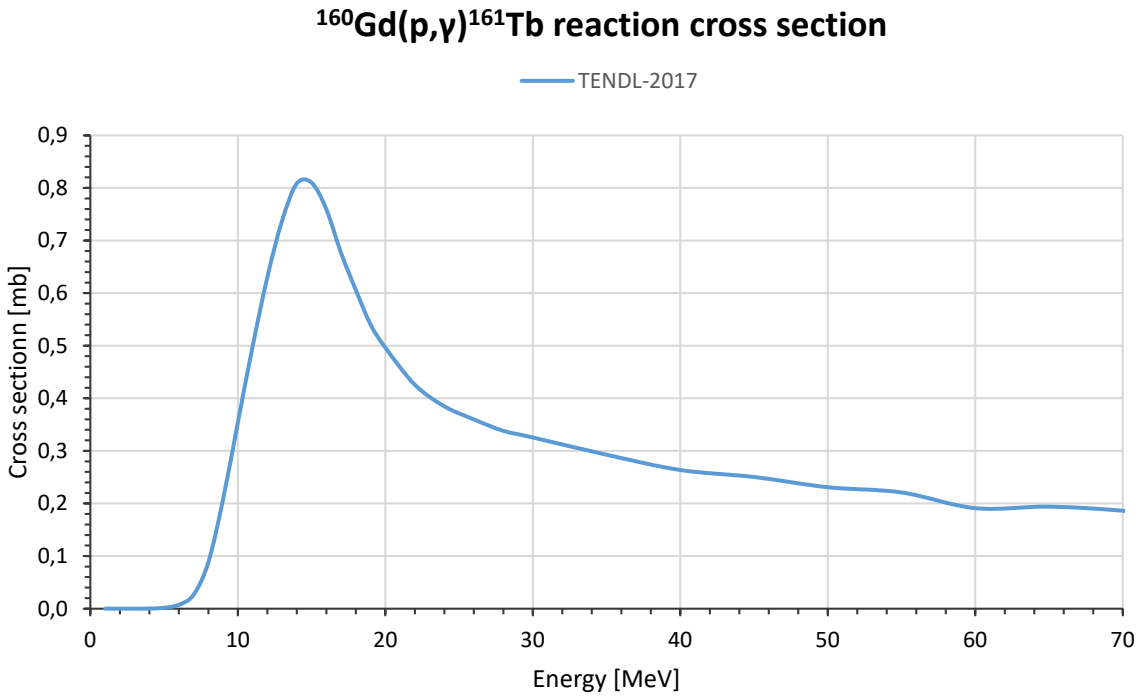

Figure 6.9: *cross section data for the ^{160}Gd(p,γ)^{161}Tb reaction taken form TENDL-2017* [6.17]

6.2.4 Expected in-target production of ^{149}Tb, ^{152}Tb, ^{155}Tb and ^{161}Tb

Since the MC code FLUKA was taken as for the further evaluations of the presented feasibility study, it was also used to simulate the in-target produced activities at different irradiation times, as done also in the case of Copper and Scandium. Differently from the yields calculations, for the performance of such simulations, the radioactive decays were activated, and timepoints of 0.5, 1, 2, 3, 4, 5 and 6 days were considered, in accordance with the maximum expected irradiation time for the SPES targets, namely 15 days. A primary proton beam of 70 MeV energy and 100 μA intensity was considered, similarly to the yields simulations.

Table 6.1 summarizes the calculated activities for the relevant Terbium radioisotopes, ^{149}Tb, ^{152}Tb, ^{155}Tb and ^{161}Tb; showing promising results. In fact, for ^{149}Tb the expected produced activity after 5 days of irradiation was 36.5 GBq, for ^{152}Tb it was 1.12 TBq while for ^{155}Tb it was 1.09 TBq. Concerning ^{161}Tb, FLUKA simulations highlighted the generation of 6.86 GBq within 5 days of proton irradiation. Since such nuclide was not reported among the yield spectrum in figure 6.7, such high produced activity may be due to the decay of eventual parents (such as ^{161}Gd, present in figure 6.7). Anyway, ^{161}Tb is not regarded as one of the primary aim of such feasibility study since conventional production routines provide sufficient amounts of the aforementioned nuclide.

Table 6.1: *the expected in-target activity for ^{149}Tb, ^{152}Tb, ^{155}Tb and ^{161}Tb at different irradiation timepoints*

GdB_4 target (100 μA 70 MeV PPB)												
	^{149}Tb prodcution ($t_{1/2}$: 4.12 h)			^{152}Tb prodcution ($t_{1/2}$: 17.5)			^{155}Tb prodcution ($t_{1/2}$: 5.32 d)			^{161}Tb prodcution ($t_{1/2}$: 6.91d)		
Time	Activity		Nuclei	Activity		Nuclei	Activity		Nuclei	Activity		Nuclei
[days]	[Bq]	[Ci]	[#]	[Bq]	[Ci]	[#]	[Bq]	[Ci]	[#]	[Bq]	[Ci]	[#]
0.5	3.16E+10	0.85	6.76E+14	4.26E+11	11.51	3.87E+16	1.43E+11	3.86	9.48E+16	8.46E+08	0.02	7.26E+14
1	3.58E+10	0.97	7.67E+14	6.92E+11	18.70	6.29E+16	2.77E+11	7.49	1.84E+17	1.66E+09	0.04	1.42E+15
1.5	3.64E+10	0.98	7.79E+14	8.57E+11	23.17	7.79E+16	4.02E+11	10.88	2.67E+17	2.43E+09	0.07	2.08E+15
2	3.65E+10	0.99	7.80E+14	9.60E+11	25.95	8.73E+16	5.20E+11	14.06	3.45E+17	3.16E+09	0.09	2.71E+15
3	3.65E+10	0.99	7.81E+14	1.06E+12	28.75	9.67E+16	7.33E+11	19.82	4.86E+17	4.52E+09	0.12	3.88E+15
4	3.65E+10	0.99	7.81E+14	1.10E+12	29.83	1.00E+17	9.21E+11	24.89	6.11E+17	5.75E+09	0.16	4.93E+15
5	3.65E+10	0.99	7.81E+14	1.12E+12	30.25	1.02E+17	1.09E+12	29.33	7.20E+17	6.86E+09	0.19	5.89E+15
6	3.65E+10	0.99	7.81E+14	1.13E+12	30.41	1.02E+17	1.23E+12	33.24	8.15E+17	7.86E+09	0.21	6.75E+15

6.3 Early offline ionization tests of stable Terbium

After then identification of a suitable ISOL target material and the evaluation of the expected in-target yields and produced activities, the feasibility study for the production of Terbium radionuclides according to the ISOLPHARM method foresees the subsequent investigation of the ionization, extraction and mass separation of the Tb isotopes with the SPES technologies. Indeed, even if the in-target production of Terbium nuclides is extremely high, the amount of radioisotopes available for the subsequent radiochemistry studies can be significantly lower,

because a fraction of the produced nuclei is lost in the ionization process. Thus, the ionization efficiency has to be carefully evaluated with dedicated tests. As previously done in the cases of Strontium, Yttrium, Iodine, Silver, Copper and Scandium [6.40, 6.41], such tests were performed with the SPES Front End prototype in offline modality, meaning that the stable counterparts of the desired elements were ionized. In fact, since the ionization process involves only chemical properties of the wanted nuclides, the use of stable isotopes of Terbium (^{161}Tb, natural abundance 100%) does not affect the reliability of results for their radioactive counterparts.

The experimental apparatus used for the ionization tests, already widely described in the previous chapters, is the offline prototype of the SPES Front End. Such apparatus includes six main subassemblies, that are: the Target - Ion Source (TIS) unit, the first beam optics subsystem, including four steers, the first triplets, and the first diagnostic box, the Wien filter (WF), namely the electromagnetic mass separator, the second diagnostic box including the slits, the second beam optic subsystem, namely the second triplets and the secondary target station for the collection of the beam. The pressure levels within the beamline normally range between 10^{-5} and 10^{-6} mbar.

Since Terbium first ionization energy is 5.86 eV [6.42], the SPES Plasma Ions Source (PIS) can be employed, which is capable to ionize a wide set of elements, also the most electronegative [6.43], but also the SPES SIS could potentially be used, since it ionized successfully Strontium [44], whose ionization energy is 5.69 eV [6.42].

For the first tests, however, the SPES PIS was used. Thus, the following parameters were used for the performance of the experiments:

- The ion source and transfer line were heated by Joule effect with a current intensity of 415 A, thus reaching a temperature level generally above 2000°C
- The extraction electrode was positioned at 50% of its maximum stroke, and potential drop of 25 kV was applied between the latter and the TIS unit
- Concerning the first beam optics subassembly, the deflectors S1, S2, S3 and S4 were set at respectively 50 V, 320 V, 10 V and 100 V, whereas the three quadrupoles Q1, Q2 and Q3 forming the first triplet were set respectively at 914, 759 and 1521 V.
- The Wien Filter settings were studied in order to allow the selection of only ^{161}Tb, the only stable isotope of Scandium. A constant electric field of 74.96 kV/m was set into the WF by means of two couple of electrodes, respectively at 343 V (pre-electrodes) and 1874 V (electrodes). The magnetic field was adjusted by means of the WF coil current, set at 129.5 A, in order that only mass 161 atoms are not diverted.
- The slits were left open.

- The second Faraday Cup (FC2) was left into the beam line, in order to measure constantly the beam current.
- The subsequent triplets were left off, since the beam was dumped onto the second Faraday cup.

Concerning the introduction of Terbium in the TIS unit, several methods were considered, as in the case of Scandium.

As first attempt, the Mass Marker (MM) technique was used [6.44], as in the case of Silver and Copper [6.41]: it consisted in the deposition of 40 μL of Terbium standard solution for AAS ($Tb(NO_3)_3$ 1 g/L, Fluka Analytics) on a thin tantalum foil, namely the Mass Marker (MM), lately accurately folded and inserted inside a small tubular oven. The stepwise heating of the oven by Joule effect should allow the atomization of the previously deposed $Tb(NO_3)_3$ substrate, and the migration of the released neutrals towards the ion source through the transfer line.

Using the presented MM method, extremely low Tb ion current (<1 nA) was reported even increasing oven heating current intensity to its maximum value (80 A) corresponding to more than 2000°C at the MM location. Such result suggested that very few Terbium nuclei were reaching the ion source for the eventual presence of cold-spots along the path leading to the source. In presence of such cold-spots Terbium might indeed might stick, being a high boiling point element (3123°C in atmosphere). Thus, as in the case of Yttrium and Scandium, that showed similar behaviours, the second attempt was the direct insertion of the MM within the transfer line, without the use of the oven system. In such way, as already discussed in chapter 4, the heating of the sample is not decoupled by the temperature increase of the source, and part of the loaded nuclei may escape prior that the ion source is ready to operate efficiently, however, because of the refractoriness of Terbium, such amount is expected to be negligible, and the reliable estimation of its ionization efficiency should still, be possible.

Also adopting the second solution the recorded Tb beam current was extremely low (<2 nA), but, otherwise than the case of the employment of the oven, it was possible to recover the Ta sample after the test. Consequently, by inspecting the heated sample, a whitish stain was found in place of the $Tb(NO_3)_3$ deposition, implying the occurrence of chemical reactions within the MM, causing the formation of the non-volatile Terbium Oxide (Tb_2O_3).

Thus, in order to avoid such issue, the MM sample was loaded in an Oxygen-free chemical form, namely Terbium Chloride ($TbCl_3$). The sample loaded with 40 μL of $TbCl_3$ aqueous solution (1 g/L) was again placed directly in the transfer line, but also in such case a very low mass 161 ion current was detected (~2 nA).

Provided that the transfer line of the SPES PIS prototype employed for such tests (figure 6.10a) was not optimized in order to ensure a uniform temperature distribution along its length, it was speculated that such low current was caused by the presence of cold-spots within the PIS assembly, where Tb atoms may stick. Thus, being Tb ionization possible also with the SPES SIS (figure 6.10b), the further tests were performed with the latter technology. Indeed, the SIS available for the offline tests is provided with a thermally optimized transfer line.

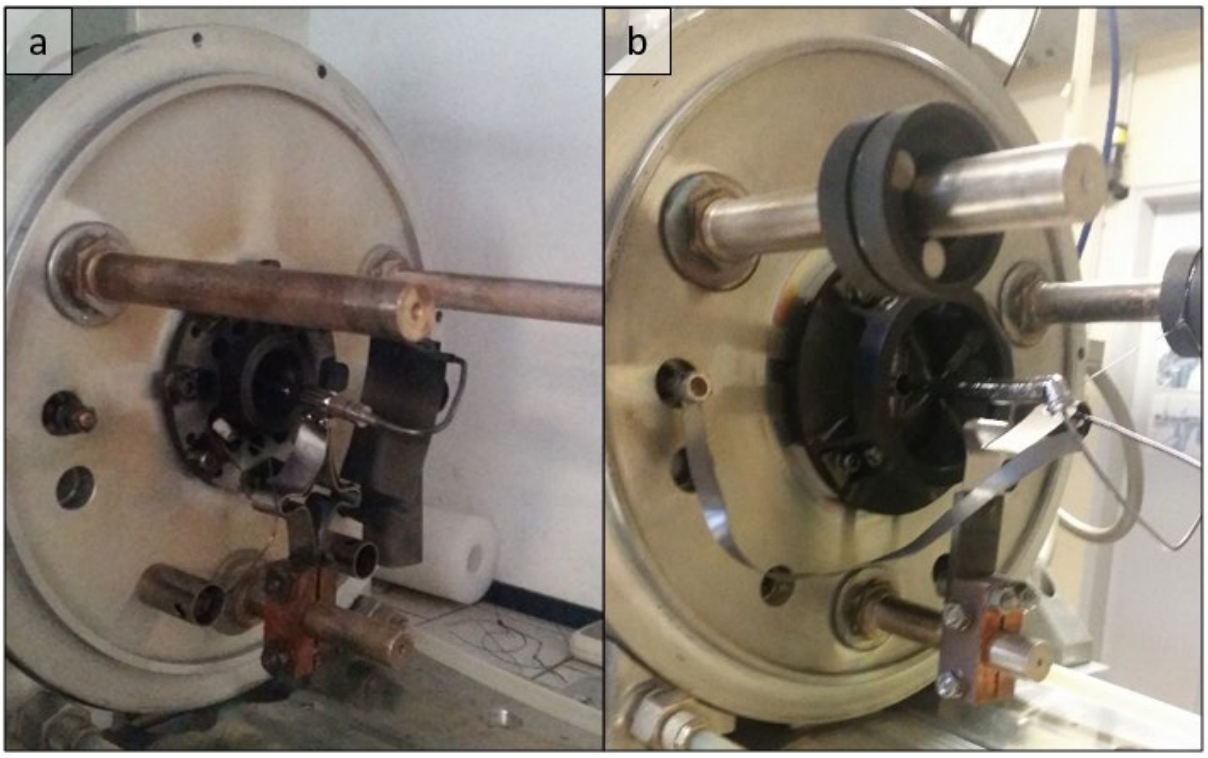

Figure 6.10: *the two ion sources used for the Tb ionization tests, namely the SPES-PIS (a) and the SPES-SIS (b). It is possible to notice the different transfer line design*

As a consequence, one the SIS was coupled to the SPES offline Front End, a Ta MM loaded with 40 μL of $TbCl_3$ was inserted in its transfer line, and the source was heated with current intensities up to 350 A [6.45], corresponding to a temperature level 2100°C at the MM location. Finally, a relatively intense mass 161 current was reported (10 nA), and the beam composition was analysed by means of a Mass Scan (figure 6.11).

Terbium was clearly identified thanks to the presence of a peak at mass 161, but also an unexpected peak of comparable order of magnitude was reported at mass 177. Such peak is compatible with the incomplete oxide TbO, thus suggesting that the release of terbium might be again hindered by the presence of Oxygen within the ion source.

Analysing the previously performed tests with the PIS, indeed it was possible to notice the presence of Tantalum Oxide (in its incomplete form TaO, because Ta_2O_3 is out of range of the Mass Scan) within the beam composition. Such oxide may be originated by the self-oxidation of tantalum at low temperatures [6.46], since the Ta samples for the MM were kept in air prior

their utilization. Consequently, during heating, the Tantalum Oxide layer might have acted as Oxygen donor for the formation of the non-volatile Terbium Oxide, thus hindering the release of the loaded Tb atoms.

Since such Tantalum Oxide layer can be eliminated if the Ta MM sample are conditioned at high temperatures, the next tests will be performed either with conditioned foils or with different material as loaded substrates.

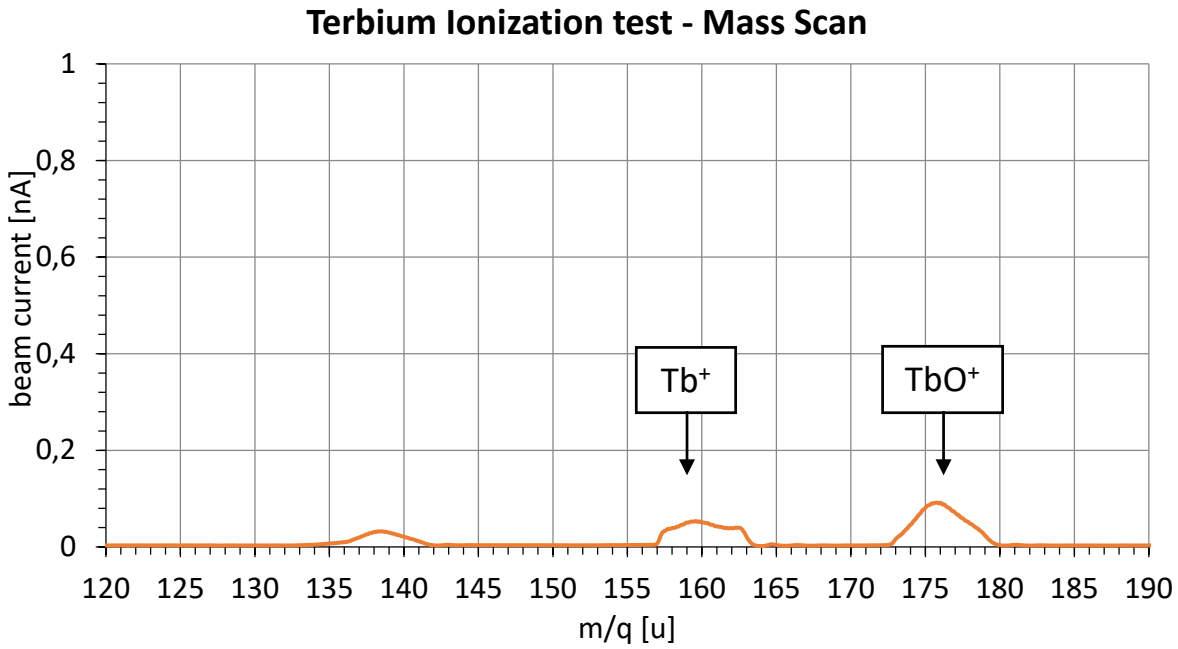

Figure 6.11: *mass scan performed during the copper ionization tests. Mass 63 and 65 correspond to the stable isotopes of copper ^{63}Cu and ^{65}Cu*

6.4 Discussion and conclusions

The study presented in this chapter was aimed to evaluate the feasibility of the production of ^{149}Tb, ^{152}Tb and ^{155}Tb at SPES facility according to the ISOLPHARM patented method.

Previously performed studies assessed the possibility of the proton irradiation of natural Gadolinium targets, highlighting remarkable production of the desired nuclides, but the side production of several Terbium radioisotopes decreased significantly the achieved radionuclidic purity to levels unsuitable for radiolabelling.

The production of extremely pure Terbium radionuclides was achieved only at ISOLDE, where a spallation Tantalum target was used the employment of electromagnetic mass separation ensured the elimination of any unwanted isotopic contaminant. The ISOL technique proved thus to be the only method capable to produce reasonable amounts of pure Terbium nuclide, but the developments of ISOLDE were difficultly replicable elsewhere, since GeV proton beams are not commonly available. Thus, ISOLPHARM has the capability to combine the

promising results of both approaches: at one side the high production rates of Gadolinium based targets when irradiated by protons from commercially available cyclotrons (with energy up to 70 MeV), at the other side the high purity achievable only with mass separation.

Concerning the target material, a refractory Gadolinium-based compound had to be identified, since ISOL targets have to operate at high temperature levels. Being carbides the most common ISOL target materials, initially, in this Study Gadolinium carbide was considered, and the first samples were synthetized. However, soon after the discovery of the chemical instability of GdC_x in air this idea was discarded, and the commercially available Gadolinium Boride, with similar refractoriness, was considered as valid alternative.

In order to have preliminary estimations of the possible production yields for ^{149}Tb, ^{152}Tb and ^{155}Tb, FLUKA and Geant4 Monte Carlo simulations were performed, showing interesting preliminary results. According to FLUKA ~36.5 GBq, 1.12 TBq and 1.09 TBq are the expected activities for respectively ^{149}Tb, ^{152}Tb and ^{155}Tb, within the GdB_4 target after 5 days of irradiation with a 100 μA 70 MeV proton beam. FLUKA simulations highlighted also the generation significant amounts ^{161}Tb, 6.86 GBq within 5 days of proton irradiation.

In addition to the evaluation of the in-target yields, such study was aimed also to preliminary evaluate the efficiencies involved in the Tb ionization process, but several issues were found during the performance of dedicated tests. In fact, as in the case of Scandium, Terbium suffered indeed of bad volatility, thus various techniques for the insertion of the neutrals within the offline Front End were used. The problem was partially solved by using the SPES SIS, which includes a transfer line with a more homogenous temperature profile, and by inserting the Mass Marker loaded with $TbCl_3$ directly within the source transfer line. The presence of the refractory Terbium Oxide was anyway reported; thus the efficiency measurements were still not performed. Provided that the MM sample might not be representative of the online processes, where Terbium is generated as atom within a GdB_4 lattice, improvements are ongoing to eliminate any Oxygen source within the test apparatus that could promote the formation of Terbium oxide and hinder the ionization efficiency measurement. Anyway, as in the case of Ag and Cu, improvements could be achieved by switching to the resonant laser ionization technique [6.47], as already done for the MEDICIS facility [6.16].

In addition, for refractory and high boiling point elements such as Terbium, other techniques could be used to boost the release, as in example the employment of molecular beams proposed also for Scandium. Indeed, according to such solution, refractory elements could be potentially released towards the ion source in the form of highly volatile molecules [6.48, 6.49].

As in the case of Scandium, Terbium may react with the gaseous Carbon tetrafluoride (CF_4), leading the formation of the volatile molecule TbF_3, that could be easily ionized and extracted

as a beam, as already done at ISOLDE for some elements [6.50]. Ongoing developments are being performed to equip the SPES offline Front End with the capability to inject CF_4 within the ion source.

As final consideration, especially in the case of Terbium, other facilities equipped with similar proton drivers may consider worth to replicate the developments performed at INFN-LNL, since both the employment of electromagnetic separation proved to be the only feasible technique for the production of Terbium, and the technology required to operate a small ISOL facility has been widely developed.

6.5 References

[6.1] C. Müller *et al.*, "A unique matched quadruplet of terbium radioisotopes for PET and SPECT and for α- and β- radionuclide therapy: an in vivo proof-of-concept study with a new receptor-targeted folate derivative.," *J. Nucl. Med.*, vol. 53 12, pp. 1951–1959, 2012.

[6.2] C. Müller *et al.*, "Preclinical in vivo application of 152Tb-DOTANOC: a radiolanthanide for PET imaging," *EJNMMI Res.*, vol. 6, no. 1, p. 35, Apr. 2016.

[6.3] C. Müller *et al.*, "Future prospects for SPECT imaging using the radiolanthanide terbium-155 — production and preclinical evaluation in tumor-bearing mice," *Nucl. Med. Biol.*, vol. 41, pp. e58–e65, May 2014.

[6.4] C. Müller *et al.*, "Folate Receptor Targeted Alpha-Therapy Using Terbium-149," *Pharmaceuticals*, vol. 7, no. 3, pp. 353–365, 2014.

[6.5] S. Lehenberger *et al.*, "The low-energy β− and electron emitter 161Tb as an alternative to 177Lu for targeted radionuclide therapy," *Nucl. Med. Biol.*, vol. 38, no. 6, pp. 917–924, Aug. 2011.

[6.6] S. K. Imam, "Advancements in cancer therapy with alpha-emitters: a review," *Int. J. Radiat. Oncol.*, vol. 51, no. 1, pp. 271–278, Sep. 2001.

[6.7] G. F. Steyn *et al.*, "Cross sections of proton-induced reactions on 152Gd, 155Gd and 159Tb with emphasis on the production of selected Tb radionuclides," *Nucl. Instruments Methods Phys. Res. Sect. B Beam Interact. with Mater. Atoms*, vol. 319, pp. 128–140, Jan. 2014.

[6.8] V. I. Levin, A. B. Malinin, and I. N. Tronova, "Production of radionuclides by photonuclear reactions Pt 1," *Radiochem. Radioanal. Lett.*, vol. 49, no. 2, pp. 111–117, 1981.

[6.9] B. J. Allen, G. Goozee, S. Sarkar, G. Beyer, C. Morel, and A. P. Byrne, "Production of terbium-152 by heavy ion reactions and proton induced spallation," *Appl. Radiat. Isot.*, vol. 54, no. 1, pp. 53–58, Jan. 2001.

[6.10] N. G. Zaitseva *et al.*, "Terbium-149 for nuclear medicine. The production of 149Tb via heavy ions induced nuclear reactions," *Czechoslov. J. Phys.*, vol. 53, no. 1, pp. A455--A458, 2003.

[6.11] P. Schmor, "Review of Cyclotrons for the Production of Radioactive Isotopes for Medical and Industrial Applications," in *Reviews of Accelerator Science and Technology*, pp. 103–116.

[6.12] G.-J. Beyer *et al.*, "Targeted alpha therapy in vivo: direct evidence for single cancer cell kill using 149Tb-rituximab," *Eur. J. Nucl. Med. Mol. Imaging*, vol. 31, no. 4, pp. 547–554, Apr. 2004.

[6.13] R. M. dos Santos Augusto *et al.*, "CERN-MEDICIS (Medical Isotopes Collected from ISOLDE): A New Facility," *Appl. Sci.*, vol. 4, no. 2, pp. 265–281, 2014.

[6.14] V. Sabaiduc and others, "BEST 70P Cyclotron Factory Test," in *Proceedings, 6th International Particle Accelerator Conference (IPAC 2015): Richmond, Virginia, USA, May 3-8, 2015*, 2015, p. THPF003.

[6.15] A. Monetti *et al.*, "The RIB production target for the SPES project," *Eur. Phys. J. A*, 2015.

[6.16] R. F. Cavaier, F. Haddad, T. Sounalet, T. Stora, and I. Zahi, "Terbium Radionuclides for Theranostics Applications: A Focus On MEDICIS-PROMED," *Phys. Procedia*, vol. 90, pp. 157–163, Jan. 2017.

[6.17] D. Rochman *et al.*, "The TENDL library: Hope, reality and future," *EPJ Web Conf.*, vol. 146, p. 02006, Sep. 2017.

[6.18] N. Otuka *et al.*, "Towards a More Complete and Accurate Experimental Nuclear Reaction Data Library (EXFOR): International Collaboration Between Nuclear Reaction Data Centres (NRDC)," *Nucl. Data Sheets*, vol. 120, pp. 272–276, Jun. 2014.

[6.19] Y. T. Mironov, "Features of excitation function study of the nuclear reactions at internal beam in the PNPI synchrocyclotron," in *International conference: Features of nuclear excitation states and mechanisms of nuclear reactions 51 Meeting on nuclear spectroscopy and nuclear structure The book of abstracts*, 2001, p. 384.

[6.20] C. Vermeulen *et al.*, "Cross sections of proton-induced reactions on natGd with special emphasis on the production possibilities of 152Tb and 155Tb," *Nucl. Instruments Methods Phys. Res. Sect. B Beam Interact. with Mater. Atoms*, vol. 275, pp. 24–32, Mar. 2012.

[6.21] T. Behrsing, G. B. Deacon, and P. C. Junk, "The chemistry of rare earth metals, compounds, and corrosion inhibitors," *Rare Earth-Based Corros. Inhib.*, pp. 1–37, Jan. 2014.

[6.22] K. H. J. Buschow, "Chapter 4 Rare earth compounds," *Handb. Ferromagn. Mater.*, vol. 1, pp. 297–414, Jan. 1980.

[6.23] J. Etourneau and P. Hagenmuller, "Structure and physical features of the rare-earth borides," *Philos. Mag. B*, vol. 52, no. 3, pp. 589–610, 1985.

[6.24] G.-Y. Adachi, N. Imanaka, and F. Zhang, "Chapter 99 Rare earth carbides," *Handb. Phys. Chem. Rare Earths*, vol. 15, pp. 61–189, Jan. 1991.

[6.25] L. C. Carraz, I. R. Haldorsen, H. L. Ravn, M. Skarestad, and L. Westgaard, "Fast release of nuclear reaction products from refractory matrices," *Nucl. Instruments Methods*, vol. 148, no. 2, pp. 217–230, Jan. 1978.

[6.26] L. Biasetto *et al.*, "Gas permeability of lanthanum oxycarbide targets for the SPES project," *J. Nucl. Mater.*, vol. 440, no. 1–3, pp. 70–80, Sep. 2013.

[6.27] L. Biasetto *et al.*, "Morphological and functional effects of graphene on the synthesis of uranium carbide for isotopes production targets," *Sci. Rep.*, vol. 8, no. 1, p. 8272, 2018.

[6.28] A. E. Barzakh *et al.*, "Investigation of the release properties of MeCx targets at IRIS," *Nucl. Instruments Methods Phys. Res. Sect. B Beam Interact. with Mater. Atoms*, vol. 126, no. 1–4, pp. 150–153, Apr. 1997.

[6.29] B. Hajek, V. Brozek, M. Popl, and J. Mostecky, "STUDIES ON HYDROLYZABLE CARBIDES. VII. DECOMPOSITION OF SOME DICARBIDES OF THE TYPE M/sup III/C$sub 2$ AND OF SCANDIUM CARBIDE WITH DEUTERIUM OXIDE.," 1971.

[6.30] H. Itoh, Y. Tsuzuki, T. Yogo, and S. Naka, "Synthesis of cerium and gadolinium borides using boron cage compounds as a boron source," *Mater. Res. Bull.*, vol. 22, no. 9, pp. 1259–1266, Sep. 1987.

[6.31] A. Andrighetto, C. M. Antonucci, S. Cevolani, C. Petrovich, and M. Santana Leitner, "Multifoil UCx target for the SPES project --An update," *Eur. Phys. J. A - Hadron. Nucl.*, vol. 30, no. 3, pp. 591–601, 2006.

[6.32] G. Battistoni *et al.*, "Overview of the FLUKA code," *Ann. Nucl. Energy*, 2015.

[6.33] G. Battistoni, F. Cerutti, A. Ferrari, J. Ranft, S. Roesler, and P. R. Sala, "Hadron production simulation by FLUKA," *J. Phys. Conf. Ser.*, vol. 408, no. 1, p. 12051, 2013.

[6.34] J. Allison *et al.*, "Recent developments in Geant4," *Nucl. Instruments Methods Phys. Res. Sect. A Accel. Spectrometers, Detect. Assoc. Equip.*, vol. 835, pp. 186–225, Nov. 2016.

[6.35] A. V Ivantchenko, V. N. Ivanchenko, J.-M. Q. Molina, and S. L. Incerti, "Geant4 hadronic physics for space radiation environment," *Int. J. Radiat. Biol.*, vol. 88, no. 1–2, pp. 171–175, 2012.

[6.36] D. H. Wright and M. H. Kelsey, "The Geant4 Bertini Cascade," *Nucl. Instruments Methods Phys. Res. Sect. A Accel. Spectrometers, Detect. Assoc. Equip.*, vol. 804, pp. 175–188, Dec. 2015.

[6.37] G. Folger, V. N. Ivanchenko, and J. P. Wellisch, "The Binary Cascade," *Eur. Phys. J. A - Hadron. Nucl.*, vol. 21, no. 3, pp. 407–417, 2004.

[6.38] Mancusi, D., Boudard, A., Cugnon, J., David, J.-C., Kaitaniemi, P., and Leray, S., "New C++ version of the Liège intranuclear cascade model in Geant4," *SNA + MC 2013 - Joint International Conference on Supercomputing in Nuclear Applications + Monte Carlo*. p. 5209, 2014.

[6.39] V. Ivanchenko *et al.*, "Recent Improvements in Geant4 Electromagnetic Physics Models and Interfaces," in *3th Monte Carlo Conference MC2010*, 2010, vol. 2, pp. 898–903.

[6.40] F. Borgna *et al.*, "A preliminary study for the production of high specific activity radionuclides for nuclear medicine obtained with the isotope separation on line technique," *Appl. Radiat. Isot.*, 2017.

[6.41] F. Borgna *et al.*, "Early Evaluation of Copper Radioisotope Production at ISOLPHARM," *Molecules*, vol. 23, no. 10, 2018.

[6.42] D. R. Lide, *CRC Handbook of Chemistry and Physics: A Ready-reference Book of Chemical and Physical Data*. CRC-Press, 1995.

[6.43] A. Andrighetto *et al.*, "Spes: An intense source of Neutron-Rich Radioactive Beams at Legnaro," *J. Phys. Conf. Ser.*, vol. 966, no. 1, 2018.

[6.44] F. Borgna, "Pharmaceutical Deveolpment of the ISOL Technique for the Production of Radionuclides and their Applications in Targeted Radionuclide Therapy," University of Padova, 2018.

[6.45] M. Manzolaro, G. Meneghetti, and A. Andrighetto, "Thermal–electric numerical simulation of a surface ion source for the production of radioactive ion beams," *Nucl. Instruments Methods Phys. Res. Sect. A Accel. Spectrometers, Detect. Assoc. Equip.*, vol. 623, no. 3, pp. 1061–1069, Nov. 2010.

[6.46] D. . Vermilyea, "The oxidation of tantalum at 50–300°C," *Acta Metall.*, vol. 6, no. 3, pp. 166–171, Mar. 1958.

[6.47] V. N. Fedosseev *et al.*, "ISOLDE RILIS: New beams, new facilities," *Nucl. Instruments Methods Phys. Res. Sect. B Beam Interact. with Mater. Atoms*, vol. 266, no. 19–20, pp. 4378–4382, Oct. 2008.

[6.48] C. Seiffert, "Production of radioactive molecular beams for CERN-ISOLDE," Technische Universität, Darmstadt, 2015.

[6.49] K. Baechmann, "CHEMICAL PROBLEMS OF THE ON-LINE SEPARATION OF SHORT-LIVED NUCLIDES.," *Forschungsbericht K70-28*, vol. BMBK-FB-L7, 1970.

[6.50] T. Bjørnstad *et al.*, "Recent development of high-temperature metal targets for ISOLDE," *Nucl. Instruments Methods Phys. Res. Sect. B Beam Interact. with Mater. Atoms*, vol. 26, no. 1–3, pp. 174–182, May 1987.

Chapter 7

Nuclide production and release simulations with Geant4 and FLUKA for ISOLPHARM

“ Para hacer las cosas bien es necesario: primero, el amor, segundo, la técnica.”

“To do things properly it is necessary: firstly, love, secondly, the technique”

Antoni Gaudí i Cornet (Spanish architect, 1852 – 1926), reported in *Gaudí: Arquitecto de Dios, 1852-1926*, Rafael Álvarez Izquierdo

7.1 Introduction

When a feasibility study for the evaluation of the ISOL production of medical radionuclides is performed, the estimation of the effectively achievable produced amounts of such nuclei is an important step to identify the best candidates. Indeed, if too low quantities are produced, the subsequent steps foreseen in ISOLPHARM, namely the radiochemical and radiopharmaceutical studies, can’t be carried out. Therefore, such indication can highlight if the ISOL process has to be updated, when possible, by, for example, considering a different target material or material microstructure or implementing a more efficient ionization technique. The ISOL technique is a complex method for the production of radioactive nuclei, and foresees many steps, each of them affecting the final amount of radionuclides that can be recovered at the end of the process. Indeed, the species of interest are firstly generated in target through nuclear reactions induced by the primary beam, subsequently they diffuse through the target material and then effuse in

vacuum towards the ion source. There they are ionized, extracted and then mass separated, and finally transported as a beam to the desired experimental hall [7.1]. Thus, according to the ISOL technique, the final beam intensity available at the radioisotope collection target station can be expressed with the formula 7.1 [7.2].

$$Y = \sigma \Phi N \varepsilon_d \varepsilon_e \varepsilon_i \varepsilon_t \tag{7.1}$$

- The symbol σ identifies the nuclear cross section for the desired reaction, and consequently is a function of the targeted nuclide and the beam energy.
- Φ is the primary beam flux, expressed in particle per second and per square meter, as it is available from the primary accelerator of the ISOL facility (proton beam form a cyclotron in the case of SPES-ISOLHARM).
- N is referred to the number of nuclei of the target species present in the target.
- ε_d is an efficiency coefficient related to the in target diffusion process. It varies according to the microstructure of the target (grain size, porosity, density) as well as to the target temperature.
- ε_e is another efficiency factor related to the effusion process, that depends on both the working temperature and the materials used for the targets and ion source system components.
- the efficiency factor ε_i represent the influence of the ionization process and may vary according to the ionization technique used. As showed in the previous chapters, such coefficient is often experimentally determined using stable isotope beams of the element of interest, since the ionization is a property of the chemical element.
- ε_t is the efficiency coefficient that summarizes the beam purification and transport processes. Generally, such a coefficient is high, since the optical devices and the mass separator resolution are designed to minimize the beam losses. Such factor is dependent on the number and type of devices installed along the beam line, thus also to its length. The longer the beam line, the higher are the beam losses. In the particular case of ISOLPHARM, if the collection station will be installed close to the ISOL bunker, such factor can be considered close to 80-90%.

The product $\sigma \Phi N$ corresponds to the in-target production of the desired nuclides, and can be calculated using various standard Monte Carlo codes (i. e. Fluka, MCNPX, Geant4) [7.3, 7.4]. For the activated reactions, such codes may consider both experimental cross sections and/or calculated excitation functions, especially in case of reactions that lack experimental data. This is particularly true in the proton energy range of SPES (35-70 MeV), where few experimental

cross section data were collected, as shown in chapter 4. Consequently, in such cases, trusting a single MC model for the estimation of the in-target production may be misleading.

Whereas the value of the coefficients ε_i and ε_t can be determined with dedicated tests, even using stable beams, as showed in the previous chapters, the effusion and diffusion coefficients are difficult to find out experimentally. However, in some rare cases, it is possible to evaluate the release behaviour of ISOL targets with dedicated experiments [7.5-7.7] obtaining release times of different elements, and consequently the release efficiency ($\varepsilon_r = \varepsilon_d * \varepsilon_e$), a factor that takes into account both processes. Alternatively, such efficiency coefficient can be estimated with Monte Carlo simulations using properly designed codes such as Diffuse II [7.8] and RIBO [7.9]. Although such codes proved to be reliable and able to replicate experimental data under specific conditions, they cannot be adapted to specific setups without the interaction with the developers, and are consequently unlikely to be used to simulate various target configurations. Considering such background, new numerical approaches are required, if researchers wish to delve deeper the possibility of estimating the efficiency of the release processes in ISOL targets. In the framework of ISOLPHARM the Monte Carlo toolkit Geant4 was chosen to develop a new model able to simulate both diffusion and effusion. Such toolkit is publicly available and open-source, allowing the user to exploit the existing physics processes and to add custom libraries for the missing ones, e.g. the effusion and diffusion processes. The flexibility of the Geant4 code is its biggest advantage the other available Monte Carlo codes, permitting the user to customize it for its goals. Once the code would be validated, it could be used to evaluate different target configuration, allowing to improve the target design in order to increase the release efficiency.

Such a code requires however a large deployment of computing resources to produce reliable results, and a simulation may require a long time to be completed. Such peculiarities indicate that the aforementioned code may greatly profit by parallel cloud computing. For this reason, in the framework of the collaboration project ISOLPHARM_Ag, an IT infrastructure for ISOLPHARM is being developed, exploiting the resources of the existing "CloudVeneto", an IaaS (Infrastructure as a Service) cloud service. The aim of such infrastructure is to allow users to launch through a web portal not only the custom Geant4 code for the release simulations, but also various standard codes (FLUKA and Geant4 with different physics settings) for the evaluation of the in-target production, in order to increase the reliability of the results. Finally, the produced data will be shared with a community of users through the ISOLPHARM website, currently under construction.

7.2 Nuclide production simulations with FLUKA and Geant4

The first type of simulations for ISOLPHARM are aimed to evaluate the in-target production of the desired nuclide, in order both to compare different target materials and to provide an estimation of the producible activities with the ISOL technologies. Such simulations are basically standard beam-target interaction simulations. However, the obtained results rely on the nuclear interaction model that is referred to the selected MC code, that may not be fully representative, especially in case of particularly "exotic" nuclear reactions. As a consequence, in order to increase the reliability of the calculated results, it is necessary to perform the same simulation considering different models. Currently, in the framework of ISOLPHARM the Monte Carlo codes FLUKA [7.3] and Geant4 [7.10] are being implemented in the IT infrastructure. Indeed, even if the first step simulations are standard and not very computing-intensive, they may profit of the benefits of parallel computing in terms of calculations time and the different codes can be launched simultaneously for a faster comparison.

In FLUKA, hadron-nucleus interactions are modelled exclusively according to the PEANUT (PreEquilibrium-Approachto-NUclear-Thermalization) event generator [7.11]. Such nuclear interaction model can be summarized as a sequence of four main steps:

i) Glauber-Gribov cascade and high energy collisions,
ii) Generalized IntraNuclear cascade
iii) Preequilibrium emission
iv) Evaporation/Fragmentation/Fission phase and γ deexcitation.

Some of the steps may be skipped according to the projectile particle type and to its energy.

Otherwise, Geant4, allows the user to select a nuclear interaction model among the existing nuclear physics lists, based for example on the Bertini cascade model or on the Binary Light Ion Cascade (BIC) model [7.12] or on databases such as TENDL[7.13]. Additionally, Geant4 allows the user to compile the code with his/her own eventual hadron-nucleus interaction model, that can be developed either empirically with suitable experiments or through numerical calculations with modern nuclear model codes such as TALYS[7.13] or EMPIRE [7.14]

Figure 7.1 compares the different workflows followed to launch a nuclide production simulation with both FLUKA and Geant4.

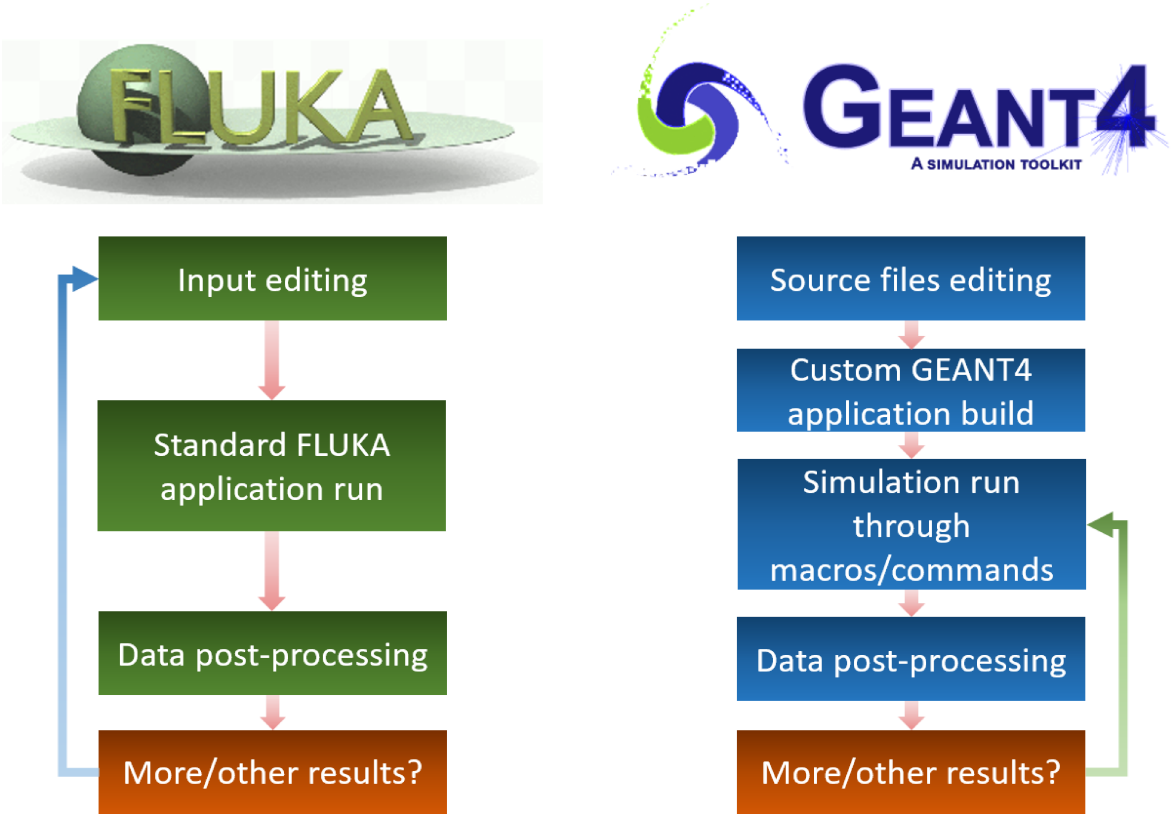

Figure 7.1: *the two workflows for the production simulations with FLUKA and Geant4*

Since FLUKA is a Monte Carlo code, not a toolkit as Geant4, it does not allow a wide customization level for user's simulations. Generally, the user edits the input file as a combination of code blocks called "cards". Such input is subsequently used to launch the desired simulation. In order to reduce the statistical error, FLUKA foresees the possibility to re-run the same input file a certain amount of times, varying automatically each time the seed number used, providing thus results that might be slightly different. Each of such runs is called "cycle", and produce different output files. The final results for the simulation are obtained by merging outputs from the single cycles. The same procedure has to be executed each time the user wishes to modify one or more simulation parameters.

Since Geant4 is a toolkit and no standard application as FLUKA is provided to the user, consequently a different approach has to be considered while setting an in-target isotope production simulation. The first step is indeed the editing of the source files, that are successively used to build the custom Geant4 application. Once the application is created and started, the simulation is launched through commands, aimed both to define the simulation parameters and to initialize the run. When a long set of commands has to be defined, it is more convenient to use macros, text files containing a list of commands, that can be read by the custom application. If the user is not satisfied of the simulation results, it is not necessary to rebuild the custom application, but simply either to modify one or more parameters through commands or to use a new input macro and relaunch the simulation.

7.3 The Geant4 custom model for the release simulations

As already introduced, Geant4 is a Monte Carlo toolkit [7.10, 7.12, 7.15] that provides a diverse, wide-ranging, yet cohesive set of software components, which can be employed from simple single studies of basic phenomena and geometries to full-scale detector simulations for experiments at large facilities as the Large Hadron Collider at CERN.

The definition and implementation of the software components has to include all aspects of the simulation process, as for example the simulated system geometry and materials, the fundamental particles of interest, the generation of primary particles of events, the tracking of particles through materials and external electromagnetic fields, the physics processes governing particle interactions, the response of sensitive detector components, the generation of event data, the storage of events and tracks.

Since Geant4 usually tracks particles with energies of the order of magnitude of keV, a specific list of activated physical process has to be built, if the user wishes to simulate the transport of evaporated isotopes at thermal energies of the order of eV, as in the case of the diffusion and effusion phenomena. Consequently, in such case, all the standard Geant4 processes have to be deactivated except for the in-flight decay, that may occur to the in-target generated species. As a consequence, a novel physics list was developed with two main processes, the diffusion in the target material and the effusion in the vacuum vessel containing the target disks.

The diffusion process was modelled in two different stages (figure 7.2a and 7.2b). The first is the proper diffusion, occurring in the molecules/grains of the target material; the second "diffusion" process is actually the effusion through the pores of the target disk material. In the code, the main difference between the aforementioned two stages is the mean free path of a nuclide in these two media.

In the case of actual diffusion, the number of interactions in a molecule is very high due to the very short mean free path, generally of the same order of magnitude of the atomic distance. Considering the reasonable assumption of spherical target material grains/molecules, the average time t_D spent by a particle to exit the grain/molecule can be calculated solving exactly the second Fick's Law for a perfect sphere [7.16], which leads to

$$t_D = \frac{a^2}{\pi^2 D_M} \tag{7.2}$$

where D_M is the diffusion coefficient and a is the radius of the sphere. In the code, the user provides a diffusion coefficient at a given temperature $D_{M,0}$ that the code uses to compute the mean free path depending on the target temperature, whereas the distribution of the molecule sizes a is known, since the material microstructure is generally experimentally characterized.

Taking into account both the user defined $D_{M,0}$ and the distribution of a sizes, the code randomly generates a t_D for each tracked nuclides, and sums it to the isotope lived time, affecting its decaying probability.

After the isotope has left the grain/molecule, the second "diffusion" step is initiated, namely the effusion through the target material pores. In such case, the random walk of the nuclide is longer, of the order of magnitude of the average pore size, and is modelled as an isotropic diffusive process. In such case the user is requested to define an additional "diffusion" coefficient at a given temperature $D_{P,0}$.

After the nuclide reaches the target surface, it can be ejected and travels freely in the vacuum system until it reaches another solid surface (figure 7.2c). At this point, the effusion process is initiated. The code takes into account also the eventual probability of being definitively captured and bounded to the surface, parameter that has to be provided by the user and can eventually be estimated with dedicated effusion tests involving the target assembly materials. If the particle is not permanently captured, it can be absorbed for a limited amount of time by the surface and successively desorbed, affecting its decaying probability. The average delay between an adsorption and the consecutive desorption is referred as "sticking-time" and has to be supplied by the user. Various distributions can be used to model the random exiting angle of a particle from a surface. In the code a Lambertian distribution was considered, because it better describes the reflection of atoms in vacuum systems [7.9].

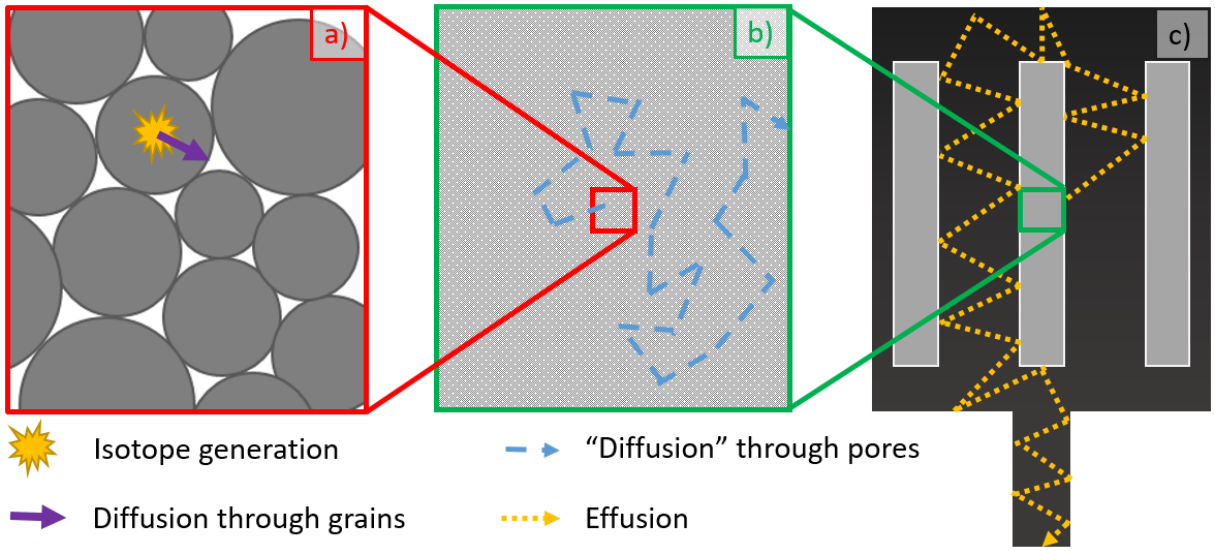

Figure 7.2: *Scheme of the isotope release process*

As a result, in order to launch a simulation, the user has to set the following parameters:

- Target temperature (T);
- Mean (μ_a) and standard deviation (σ_a) of the distribution of radius a of the molecule;
- Diffusion coefficients at a given temperature $D_{M,0}$ and $D_{P,0}$ for each nuclide element;

- Probability of absorption and full absorption for each nuclide element and material;
- Sticking-times for each nuclide element and target assembly material combination.

Some of such parameters can be estimated in advance and inserted in the simulation, other can be hypnotized and consequently extrapolated later from the simulation itself. Generally, the user can easily provide the target temperature T, usually known from both experimental measurements and Finite Element Method numerical models [7.17, 7.18], while μ_a and σ_a can be estimated from the target material microstructural analysis. The diffusion coefficients for the combination of nuclide chemical element and target material can be found in literature only for some isotopes; otherwise, molecular dynamics simulations could be employed to estimate a reasonable value. Sticking-times and the probability of absorption - desorption and/or permanent absorption can be found in literature for some combination of material and nuclide chemical element or calculated with empirical models [7.19], eventually supported by dedicated tests.

After the code has simulated the diffusion from the target material molecule, the inter-grain effusion in the target pores, and the effusion in the vacuum system with thousands of reflection (figure 7.3), the tracked isotope may either decay along the path or reach the end of the transfer line. At such point the simulation ends and the time-of-flight for each survived isotope is stored.

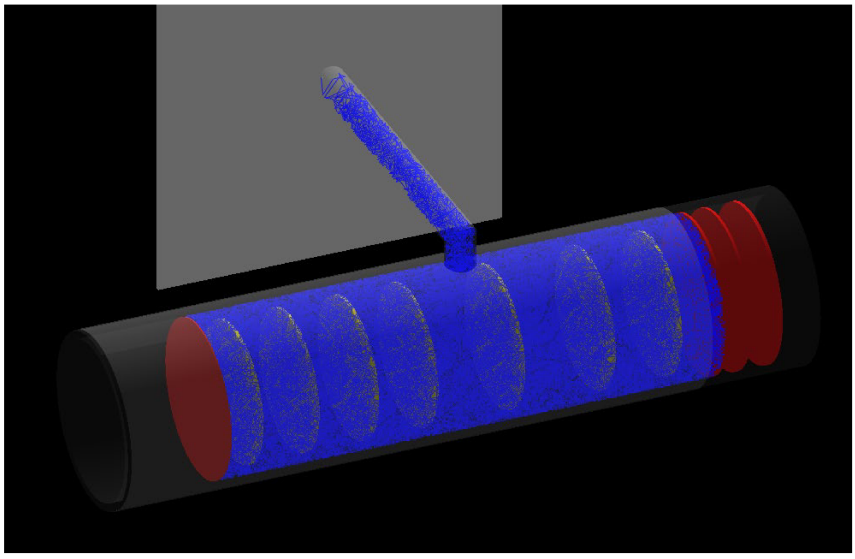

Figure 7.3.: *Visual example of the effusion paths (in blue) of ten particles in the SPES target assembly*

Such results will be extremely useful calculate the release efficiency as the ratio between the number of nuclides of that specific specie tracked up to the end of the transfer line and the amount produced in the target. In addition, in case of experimentally measured beam intensities, it will be possible either to validate the model or to adjust the hypothesized diffusion and effusion parameters in order to match the experimental data.

7.3.1 Testing the code: rubidium isotopes release simulations from the SPES UC_x target

With the aim of testing the code, the case study of rubidium isotopes release from a uranium carbide target was taken into account, since some of the simulation parameters, as for example the sticking times, could be found in literature. The apparatus reproduced in the simulation includes all components of the target block assembly, namely the 7 UC_x disks, the tantalum heater and transfer line and the graphite box with the windows and dumpers. The implemented geometry is shown in figure 7.4.

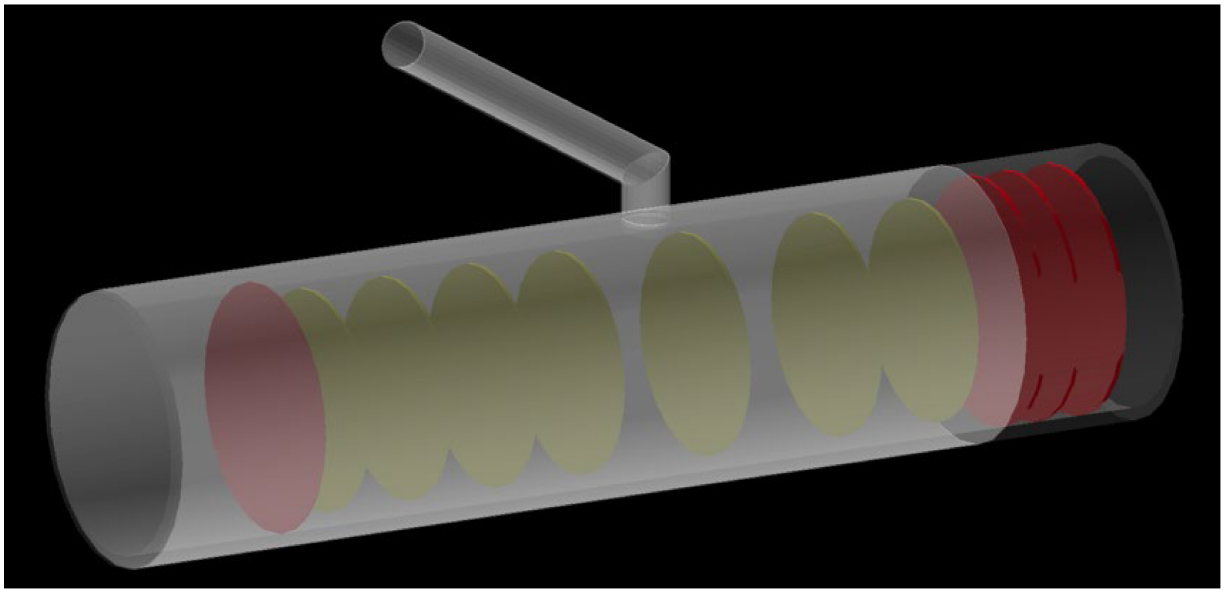

Figure 7.4: *Geometry implemented in the Geant4 simulation. The UC_4 disks are yellow, the carbon disk red and the tantalum walls grey.*

In the simulation, the user must provide in the input the average number of isotopes of the selected specie that are produced in each disk. Such results can be retrieved from the previously run production simulations with any of the considered Monte Carlo code.

For rubidium, the values for the sticking times are 100 ns for interaction with Tantalum [7.20] and 4.42 μs for Carbon [7.21], as found in literature. The sticking time on UC_4 was set to zero. and the probability of full absorption was hypnotised null, whereas the probability of adsorption before a reflection was considered one. The $D_{M,0}$ coefficient for Rubidium was supposed to be similar to the $D_{M,0}$ for the noble gas Kripton and set to 7.943 10^{-13} cm^2/s [7.22], while for the $D_{P,0}$ three different values were taken into account: 10^{10} cm^2/s and 10^{8} cm^2/s for an almost immediate release, 10^{0} cm^2/s for a slow release. The μ_a and σ_a parameters were set to 10^{-2} and 10^{-3} nm [7.23], respectively.

Figure 7.12 shows the released yields normalized for μA of proton beam for the Rubidium for two different target temperatures, 1600 °C and 2000 °C. Exclusively the Rubidium isotopes were tracked in the simulation. The amount of isotopes simulated correspond to the expected

in-target production for a 40 MeV 50 µA proton beam impinging the UC_x target. The Monte Carlo yields are successively weighted by the ionization and the transport efficiency, 80% and 10% respectively. As shown in figure 7.5, if the atoms diffuse freely in the porous material, the temperature range does not affect the release efficiency for isotopes with atomic number A≤90. On the contrary, for higher mass-number isotopes (A≥91) the temperature range effect becomes relevant even in case of fast release. Indeed, such isotopes are farther from the stability valley, and consequently have shorter half-life. Thus, as expected, at high masses the curves at 1600 °C drop drastically, while the yields at 2000 °C remain generally higher. Additionally, in the case of slow release (low $D_{P,0}$) the release of all the isotopes is affected by the temperature effect.

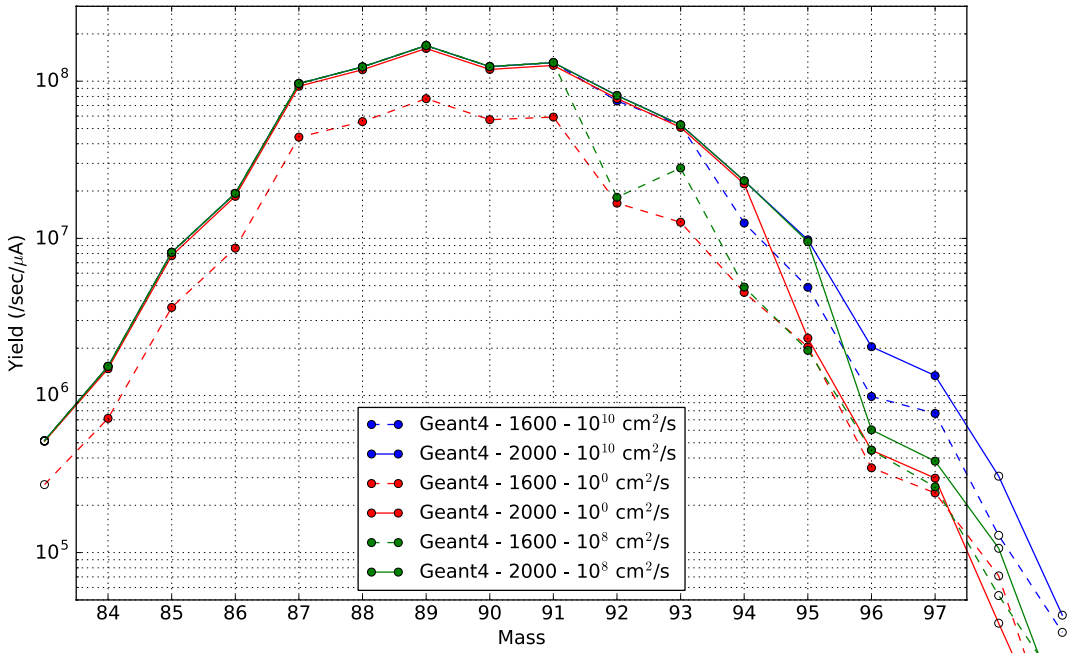

***Figure 7.5**: Expected yields (normalized by µA of proton beam) from the Geant4 simulations of the release process, considering different parameters. The Monte Carlo yields are weighted by the ionization and the transport efficiency, 80% and 10% respectively.*

The Geant4 simulation allows on to have an insight not only on the expected beam intensities, but also on the release time. Figure 7.6 shows the distribution of the Rubidium 90 isotope yield as a function of the calculated release time. If the diffusion coefficient is negligible, the temperature dominates the release time. On the other side, the release time is almost independent from the temperature if the contribution of the diffusion process becomes significant. It is interesting to highlight that, in case of 1600°C in the target with a 10^{10} cm^2/s coefficient $D_{P,0}$, amounts of the generated particles are released not immediately in the first few seconds, but also in the following seconds, as for the case of 2000°C in target with a 10^8 cm^2/s $D_{P,0}$. As a consequence, if only the particles released in the first second are selected, a slightly different scenario can be found. Figure 7.7 shows the released yields as a function of the isotopic

mass for the Rubidium, but only the isotopes released in the first second after the generation are considered. As expected both the temperature and the $D_{P,0}$ coefficient affect significantly the calculated beam intensities. This aspect is particularly relevant for other SPES applications were short-lived nuclei have to be delivered to the experiments.

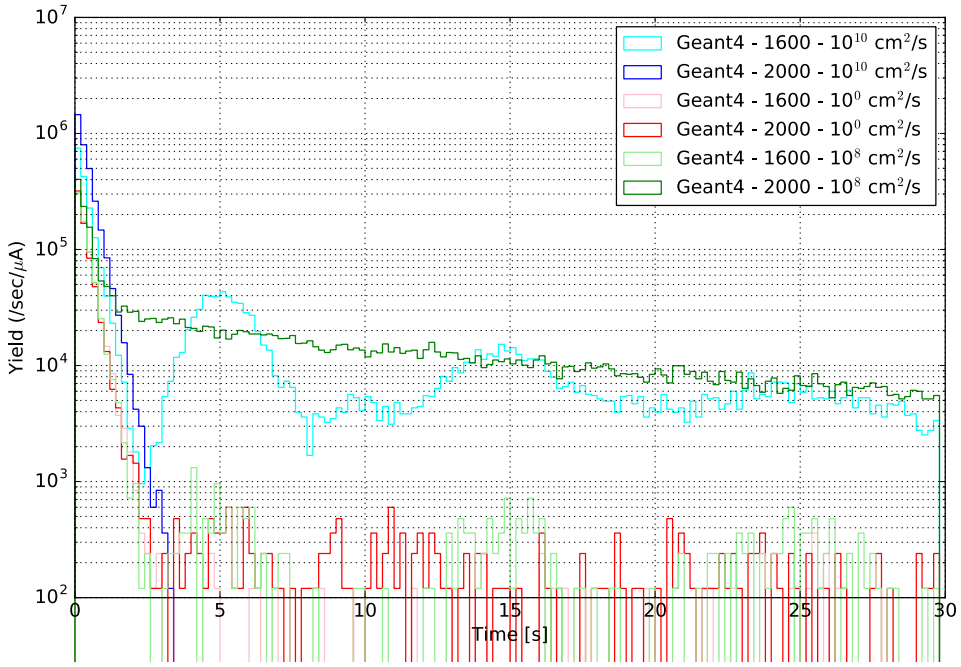

***Figure 7.6**: Geant4 simulations of the distribution of the release time for Rubidium 90 isotope. In the simulation only the Rubidium atoms generated by the primary beam were used. For the sake of comparison, the Monte Carlo yields are weighted by the ionization and the transport efficiency, 80% and 10% respectively.*

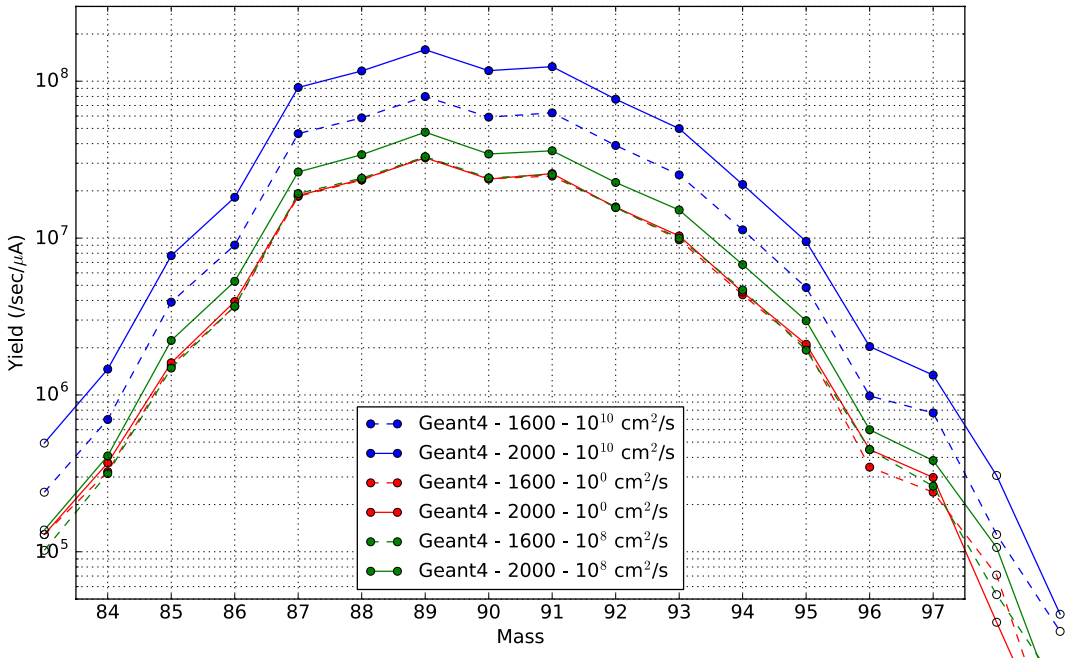

***Figure 7.7**. Expected yields (normalized by μA of proton beam) from the Geant4 simulations of the release process, considering different parameters Only the particles released within a second after generation are tracked. The Monte Carlo yields are weighted by the ionization and the transport efficiency, 80% and 10% respectively.*

7.4 The ISOLPHARM web portal for cloud simulations

One of the aims of the ISOLPHARM_Ag collaboration project is the development of an ISOLPHARM web based portal, that will be used to launch the presented complex and computing resources demanding Monte Carlo codes. Indeed, as previously introduced, such simulations will be used as fundamental tool firstly to evaluate the feasibility of the ISOL production of certain nuclides of medical interest, secondly to test eventual upgrades that could increase both the efficiency and the productivity of the ISOL process.

Both types of Monte Carlo simulations, namely the first step for the evaluation of the in-target production of the desired nuclide and the second step for the estimation of the efficiency of the subsequent release process, can widely benefit of the cloud-based powerful computing resources, in order to perform faster and more efficient simulations. In addition, the possibility of parallel computing can further decrease the calculation times, thus boosting the possibility to compare different dataset from different simulations. Finally, the use of a common interface for the implemented FLUKA and Geant4 Monte Carlo codes can simplify the simulation setting and launch since no knowledge of the specific code syntax is required.

Considering such requirements, the setting of a new dedicated cloud infrastructure for ISOLPHARM can be challenging, since the codes have to be slightly modified to be adapted for the cloud environment and a common syntax and workflow has to be defined. Moreover, whereas Geant4 is provided with the capability of parallel computing thanks to the multithreading option, the original FLUKA code does not have such capability. As a consequence, in order to allow a similar management system for both codes, a parallel computing option for FLUKA had to be designed. In particular, FLUKA foresees to run the simulation with cycles, meaning that the simulation is stepwise repeated a user-defined amount of times with different seed numbers. Such feature was used to develop a parallelization option for FLUKA. Indeed, by previously forcing the assignment of the seed number for each cycle, it is possible to run simultaneously all cycles in different threads. Such development, performed by INFN-PD scientists, members of ISOLPHARM collaboration, was noticed FLUKA developers, that are now interested to cooperate.

Figure 7.8 shows the processing workflow that will be adopted to perform both simulation steps. The first simulation to be set is the in-target nuclide production evaluation: firstly, the user is requested to specify in an intuitive graphic interface some input parameters, regarding the characteristic of the primary beam, the type of target material and the target geometry to be simulated. Such parameters are subsequently processed by the web portal and automatically translated into the input macros or files for both Geant4 and FLUKA.

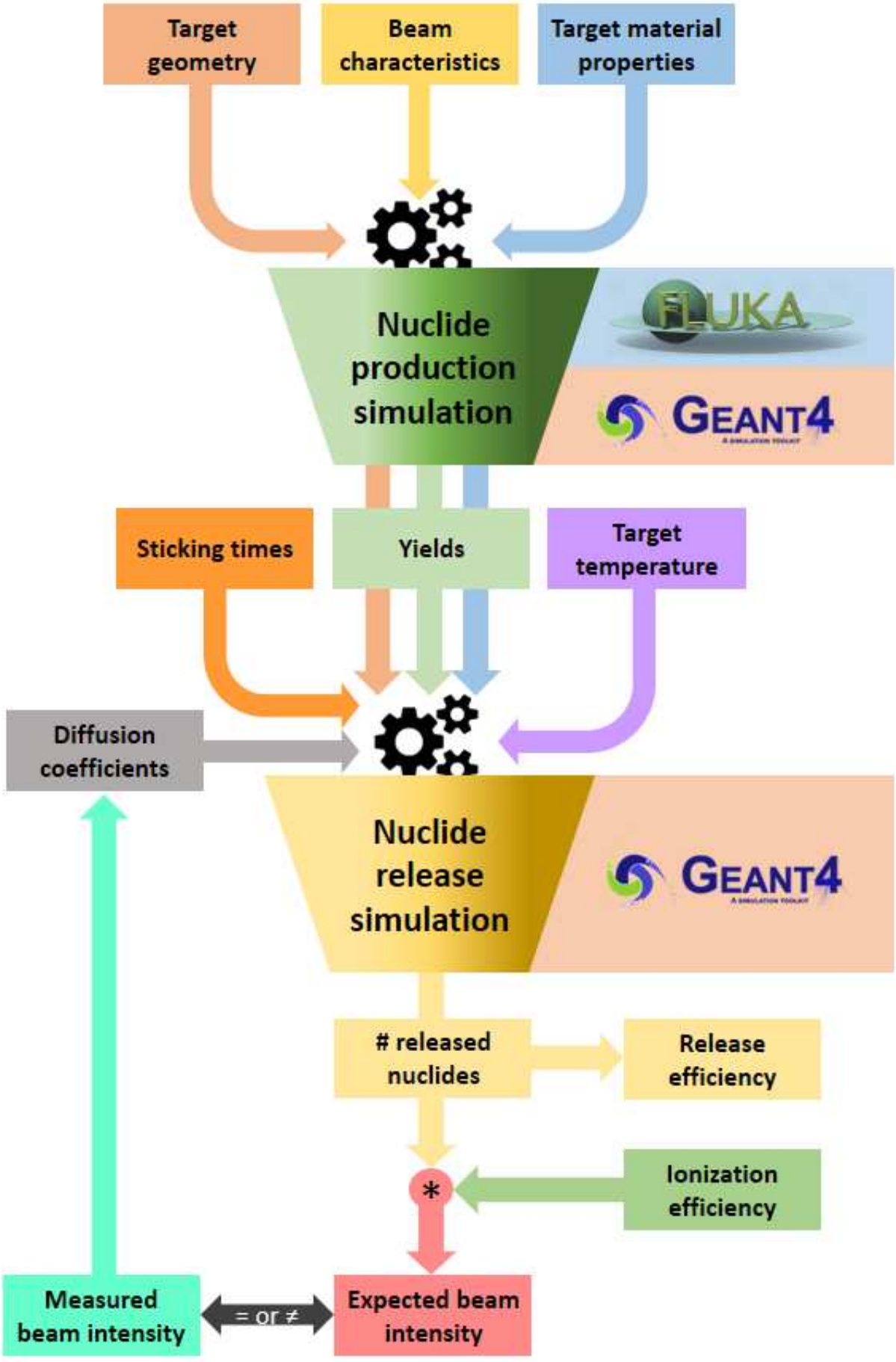

***Figure 7.8**: Processing workflow for the two simulation steps*

Both codes are simultaneously launched in cloud environment, and produce result data. Such data are finally processed and shown with a common and intuitive format, thus simplifying the retrieve of the desired information.

The second simulation step, in other words the release simulations, will be launched subsequently, and will inherit form the previous step both the target configuration settings and the calculated yields. In addition, the user is requested to specify the target temperature, since the diffusion and effusion processes are temperature dependent. The simulation of the effusion process requires the specification of sticking times, namely the time delay between each absorption and desorption of the effusing nucleus on a hot surface. The code itself will extract from a given database the sticking times for each target unit material - radionuclide combination, if such values are known, or will fix randomly such parameters. The diffusion coefficient is generally unknown, consequently the code will randomly select it a set of possible values. The code will provide as output the average release time for the considered nuclide, thus providing indirectly the rate of the released nuclei. If such rate is known, the release efficiency can be estimated. Finally, the code will multiply the obtained nuclide release rates for the experimentally determined ionization and transport efficiency factors (also stored in an internal database), thus providing as final output the expected beam intensity. If some ISOL experimental data exist for such target-nuclide combination, it will be possible to iterate the simulation, varying the arbitrary selected diffusion coefficient up to convergence to the experimental value. In that way it will be also possible to estimate indirectly the diffusion coefficient for such target material – nuclide combination at that given target temperature.

As a conclusion, such complex simulation workflow requires a powerful cloud computing infrastructure to produce and store such large amount of data. In the framework ISOLPHARM_Ag the CloudVeneto infrastructure was chosen.

7.4.1 CloudVeneto

CloudVeneto (figure 7.9) is a project that involves the INFN division of Padova, INFN-LNL and ten departments of the University of Padova (Department of Biology, Department of Physics and Astronomy, Department of Geosciences, Department of Civil, Environmental and Architectural Engineering, Department of Information Engineering, Department of Mathematics, Department of Molecular Medicine, Department of Biomedical Sciences, Department of Chemical Sciences, Department of Pharmaceutical and Pharmacological Sciences). It is aimed to develop a Cloud computing reference center, addressed not only to the research environment but also to enterprises and Public Administration.

***Figure 7.9**: the CloudVeneto logo*

The infrastructure of CloudVeneto is a Cloud service of the IaaS (Infrastructure as a Service) family, that allows to manage efficiently a pool of computing resources that can be allocated dynamically and rapidly to the requesting users. Users can consequently easily customize complex computing systems, that are automatically scaled in order to guarantee the needed calculation power. Indeed, CloudVeneto is particularly suitable for scalable applications, where the availability of a wide pool of computing resources can reduce drastically the calculation times. When a new job is submitted, the cluster size (in terms of number of worker nodes) is automatically scaled out depending on the job queue filling level: worker nodes are created when jobs are waiting in the queue and are eventually destroyed when they are free.

Currently CloudVeneto infrastructure includes 44 compute nodes, for a total of more than 1750 logic cores, 2 GPUs, and an overall storage of 230 TB. 13 compute nodes are owned by the University of Padova, 18 by the INFN division of Padova and finally 13 nodes are hosted at INFN-LNL.

CloudVeneto uses the Cloud middleware OpenStack [7.24], that has a wide and rapidly growing community of users and developers, and is also supported by industry. In addition, various services have been implemented (figure 7.10), thus enabling, for example, the management of the launched virtual machines, the sign on with the member institution accounts (INFN and University of Padova) or the use of web-based interface. In detail, the activated OpenStack services are:

- Keystone (authentication, authorization, service discovery)
- Glance (images management)
- Nova (virtual machine management)
- Neutron (networking)
- Cinder (block storage)
- Heat (orchestration)
- Horizon (web-based interface)
- Ceilometer (accounting)
- EC2 (compatible interface with Amazon EC2)

Additional services were included to add other functionalities, in particular:

- The integration with Identity Provider (particularly the Single Sign-On sytem of Padova University and the INFN Authentication and Authorization Infrastructure – INFN-AAI) for the users' authentication.
- Support for the registration of users and projects
- Management of accounting information
- Support for the setting of flexible batch clusters for the execution of both standard applications and Docker containers

Typical examples of use of the CloudVeneto resources are:

- The execution of interactive applications
- The deployment of services
- The configuration of clusters for the execution of multiple instances of compute-intensive applications (or containers) in batch mode
- The parallel execution of compute-intensive applications that require the simultaneous use of more virtual machines.

The services of CloudVeneto were configured with high reliability, in order to ensure the availability of the system even in case of failures in one or more compute nodes.

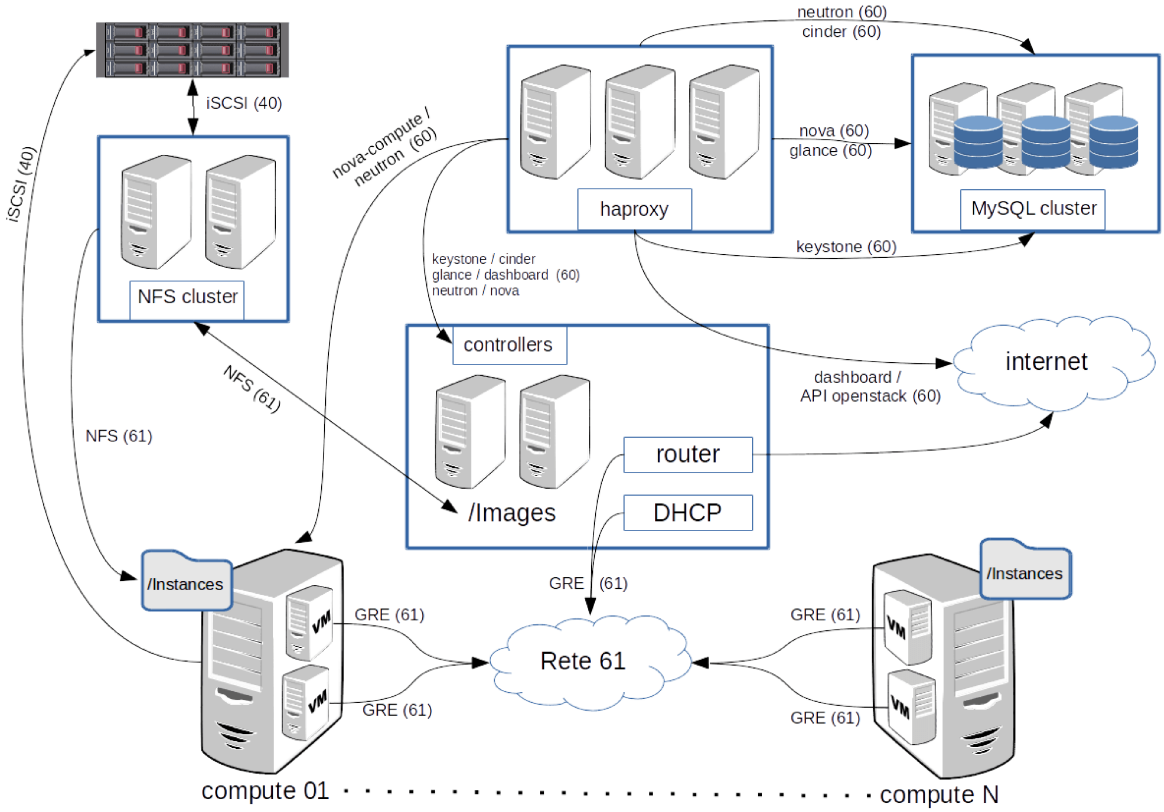

***Figure 7.10**: the architecture of CloudVeneto. For each arch, the communication protocol and subnetwork are indicated into brackets.*

7.4.2 Architecture of the ISOLPHARM IT infrastructure

As already introduced, in the framework of ISOLPHARM, a large amount of FLUKA and Geant4 MC simulations are required to evaluate both the nuclide production and release, considering in addition different target configurations. Such simulations, especially the release calculations, are computing intensive and may benefit in term of calculation time if the computing tasks are parallelized. Thus, a custom Information Technology (IT) infrastructure was designed taking into account the aforementioned computing needs, including in particular:

- the capability to execute independent and parallel Monte Carlo simulations;
- the possibility to analyze the produced data through different tools including graphical and Big Data facilities;
- a Web based portal to allow users to submit their Monte Carlo simulations and then collect/view the produced data

Considering such requirements, the OpenStack CloudVeneto infrastructure was considered suitable, and was chosen for the provisioning of the required computing resources. The computing architecture to be adopted, should include the most modern technologies with the support for the fast application deployment (even in Cloud) and the possibility to scale applications to the required computing power. In addition, high availability of the resources should be ensured, in order to prevent the loss of data due to eventual failures, and a security system should enable only expert registered users to access and modify the codes.

For this reason, the adopted solution was to deploy the custom applications for ISOLPHARM in Linux containers instead of Virtual Machines. Indeed, such containers are small, fast and portable runtime environments, that use the OS-level virtualization, and are isolated from each other and from the host. Basically containers can be considered “micro services” that are automatically created when a job is submitted, and finally killed when the job queue is empty and the produced data are stored.

The use of container requires however to be managed by the so called “Container orchestrators”. Such software is the entity which manages complex cross-domain processes and handles eventual exceptions. Its main features are the automating deployment, the auto-scaling, the high availability, the monitoring and the management of containerized applications. Some examples of open source orchestrators for large computing clusters are Apache Mesos, Docker swarm, and Kubernetes. For the ISOLPHARM infrastructure Kubernetes [7.25] was chosen.

Kubernetes supports several AuthN (authentication) technologies (as in example OpenId Connect - OIDC) and its security is based on INDIGO IAM (Identity and Access Management).

The authorization (AuthZ) is based on Kubernetes RBAC (Role-Based Access Control).

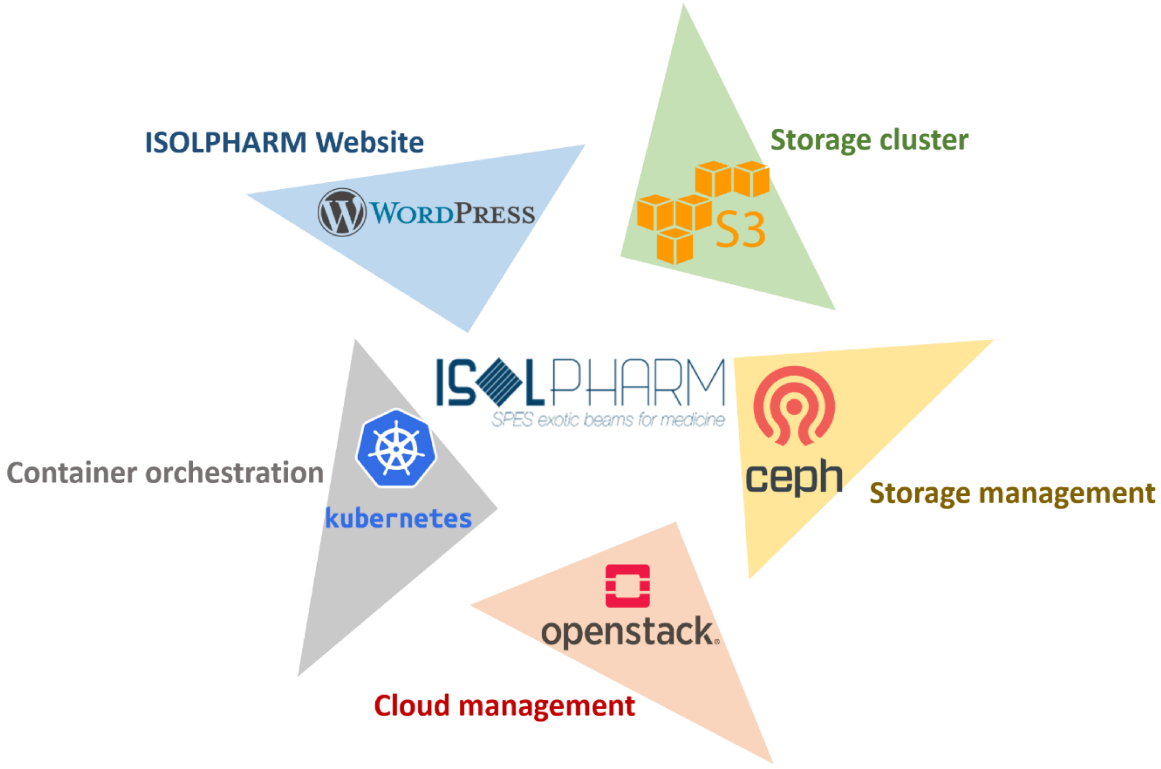

***Figure 7.11**: the software soltions adopded for the ISOLPHARM IT infrastructure*

For the management of the data produced by the simulation the object storage interface Ceph [7.26] was chosen, since it supports the selected S3 [7.27] data storage cluster and it is already implemented in CloudVeneto. Finally, a web portal has to be designed to allow user to customize and launch their own simulations. Such web portal, as well as the ISOLPHARM website, will be based on Wordpress [7.28] (figure 7.11).

For the ISOLPHARM IT infrastructure three types of users are foreseen:

- Guests: such users can simply consult the published results of the simulation and the website
- Standard users: they can launch simulations, and edit certain pages of the website. Once the simulation is over, they can decide either to publish the results in the website, or to keep them in the private area, not accessible to guests
- Superusers: they can modify/update the codes and add new codes if necessary, thus allowing new simulation configurations. They can edit the full website and add pages if necessary.

Figure 7.5 shows the typical workflow that will be undertaken by the IT infrastructure when a simulation is submitted by a standard user.

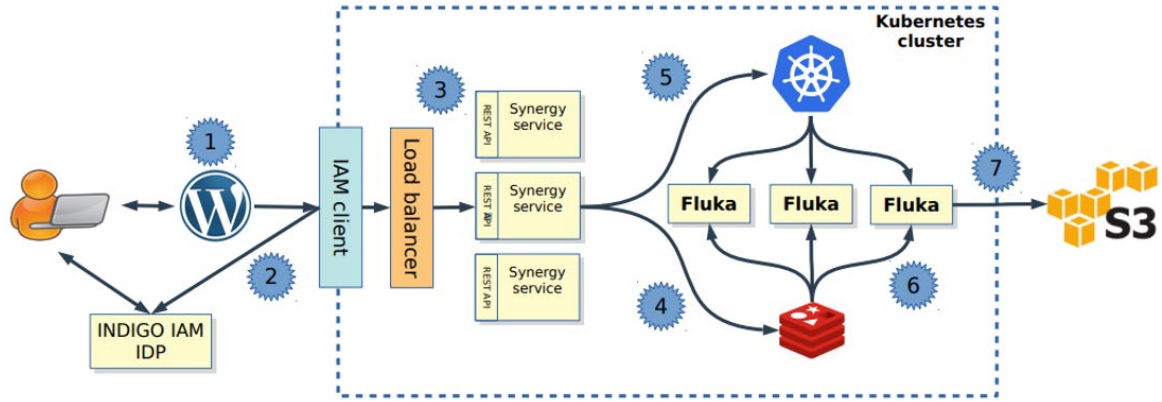

***Figure 7.12**: the ISOLPHARM IT infrastructure workflow for the submission of job (with three FLUKA tasks in the example)*

The first step (1 in figure 7.12) is the submission of the job: the user is requested to insert a set of parameters and settings that univocally define the desired simulation and the code to be launched. To insert properly such values, the user does not need to know the exact syntax for the two codes, because a script will automatically convert the raw input values in different input files. The insertion of such values will be performed through an intuitive web interface, currently under development.

The IAM client (2) checks if such user is authorised to submit such job: if not, the security system blocks the submission and request the authentication of a registered user. If the job is accepted it is sent to the Load Balancer (LB), that allocates the computing resources for its elaboration. Subsequently the LB forwards the job to the Synergy service (3), launched in three replicas in high availability to ensure the continuity and stability of the service. When Synergy validates the user job request, a new queue is created in Redis (4), a temporary key-value database, where the simulation parameters are stored. Simultaneously Synergy creates a new parallel job (FLUKA or Geant4) in Kubernetes (5). In the example in figure 7.12 the FLUKA job is parallelized in three tasks. Thereafter, each of the generated task takes the parameters from the queue and populates its template (6), generating the input file, as shown in figure 7.13. Finally, the output files produced by the task execution are stored into a S3 storage cluster (7), where they will be merged and further processed if the user intend to display them in the ISOLPHARM website.

***Figure 7.13**: A script insert automatically the input parameter in the template for both codes.*

7.4.3 The simulation input parameters

As previously declared, when setting a new simulation, a standard user is not requested to know the syntax for each of the implemented MC codes, but he/she will be able to insert the simulation parameters through a user-friendly intuitive web interface, currently under development. Yet, since both MC codes allow to widely customize the simulations by setting a large amount of parameters, it is necessary to simplify the input generation process, by identifying the values that have necessary be user-defined and the settings that can be hardcoded, thus normally hidden to standard users. As a result of such simplification process, a final list of parameters that the user must define for both simulation steps was produced, and is reported in table 7.1.

***Table 7.1**: Detailed list of the simulation input parameters*

Parameters					Production simulation		Release simulation
Topic	**Parameter name**		**Variable Type**	**Unif of Measure**	**FLUKA**	**Standard G4**	**Custom G4**
Target	**Target material**	Material type	string	-	Yes	Yes	Yes
		Target density	double	g/cm3	Yes	Yes	Yes
	Target temperature		array<double>[disk number]	°C	No	No	Yes
	Target geometry	Disk number	int	-	Yes	Yes	Yes
		Disk position	array<double>[disk number]	cm	Yes	Yes	Yes
		Disk radius	double	cm	Yes	Yes	Yes
		Disk thickness	array<double>[disk number]	cm	Yes	Yes	Yes
		Target box init	double	cm	Yes	Yes	Yes
		Target box end	double	cm	Yes	Yes	Yes
Beam	Particle (beam)		string	-	Yes	Yes	No
	Energy		double	MeV	Yes	Yes	No
	Beam center position (horizontal)		double	cm	Yes	Yes	No
	Beam center position (vertical)		double	cm	Yes	Yes	No
	beam position rms horizontal		double	cm	Yes	Yes	No
	beam position rms vertical		double	cm	Yes	Yes	No
	beam divergence rms horizontal		double	mrad	Yes	Yes	No
	beam divergence rms vertical		double	mrad	Yes	Yes	No
	beam current		double	mA	Yes	Yes	No
Yelds	Radioactive particle input file		string	-	No	No	Yes
Other	Physics list		string	-	No	Yes	Yes
	Precision		double	-	Yes	Yes	Yes
	Random generator seeds		array<int>[2]	-	Yes	Yes	Yes

Firstly, the user must define the production target characteristics, information that will be employed by both simulation steps. Standard user can select the target material from a previously created database, that contains for each entry a subset of material properties. Only superusers are allowed to insert new material configurations such database. The creation of the target geometry has been simplified by considering few parameters, as for example the number of target disks and their diameter. The other target dimensions will be automatically calculated as function of such subset of values. For the release simulations the target temperature has to be defined as additional parameter: the user can also define a temperature distribution by assigning different temperatures for each disk. The definition of the primary beam characteristics is obviously required only for the production simulations: the beam shape

customization has been restricted to the more realistic Gaussian profile. Instead of the primary beam, for the release simulations the user can select the type of nuclide he/she wishes to simulate, and the code will automatically retrieve the calculated yields for the given target configuration. Additional parameters that the user can define are the physics list (only for Geant4) that allows to select from the available options the desired library of cross sections or physical model, and the precision grade of the simulation. The latter will be expressed as a grade from 1 to 10 and implying the number of primary particles to be simulated. The higher the precision required, the higher will be the number of simulated particles, but consequently also the calculation time. Finally, the user can set a different random seed if he/she wishes to relaunch the same simulation and increase the statistics.

7.4.4 The results visualization

During and at the end of the simulation different data could be presented as output through the ISOLPHARM web portal, in the form of images, videos, tables, documents, etc. which can be saved for future uses. When the produced results will be ready to be shared with the ISOLPHARM community they will be uploaded in the website and shown by means of an interactive nuclide chart. Such interactive image will contain the yields of different radionuclides from the various target configurations, with colors representing different production rates. By clicking on each box, representing a particular radionuclide, users will be provided with data regarding that radionuclide such as production rate with different models (simulation step 1), and release efficiency (simulation step 2). Graphs of production and release efficiency of all radionuclides of an element will be presented when clicking a specific space of the image relative to a particular line of equal Z (number of protons), whereas data of different radionuclides of the same mass will be presented when clicking a particular diagonal of equal A (mass number).

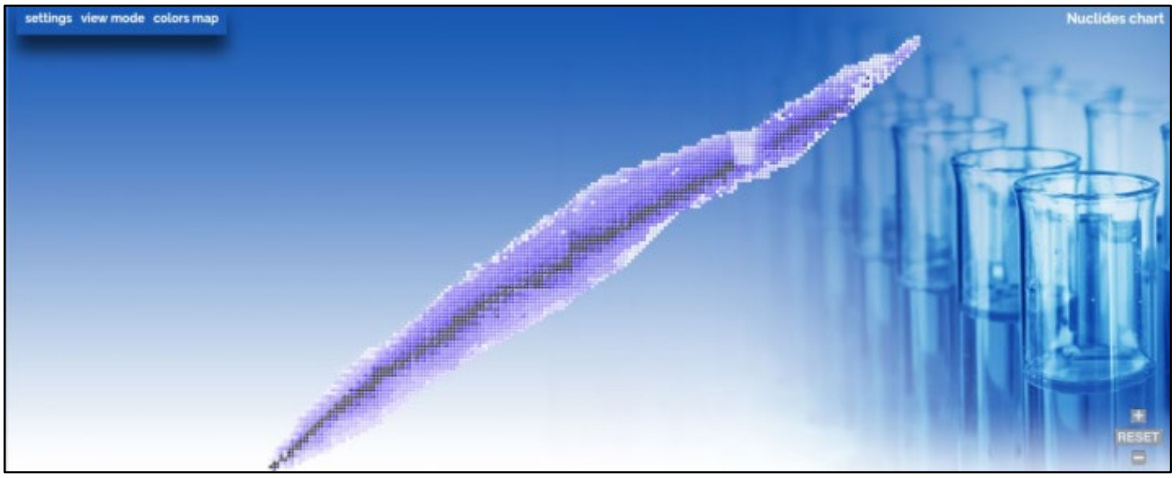

***Figure 7.14**: Prototype of the interactive nuclide chart for results visualization*

Other possible data presentation layouts will be discussed and implemented by the ISOLPHARM_Ag collaboration. Currently a prototypical applet for such interactive nuclide chart has been developed, as shown in figure 7.14

7.5 Discussion and conclusions

As shown in this chapter, the feasibility study for the production of nuclides of medical interest with the ISOL technique requires a complex set of Monte Carlo simulations, some of which highly computing demanding. In order to meet such need of computing resources, in the framework of ISOLPHARM_Ag, a powerful cloud based infrastructure is being built, with the additional feature to allow the launch of the different MC codes through a common web-based user-friendly interface, thus simplifying the process.

The simulation for the evaluation of the in-target production of the nuclides of interest will be based on both the FLUKA and Geant4 codes, with the aim to increase the reliability of the results by comparing different physics models. Additionally, as possible future development, other codes might be included.

Geant4 was used to compile a custom code aiming to simulate the release of the produced species from an ISOL target through the diffusion and effusion processes. In such case, in order to obtain plausible results, the preliminary estimation of some input parameters is required, in particular the sticking times for any of the extracted chemical element - target material combination is required. Indeed, Rubidium was chosen as test case to evaluate the custom code, since such parameters were found in literature for both the Rubidium – graphite and Rubidium – tantalum combinations. As expected, both the temperature and the diffusion coefficient effects becomes more significant in case of isotopes with shorter half-life, thus medical nuclides, that generally have half-lives of the order of magnitude of hours or days should be released more efficiently.

In general, if compared with experimental data, namely real beam intensities, the Geant4 model could be used to estimate the value of the diffusion coefficient at the testing temperature. A representative estimation of such a parameter could potentially guide the optimisation the target material design (i.e. pore sizes and density) in order to maximise the release efficiency for the desired chemical element. As a consequence, the available radioactive beam intensity could be increased, especially in the case of isotopes with shorter half-life.

A future upgrade of the model could potentially be used to characterize the sticking times and the diffusivity of the elements of interest, through inverse analyses. Indeed, if the experimental beam intensity for different isotopes of the same elements will be available, the release

efficiency of the desired isotope can be experimentally derived, and consequently the average release time for each chemical element. Since the Geant4 model calculates the release time considering its dependency on exclusively the diffusivity coefficient and the sticking times, such parameters could be estimated by means an iterative optimization algorithm with the goal to minimize the deviation from the experimental average release time.

7.6 References

[7.1] N. Orr, "Physics with Reaccelerated ISOL Beams," *J. Phys. G Nucl. Part. Phys.*, vol. 38, no. 2, p. 20301, 2010.

[7.2] S. Corradetti *et al.*, "Temperature dependence of yields from multi-foil SPES target," *Eur. Phys. J. A*, vol. 47, no. 10, p. 119, 2011.

[7.3] G. Battistoni *et al.*, "Overview of the FLUKA code," *Ann. Nucl. Energy*, 2015.

[7.4] A. Ferrari, P. R. Sala, A. Fasso, and J. Ranft, "FLUKA: A multi-particle transport code (Program version 2005)," 2005.

[7.5] E. H. Spejewski, H. K. Carter, B. Mervin, E. Prettyman, A. Kronenberg, and D. W. Stracener, "ISOL yield predictions from holdup-time measurements," *Nucl. Instruments Methods Phys. Res. Sect. B Beam Interact. with Mater. Atoms*, vol. 266, no. 19–20, pp. 4271–4274, Oct. 2008.

[7.6] F. Hosni *et al.*, "Yields of neutron-rich rubidium and cesium isotopes from fast-neutron induced fission of 238U, obtained by studying their release from a thick ISOL target," *Nucl. Instruments Methods Phys. Res. Sect. B Beam Interact. with Mater. Atoms*, vol. 247, no. 2, pp. 205–209, Jun. 2006.

[7.7] K. Peräjärvi *et al.*, "Studies of release properties of ISOLDE targets," *Nucl. Instruments Methods Phys. Res. Sect. B Beam Interact. with Mater. Atoms*, vol. 204, pp. 272–277, May 2003.

[7.8] Y. Zhang, I. Remec, G. D. Alton, and Z. Liu, "Simulation of rare isotope release from ISOL target," *Nucl. Instruments Methods Phys. Res. Sect. A Accel. Spectrometers, Detect. Assoc. Equip.*, vol. 620, no. 2–3, pp. 142–146, Aug. 2010.

[7.9] M. Santana-Leitner, "A Monte Carlo code to optimize the production of Radioactive Ion Beams by the ISOL technique," Catalonia TU, 2005.

[7.10] S. Agostinelli *et al.*, "Geant4—a simulation toolkit," *Nucl. Instruments Methods Phys. Res. Sect. A Accel. Spectrometers, Detect. Assoc. Equip.*, vol. 506, no. 3, pp. 250–303, Jul. 2003.

[7.11] G. Battistoni, F. Cerutti, A. Ferrari, J. Ranft, S. Roesler, and P. R. Sala, "Hadron production simulation by FLUKA," *J. Phys. Conf. Ser.*, vol. 408, no. 1, p. 12051, 2013.

[7.12] J. Allison *et al.*, "Recent developments in Geant4," *Nucl. Instruments Methods Phys. Res. Sect. A Accel. Spectrometers, Detect. Assoc. Equip.*, vol. 835, pp. 186–225, Nov. 2016.

[7.13] A. J. Koning and D. Rochman, "Modern Nuclear Data Evaluation with the TALYS Code System," *Nucl. Data Sheets*, vol. 113, no. 12, pp. 2841–2934, Dec. 2012.

[7.14] M. Herman *et al.*, "Recent Developments of the Nuclear Reaction Model Code EMPIRE," *AIP Conf. Proc.*, vol. 769, no. 1, pp. 1184–1187, 2005.

[7.15] J. Allison *et al.*, "Geant4 developments and applications," *IEEE Trans. Nucl. Sci.*, vol. 53, no. 1, pp. 270–278, Feb. 2006.

[7.16] M. Fujioka and Y. Arai, "Diffusion of radioisotopes from solids in the form of foils, fibers and particles," *Nucl. Instruments Methods Phys. Res.*, vol. 186, no. 1–2, pp. 409–412, Jul. 1981.

[7.17] A. Monetti *et al.*, "The RIB production target for the SPES project," *Eur. Phys. J. A*, 2015.

[7.18] M. Ballan *et al.*, "A combined experimental and numerical approach for the control and monitoring of the SPES target during operation at high temperature," *Nucl. Instruments Methods Phys. Res. Sect. B Beam Interact. with Mater. Atoms*, 2016.

[7.19] U. Köster, "Ausbeuten und Spektroskopie radioaktiver Isotope bei LOHENGRIN und ISOLDE," Technischen Universität München, 2000.

[7.20] R. Kirchner, "On the release and ionization efficiency of catcher-ion-source systems in isotope separation on-line," *Nucl. Instruments Methods Phys. Res. Sect. B Beam Interact. with Mater. Atoms*, vol. 70, no. 1–4, pp. 186–199, Aug. 1992.

[7.21] A. Pichard *et al.*, "Development of a surface ionization source for the SPIRAL 2 project," *Rev. Sci. Instrum.*, vol. 81, no. 2, p. 02A908, 2010.

[7.22] H. Furuya, J. Komatsu, T. Muto, A. Doi, and K. Inoue, "In-Pile Fission Gas Release from UC at Temperature around 2,000°C," *J. Nucl. Sci. Technol.*, vol. 8, no. 5, pp. 256–261, 1971.

[7.23] B. Hy *et al.*, "An off-line method to characterize the fission product release from uranium carbide-target prototypes developed for SPIRAL2 project," *Nucl. Instruments Methods Phys. Res. Sect. B Beam Interact. with Mater. Atoms*, vol. 288, pp. 34–41, Oct. 2012.

[7.24] T. Rosado and J. Bernardino, "An Overview of Openstack Architecture," in *Proceedings of the 18th International Database Engineering & Applications Symposium*, 2014, pp. 366–367.

[7.25] D. Bernstein, "Containers and Cloud: From LXC to Docker to Kubernetes," *IEEE Cloud Comput.*, vol. 1, no. 3, pp. 81–84, 2014.

[7.26] X. Zhang, S. Gaddam, and A. T. Chronopoulos, "Ceph Distributed File System Benchmarks on an Openstack Cloud," in *2015 IEEE International Conference on Cloud Computing in Emerging Markets (CCEM)*, 2015, pp. 113–120.

[7.27] M. R. Palankar, A. Iamnitchi, M. Ripeanu, and S. Garfinkel, "Amazon S3 for Science Grids: A Viable Solution?," in *Proceedings of the 2008 International Workshop on Data-aware Distributed Computing*, 2008, pp. 55–64.

[7.28] S. K. Patel, V. R. Rathod, and S. Parikh, "Joomla, Drupal and WordPress - a statistical comparison of open source CMS," in *3rd International Conference on Trendz in Information Sciences Computing (TISC2011)*, 2011, pp. 182–187.

Conclusions

“Provando e riprovando.”

“Trying and trying again”

SIF – Società Italiana di Fisica (Italian Physical Society), *association motto*.

The framework of the presented work is the ISOLPHARM project, an innovative and patented method that allows the production of a large variety of carrier-free radionuclides of medical interest exploiting the technologies of the SPES ISOL facility under construction at LNL-INFN. Such method is an accelerator-based technique, proposed as alternative to the conventional routines, namely accelerator-based, reactor-based and generator-based methods, and it foresee the irradiation of refractory solid target with proton beams extracted from a medium to high energy cyclotron (35 – 70 MeV). The aforementioned target works at temperature levels (2000°C), thus the produced nuclides are released and migrate towards an ion source, where they are ionized and extracted into a beam. Such beam is purified in mass thanks to an electromagnetic mass separator, thus only the desired nuclide and eventual isobaric contaminants are collected. The performance of a subsequent chemical separation allows to recover only the searched radionuclides.

The possibility to virtually produce any nuclide in carrier-free form without the use of nuclear reactors is the strength point of the proposed method. This is particularly relevant for those nuclei that are normally not routinely produced for the lack of a proper production technique, able to ensure both decent yields and acceptable radionuclidic purity. Therefore, the presented work was focussed in the feasibility study of the ISOL production of some nuclides that were never studied, such as ^{111}Ag, or that are proved to be difficult to produce with conventional methods, such as ^{43}Sc, ^{47}Sc, ^{67}Cu, ^{149}Tb, ^{152}Tb and ^{155}Tb. For each of the aforementioned nuclei, each step foreseen by the ISOL technique had to be evaluated, in particular, the in-target yields,

the release from the target, the efficiency and feasibility of the ionization and mass separation, the capability to collect the extracted ions and to recover them afterwards. Regarding the in-target yields, firstly a suitable target material had to be identified, then Monte Carlo calculations with different codes (FLUKA and Geant4) were performed. Therefore, it was possible to estimate that 82.9 GBq of ^{111}Ag are produced in five days of irradiation of the Uranium Carbide target designed for SPES, when impinged by a 40 MeV 200 μA proton beam. Regarding ^{67}Cu, Zirconium Germanide was identified as suitable target material and 1.4 GBq are produced after five days of irradiation with a 70 MeV 100 μA, along with 55 GBq of ^{64}Cu. Titanium based target, such as Titanium Carbide or Titanium Boride, can be used produce 64.6 GBq of ^{43}Sc and 163 GBq of ^{47}Sc when impinged by a 40 MeV 200 μA proton beam for five days. Finally, Gadolinium Boride targets impinged by a 70 MeV 100 μA proton beam, can provide, after five days of irradiation, 36.5 GBq of ^{149}Tb, 1.12 TBq of ^{152}Tb and 1.09 TBq of ^{155}Tb.

Concerning the phases involving the ionization, mass separation, and collection on a proper target, tests with the stable counterparts of the desired nuclides were performed at the offline Front End, an apparatus reproducing the part of the SPES accelerator system that will be adopted also for ISOLPHARM. Thus stable Silver and Copper beams were successfully extracted and collected, providing an ionization efficiency factor of roughly 15% and 10% respectively, whereas tests with Scandium and Terbium suffered of bad volatility, thus other ionization strategies will be adopted. Ongoing upgrades of the apparatus will allow anyway to improve such results. It was also possible to demonstrate the capability to collect simultaneously and independently couples of stable isotopes of the same element, result that is particularly relevant in the case of the theranostic pairs ^{64}Cu/^{67}Cu and ^{43}Sc/^{47}Sc that are produced by the same target.

For the estimation of the release process, a novel code base on the Geant4 toolkit is being developed and very preliminary results were produced. However, such simulations are computing intensive, thus a dedicated cloud computing infrastructure was developed in the CloudVeneto environment, a service owned by INFN and UNIPD. Anyway, for long lived nuclei, as most of those employed in nuclear medicine, the release shouldn’t be an issue, since the half-life is generally widely longer than the release time.

Generally, ISOLPHARM can be considered as a test bench for evaluating the capability to develop new carrier-free radionuclides exploiting the nuclei producible with the ISOL technique. Indeed, as one of the application of SPES facility, ISOLPHARM beam time will be limited by the scheduled physics program. This will not be an issue, since for preclinical studies only little amounts of radionuclides are necessary, thus, for example, the irradiation during the weekends could be enough. Once the concept is proven, other ISOL facilities may be interested

in scheduling the production of medical nuclides with solutions similar to those adopted in Legnaro.

In addition, an increasing number of research institutions and production facility are being equipped with similar proton driver machines, thus the technologies developed for ISOLPHARM could be potentially replicated elsewhere, more easily than in the case of higher energy facilities.

Appendix A

Possible ISOL radionuclides of medical interest

"Melius est abundare quam deficere."

"Better too much than not enough"

Latin proverb (Anonymous).

A.1 Introduction

As already presented, the ISOLPHARM method can be used to develop new carrier-free radiopharmaceuticals exploiting the nuclei producible with the ISOL technique.

Since the latter method foresee the release of the desired nuclide through the diffusion and effusion processes, only non-refractory elements could be easily extracted from the target. Anyway, among the possible ISOL beams, a remarkable variety of nuclides can be found, many of which showing interesting decay properties in terms of half-life and decay radiations, thus their potential medical application can be studied. The strength point of ISOL is the possibility to produce any of them in carrier-free form, thus opening the possibility to study new radionuclides that were never considered, for the difficulties of producing them with acceptable purity, exploiting the conventional techniques.

The following table summarizes the identified nuclides with an effective of potential use in nuclear medicine, that can be produced with the ISOL technique, once a proper production target is identified.

A.2 List of ISOL producible nuclides of potential medical interest

Isotope	Half-life	Decay Radiations									
	$t_{1/2}$	α		β-		β+/ϵ		γ		Auger	
^{43}Sc	3,891 h	/	/	/	/	100%	β+	22.50%	373 keV	8.93%	3,3 keV
^{44}Sc	3,97 h	/	/	/	/	100%	β+	99.90%	1157 keV	4.14%	3,3 keV
^{47}Sc	3,3492 d	/	/	100%	0,6 MeV	/	/	68.30%	159 keV	0.22%	(4 keV)
^{64}Cu	12,701 h	/	/	38.50%	0,579 MeV	61.50%	β+	0.48%	(1345 keV)	22.51%	6,54 keV
^{67}Cu	61,83 h	/	/	100%	0,561 MeV	/	/	48.70%	184,577 keV	6.87%	7,03 keV
^{67}Ga	3,2617 d	/	/	/	/	100%	ϵ	16.64%	300 keV	60.70%	7,53 keV
^{73}Ga	4,86 h	/	/	100%	1,593 MeV	/	/	79.80%	297 keV	0.04%	(8,56 keV)
^{71}Ge	11,43 d	/	/	/	/	100%	ϵ	/	/	42.30%	8,56 keV
^{72}As	26,0 h	/	/	/	/	100%	β+	81%	833,99 keV	5.56%	8,56 keV
^{74}As	17,77 d	/	/	34.20%	1,352 MeV	66.20%	β+	0.29%	(1204 keV)	14.50%	8,56 keV
^{77}As	38,83 h	/	/	100%	0,683 MeV	/	/	1.59%	239 keV	0.06%	(9,67 keV)
^{77}Br	57,036 h	/	/	/	/	100%	β+	2.08%	817 keV	35.30%	9,67 keV
^{79}Kr	35,04 h	/	/	/	/	200%	β+	1.26%	831,97 keV	30.60%	10,2 keV
^{86}Rb	18,642 d	/	/	99.99%	1,776 MeV	0.01%	ϵ	8.64%	1077 keV	0.01%	(10,8 keV)
^{89}Sr	50,53 d	/	/	100%	1,5 MeV	/	/	/	/	/	/
^{86}Y	14,74 h	/	/	/	/	100%	ϵ	93.80%	208,1 keV	1.36%	12,7 keV
^{87}Y	79,8 h	/	/	/	/	100%	β+	89.80%	484,80 keV	31.10%	12,1 keV
^{90}Y	64,053 h	/	/	100%	2,28 MeV	/	/	/	/	0.00%	(13,4 keV)
^{111}Ag	7,45 d	/	/	100%	1,036 MeV	/	/	6.70%	342 keV	0.04%	(19,3 keV)
^{122}Sb	2,7238 d	/	/	97.59%	1,984 MeV	2.41%	β+	70.67%	564 keV	0.29%	(21 keV)
^{124}I	4,1760 d	/	/	/	/	100%	β+	11.15%	1691 keV	8.30%	22,7 keV
^{125}I	59,407 d	/	/	/	/	100%	ϵ	6.68%	35,49 keV	19.80%	22,7 keV
^{126}I	12,93 d	/	/	47.30%	1,258 MeV	52.70%	β+	32.90%	666,33 keV	5.53%	22,7 keV
^{130}I	12,36 h	/	/	100%	2,949 MeV	/	/	11.30%	1157 keV	0.19%	(24,6 keV)
^{131}I	8,0252 d	/	/	100%	0,970 MeV	/	/	81.50%	364 keV	0.68%	(24,6 keV)
^{133}Xe	5,2475 d	/	/	1	0,427 MeV	/	/	0.369	80,99 keV	5.67%	25,5 keV
^{129}Cs	32,06 h	/	/	/	/	100%	β+	30.60%	371,92 keV	13.10%	24,6 keV
^{131}Cs	9,689 d	/	/	/	/	100%	ϵ	/	/	9.30%	24,6 keV
^{132}Cs	6,480 d	/	/	1.87%	1,279 MeV	98.13%	β+	1.58%	464 keV	9.40%	24,6 keV
^{136}Cs	13,04 d	/	/	100.00%	2,548 MeV	/	/	80.00%	1048 keV	1.24%	26,4 keV
^{152}Tb	17,5 h	/	/	/	/	100%	β+	3.00%	974 keV	4.80%	34,9 keV
^{155}Tb	5,32 d	/	/	/	/	100%	ϵ	1.48%	367,36 keV	7.90%	34,9 keV
^{156}Tb	5,35 d	/	/	/	/	100%	ϵ	12.20%	1422 keV	8.10%	34,9 keV
^{161}Tb	6,89 d	/	/	100%	0,593 MeV	/	/	10.20%	75 keV	1.46%	37,2 keV
^{165}Er	10,36 h	/	/	/	/	100%	ϵ	/	/	4.80%	38,4 keV
^{169}Er	9,392 d	/	/	100%	0,351 MeV	/	/	0.00%	109,77 keV	0.00%	(5,67 keV)
^{167}Tm	9,25 d	/	/	/	/	100%	ϵ	1.61%	531,54 keV	5.80%	39,7 keV
^{171}Lu	8,24 d	/	/	/	/	100%	β+	2.55%	853,091 keV	6.90%	42,2 keV
^{172}Lu	6,70 d	/	/	/	/	100%	β+	2.16%	1621,92 keV	6.10%	42,2 keV
^{177}Lu	6,647 d	/	/	100%	0,498 MeV	/	/	21.30%	418,5 keV	0.29%	44,8 keV
^{194}Au	38,02 h	/	/	/	/	100%	β+	3.81%	2043,68 keV	3.40%	51 keV
^{196}Au	6,17 d	/	/	7%	0,687 MeV	93%	ϵ	87.00%	355,73 keV	3.20%	52 keV
^{198}Au	2,69 d	/	/	100%	1,373 MeV	/	/	95.62%	411,8 keV	0.11%	(53,8 keV)
^{199}Au	3,139 d	/	/	100%	0,452 MeV	/	/	40.00%	158,38 keV	0.70%	(53,8 keV)

Isotope	Half-life	Decay Radiations									
	$t_{1/2}$	α		β-		β+/ϵ		γ		Auger	
^{201}Tl	3,04 d	/	/	/	/	100%	ϵ	94.80%	588 keV	0.52%	(55,2 keV)
^{202}Tl	12,31 d	/	/	/	/	100%	ϵ	91.50%	439,5 keV	3.10%	53,8 keV
^{203}Pb	51,92 h	/	/	/	/	100%	ϵ	15.30%	1027 keV	1.57%	56,7 keV
^{206}Bi	6,243 d	/	/	/	/	100%	β+	31.90%	1718 keV	4.20%	56,7 keV
^{223}Ra	11,43 d	100%	5,979 MeV	/	/	/	/	1.29%	455 keV	1.77%	62,7 keV
^{224}Ra	3,63 d	100%	5,788 MeV	/	/	/	/	4.10%	241 keV	0.02%	(62,7 keV)
^{225}Ac	10 d	100%	5,935 MeV	/	/	/	/	1.00%	99 keV	17.00%	8,9 keV
^{226}Ac	29,37 h	0.00%	5,536 MeV	83%	1,117 MeV	17%	ϵ	26.90%	230 keV	0.41%	(65,9 keV)
^{227}Th	18,68 d	100%	6,146 MeV	/	/	/	/	1.14%	334 keV	/	/

A.3 Conclusions

As shown in the presented list, a wide variety of nuclides of potential medical interest can be produced with the ISOL technique. Such list is not intended to be exhaustive, since other nuclides might be identified as suitable for radiolabelling of pharmaceutical compounds.

In addition, the development of the technologies related to the ionization and transport of molecular beams can potentially open the possibility of including the refractory elements among the ISOL producible nuclei.

Appendix B

Secondary Target Unit Prototypes for ISOLPHARM

"Mejo un tacon, che un sbregon."

"Better a patch than a rip"

Venetian proverb (in Venetian dialect) cited in *Ozio, industria, lavoro, vol. 2, pp. 161-167,* C. Pasqualigo

B.1 Introduction

In the framework of ISOLPHARM, preliminary deposition tests were performed using as collection target station a modified diagnostic box of the existing offline Front End. However, when the SPES facility will be operating, such temporary solution will not be usable, for evident radioprotection and safety issues. Thus, a novel solution for the coupling of the collection target with SPES beamlines had to be studied. Differently from MEDICIS, that used metal coating on a small plates [B.1], the deposition substrate at ISOLPHARM will be a soluble salt disk, characterized by a diameter of 40 mm or 13 mm to limit the solvent volume required for its dissolution, thus increasing the radionuclide concentration for the pre-radiopharmaceutical preparation [B.2]. In addition to such constraints, additional requirements for the development of the ISOLPHARM Secondary Target Unit were its light weight and transportability in order to simplify the procedures required for its collocation within the hot-cell for radiochemical processes, and the capability to reasonably shield the radiation coming from the collected nuclei, in order to minimize the radioactive dose delivered to personnel.

The device developed for ISOLPHARM is presented in detail in the following appendix, along with another prototypical version, developed for the early stages of operation at SPES, where very low amounts of radionuclides will be collected.

B.2 The Secondary Target Unit prototype

The Secondary Target Unit being developed for ISOLPHARM consists in a small self-shielded aluminum vacuum chamber that could be adapted for hosting both collection substrate sizes [B.3]. The designed STU, represented in figure B.1 is mainly composed by two cylindrical shells closed by four screws. It has an average diameter of approximately 12 cm and a total length of 15 cm. Its weight is around 5 kg.

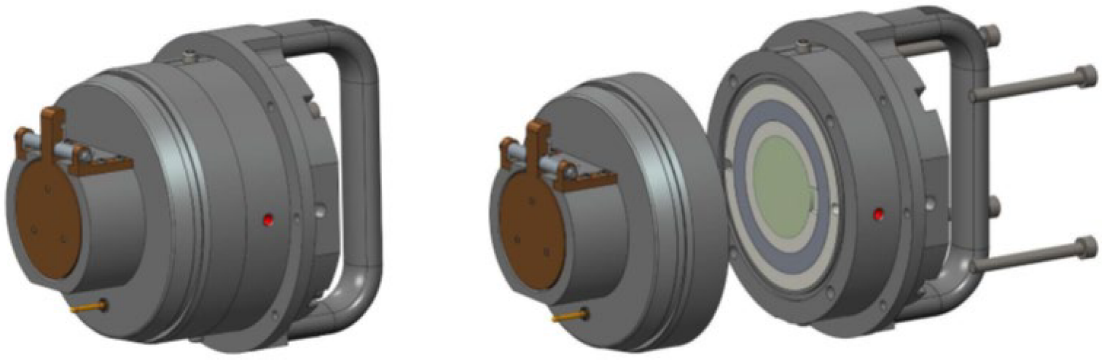

Figure B.1: *overview of the developed Secondary Target Unit* [B.3]

The right shell of the STU is composed by several concentric components, as shown in figure B.2. The component labelled with 7 is made up of polyethylene and is devoted to hold the secondary target (8). It can be replaced according to the target size. 6 is Tungsten shield devoted to attenuating or stopping the radiation coming from the irradiated target, and its thickness could be increased by replacing the polyethylene component 5 with tungsten, if energetic γ emitters are collected. All aforementioned components are hosted within an aluminum alloy vacuum chamber (4) equipped with a handle (3), for its manual transport. The different components are bound through few screws (1, 2, 8)

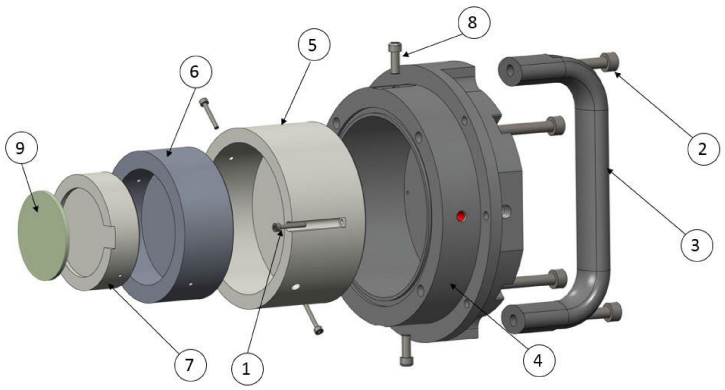

Figure B.2: *overview of the right shell of Secondary Target Unit* [B.3]

Figure B.3 represent the left part of the STU: as for the right part a polyethylene component (4) is devoted to the holding of the collection target. In addition, a copper conductive ring (5) is interposed between the collection target and its holder, allowing to detect instantaneously if the collection is taking place, and to estimate the collected amount by integrating in time the impinging beam current intensity. Such copper ring is wired with an electrical connector (14) for the transmission of the current signal. Radiation coming from the target is shielded by means of a Tungsten component (3), that can be increased in size if required by removing the polyethylene component 2. The vacuum aluminum alloy chamber (1), hosting the aforementioned components is equipped also with a shutter (8-9-10-11-12-13). Such component was designed to automatically open the STU when coupled with the beamline, as shown in figure B.4. In addition, the presence of a torsion spring (11) ensures its closure upon uncoupling the STU. The various components are jointed with threaded fastenings.

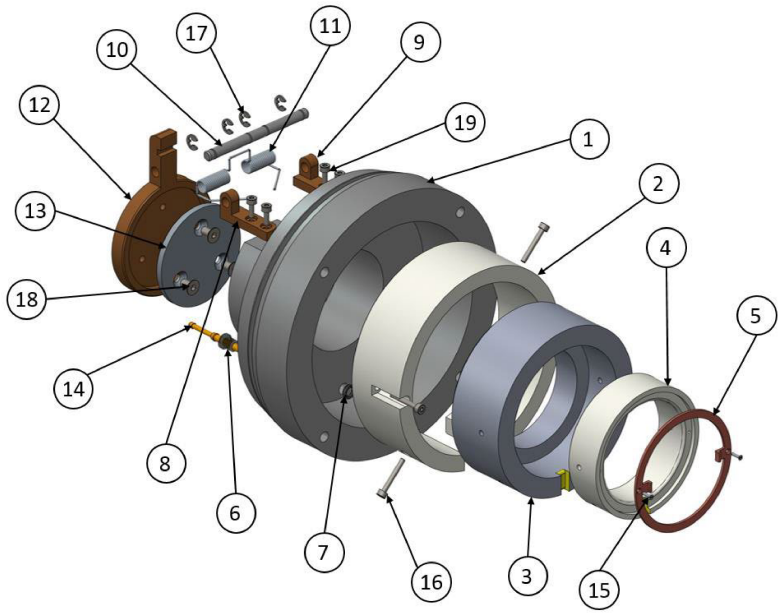

Figure B.3: *overview of the left shell of Secondary Target Unit* [3]

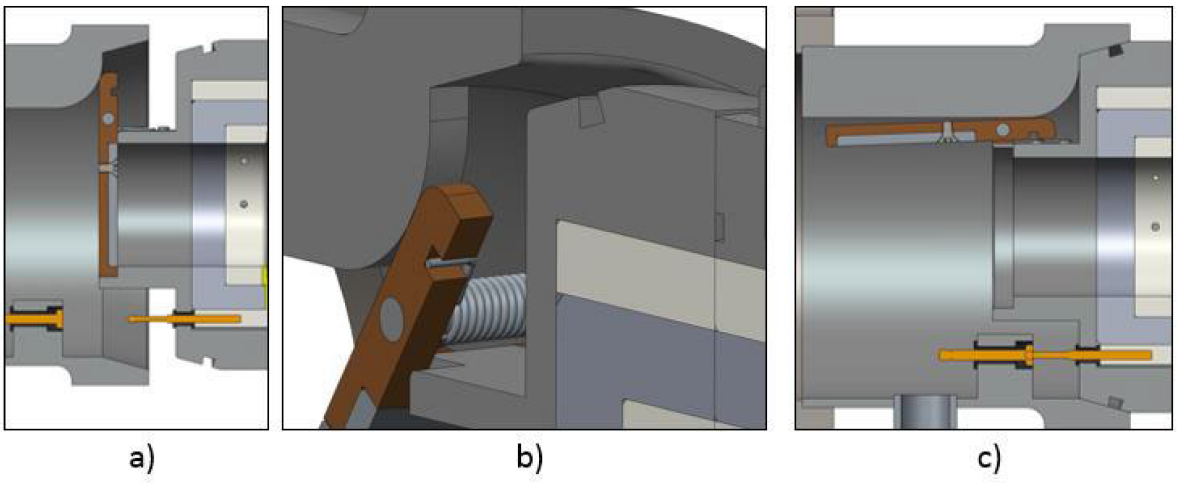

Figure B.4: *the coupling of the STU with the beamline. The automatic aperture of the shutter is highlighted* [3]

According to the presented design a preliminary prototype was manufactured (figure B.5) and is currently in testing phase to evaluate eventual improvements and modifications to be implemented.

Figure B.5: *the Secondary Target Unit Prototype* [B.3]

B.3 The Collection Target Unit for offline operation and very low activities

In addition to the presented STU, an improvement of the existing offline solution, that foresee the employment of a modified Faraday Cup, was further developed to simplify the recovery of the collection target [B.3].

Figure B.6 represent the new developed version for such device: the standard Faraday Cup, normally attached to the support stem (4) with bolts is replaced by a Tungsten cup holding the collection target (1). The coupling with the support stem is provided by a newly designed boltless joint, inserted from above.

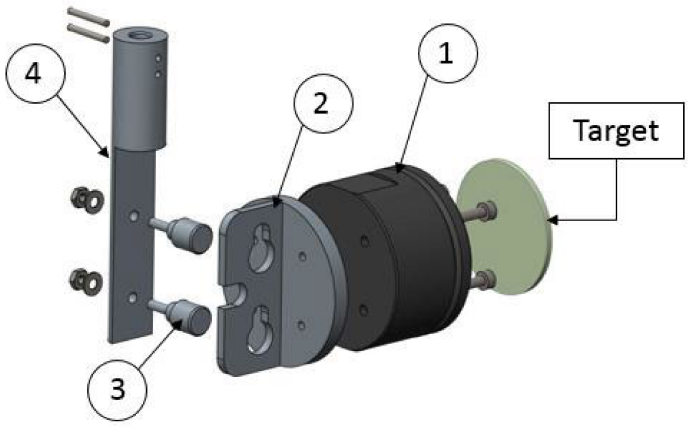

Figure B.6: *the Collection Target Unit designed for the offline tests and early collections of very low activities* [B.3]

Such device could be used also for the very early stages of ISOLPHARM, when very small amounts of radionuclides are collected for the performance of *in vitro* studies.

With such aim, a tool was designed in order to reduce the dose exposure of personnel, when retrieving the collection target. In particular, as showed in figure B.7 such tool includes a Tungsten cup, that can be coupled with the target holder, and a lever, both aimed to mitigate the radiological risk.

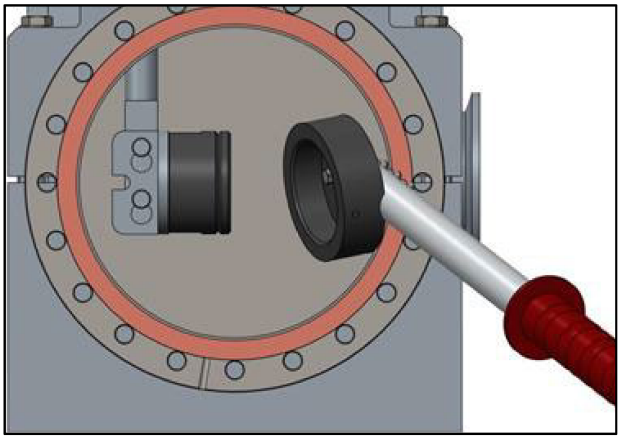

Figure B.7: *the uncoupling of the Collection Target Unit using the specifically designed tool* [B.3]

B.4 Conclusions

In this appendix, the devices designed for holding the collection targets were presented in detail. Since the manufacturing and test phases of the first prototypes is ongoing, eventual design improvements may be implemented. In particular, major changes are foreseen if the simultaneous deposition of two or more different radioisotopes is desired, since the current design was developed for the collection of a single radionuclide.

B.5 References

[B.1] A. Brown and T. E. Cocolios, “Design of the CERN MEDICIS Collection and Sample Extraction System.” 2015.

[B.2] F. Borgna *et al.*, “Early Evaluation of Copper Radioisotope Production at ISOLPHARM,” *Molecules*, vol. 23, no. 10, 2018.

[B.3] S. Popa, “Analisi e Progettazione di un Sistema di Contenimento e Movimentazione di un Bersaglio per la Raccolta di Isotopi Radioattivi di Interesse Medico,” Università di Padova, 2017.

Appendix C

Cross sections numerical evaluations for ^{nat}Ge(p, X) reactions

"Buon studio rompe, o vince rea fortuna."

"A good study stops or even wins the hostile fate"

Italian porverb (Anonymous), *IV edition, Proverbi,* Accademia della Crusca.

C.1 Introduction

^{64}Cu and ^{67}Cu are an extremely interesting theranostic pair, and the possibility of their production according to the ISOLPHARM method was studied. In particular, a ZrGe target was considered and preliminary estimations of the producible amounts with such target material were performed with FLUKA [C.1]. Furthermore, in-target yields were calculated with different models with both FLUKA and Geant4, but the two Monte Carlo models produced different results. In addition in the EXFOR database [C.2] no experimental data for the reactions ^{nat}Ge(p,X)^{64}Cu and ^{nat}Ge(p,X)^{67}Cu in the energy range 0 -100 MeV were found, consequently it was not possible to assess the reliability of the various models by comparing them with experimental measurement. Thus, the MC code FLUKA was taken as reference and its results were compared with the data calculated by means of dedicated codes as TALYS [C.3].

For such study, in addition to the desired reactions ^{nat}Ge(p,X)^{64}Cu and ^{nat}Ge(p,X)^{67}Cu other reactions such as ^{nat}Ge(p,X)^{65}Zn, ^{nat}Ge(p,X)^{65}Ga and ^{nat}Ge(p,X)^{67}Ga were considered, since for some of them experimental data were found in the EXFOR database. The leading idea is that reactions providing products close to the desired nuclides, and thus similar to the targeted ones, could be used to benchmark the various models, and the so-obtained results could be potentially expanded to prove the reliability of the models.

In particular, for each of the products considered in such study, the cross section calculations were performed for all natural isotopes of Germanium, namely ^{70}Ge (nat. abundance 20.52%), ^{72}Ge (nat. abundance 27.45%), ^{73}Ge (nat. abundance 7.76%), ^{74}Ge (nat. abundance 36.52%) and ^{76}Ge (nat. abundance 7.75%), and the final results for ^{nat}Get were calculated as the average of the single contributions of each stable Ge nuclide, considering the respective natural abundance as weight. Concerning FLUKA the cross sections were calculated in two different ways. Firstly, several simulations with a thin Ge (thickness 10 μm), in order to preserve the beam energy, were preformed and the cross section σ was calculated indirectly from the outputted yield according to the following relation:

$$\sigma = \frac{Y}{p}\frac{1}{tN_d} \tag{C.1}$$

Where Y/p is the specific yield as provided by FLUKA, namely the ratio between the number of the selected particles and the proton beam intensity in particles/s, t is the target thickness and N_d is the nuclear density in the target expressed in nuclei per volume unit.

Such simulations were performed with proton beam energy steps of 5 MeV, and FLUKA version 2011.2x.2 was used.

Secondly, the PEANUT model (FLUKA devel version 2018.0) was directly invoked [C.4]. Regarding TALYS, the data available in TENDL-2015 were originally considered [C.5]. However, since such data were not calculated with the current version, namely the 1.9, the cross sections were recalculated. In addition to the default model, a modified version was launched, since other works in literature [C.6], suggested that with such adjustment the reliability of the results could be increased. The data calculated according to the latter method will be referred TALYS mod in the figures.

In the following paragraphs all data produced in this study are reported for the sake of comparison.

C.2 Cross sections for the production of ^{64}Cu

In figures C.1, C.2, C.3, C.4 and C.5 are reported the cross sections for the reactions ^{70}Ge(p,X)^{64}Cu, ^{72}Ge(p,X)^{64}Cu, ^{73}Ge(p,X)^{64}Cu, ^{74}Ge(p,X)^{64}Cu and ^{76}Ge(p,X)^{64}Cu according to the different models. Such data were finally used to produce the plot for the ^{nat}Ge(p,X)^{64}Cu reaction, reported in figure C.6.

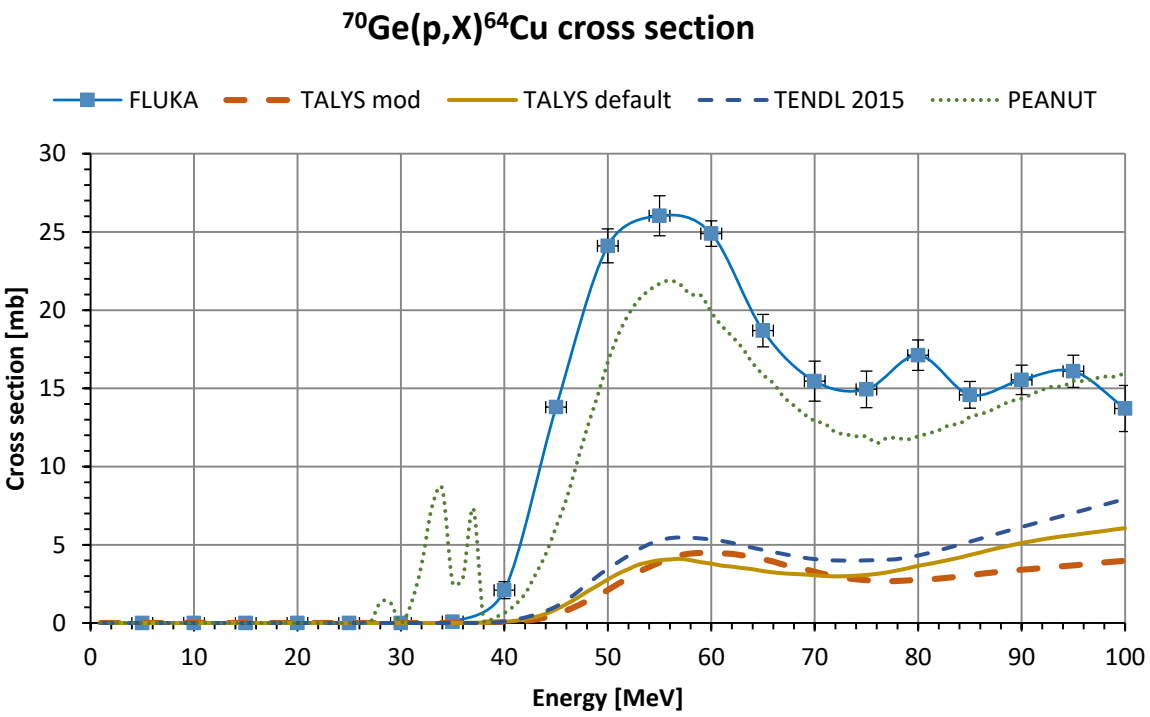

Figure C.1: *cross section for the $^{70}Ge(p,X)^{64}Cu$ reaction according to various models*

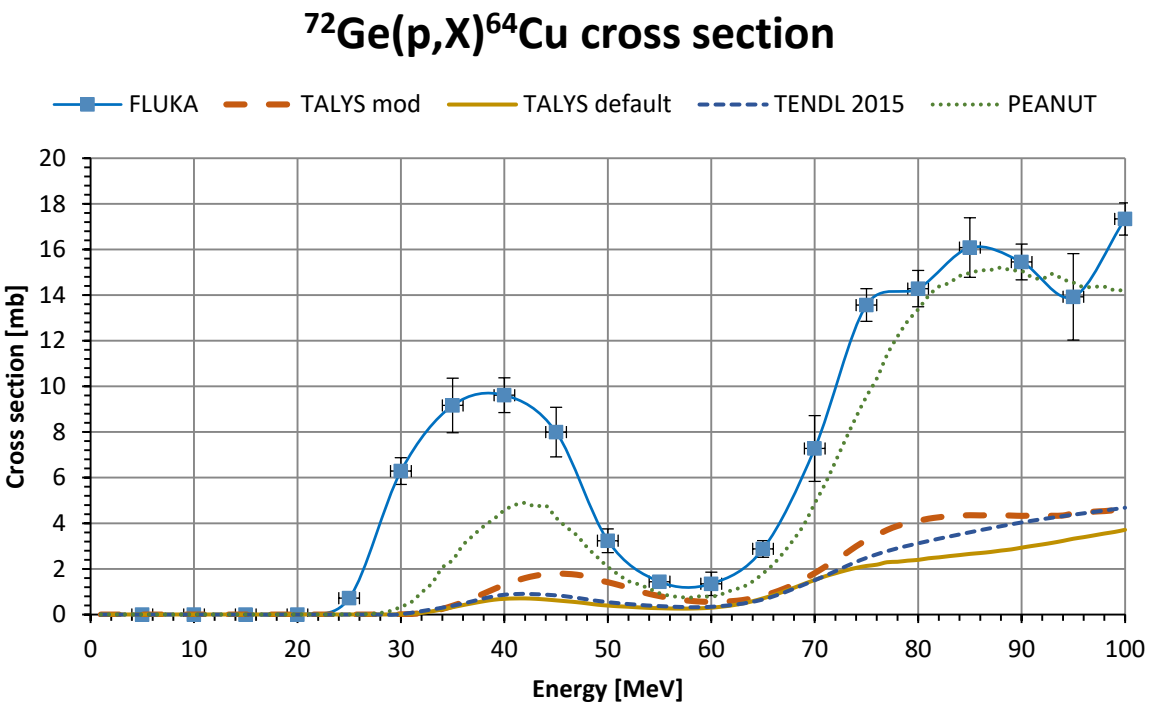

Figure C.2: *cross section for the $^{72}Ge(p,X)^{64}Cu$ reaction according to various models*

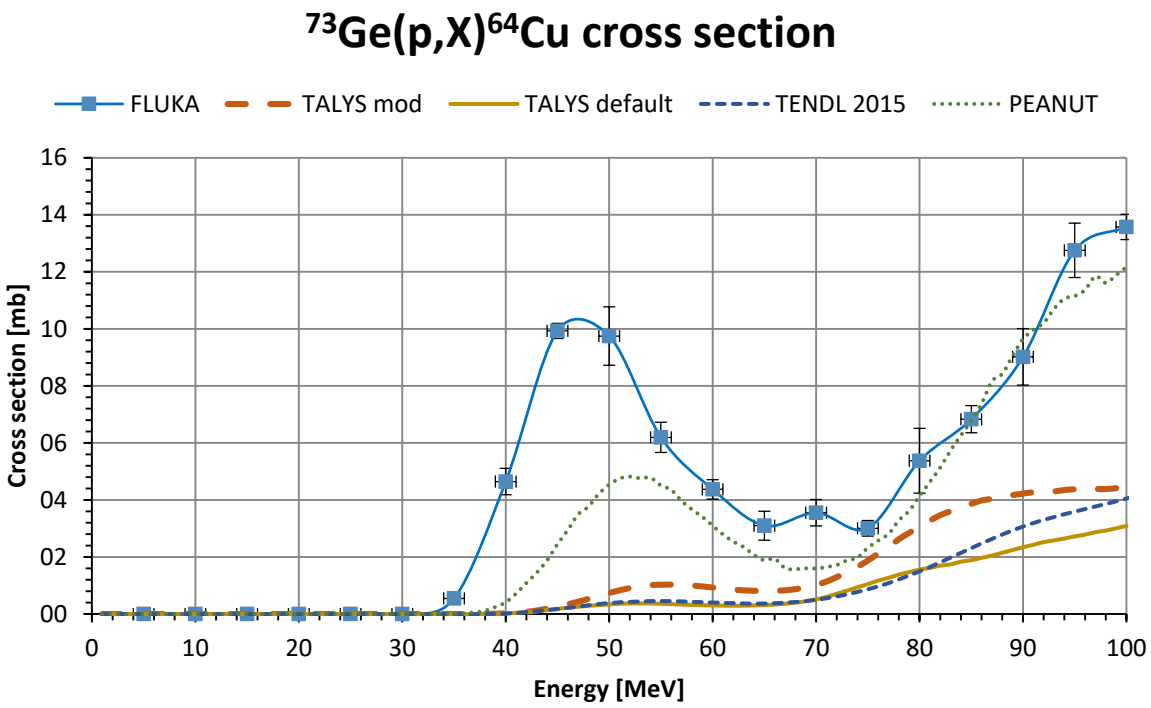

Figure C.3: *cross section for the $^{73}Ge(p,X)^{64}Cu$ reaction according to various models*

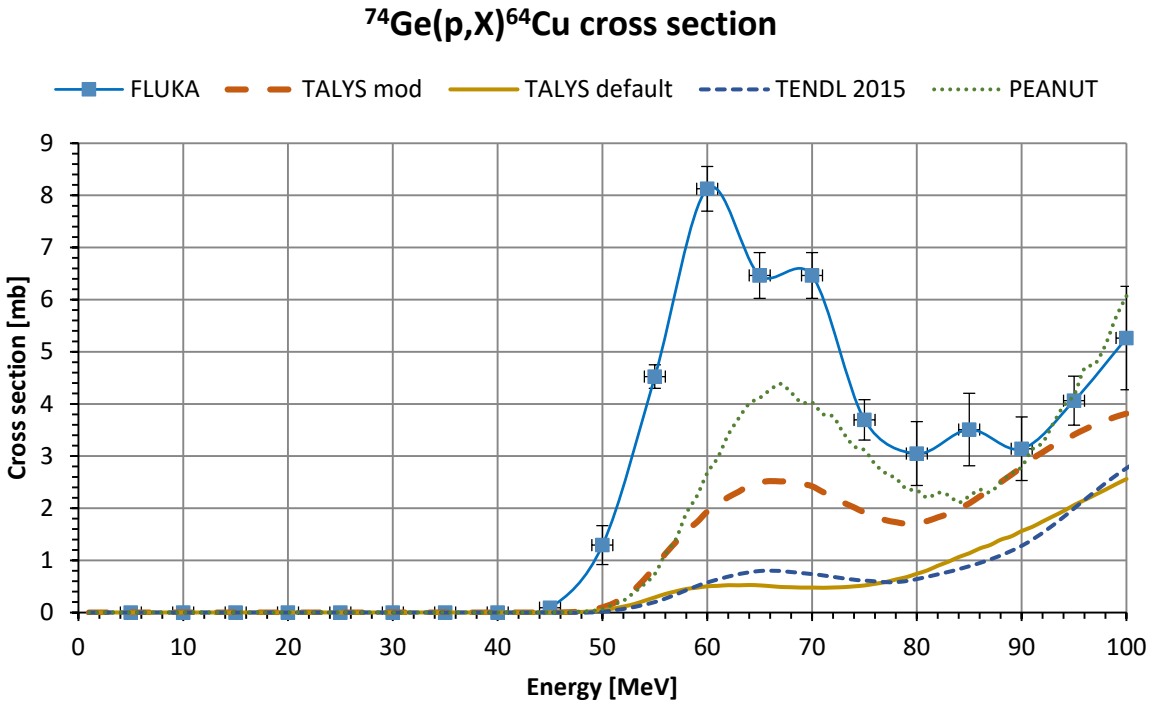

Figure 4.9: *cross section for the $^{74}Ge(p,X)^{64}Cu$ reaction according to various models*

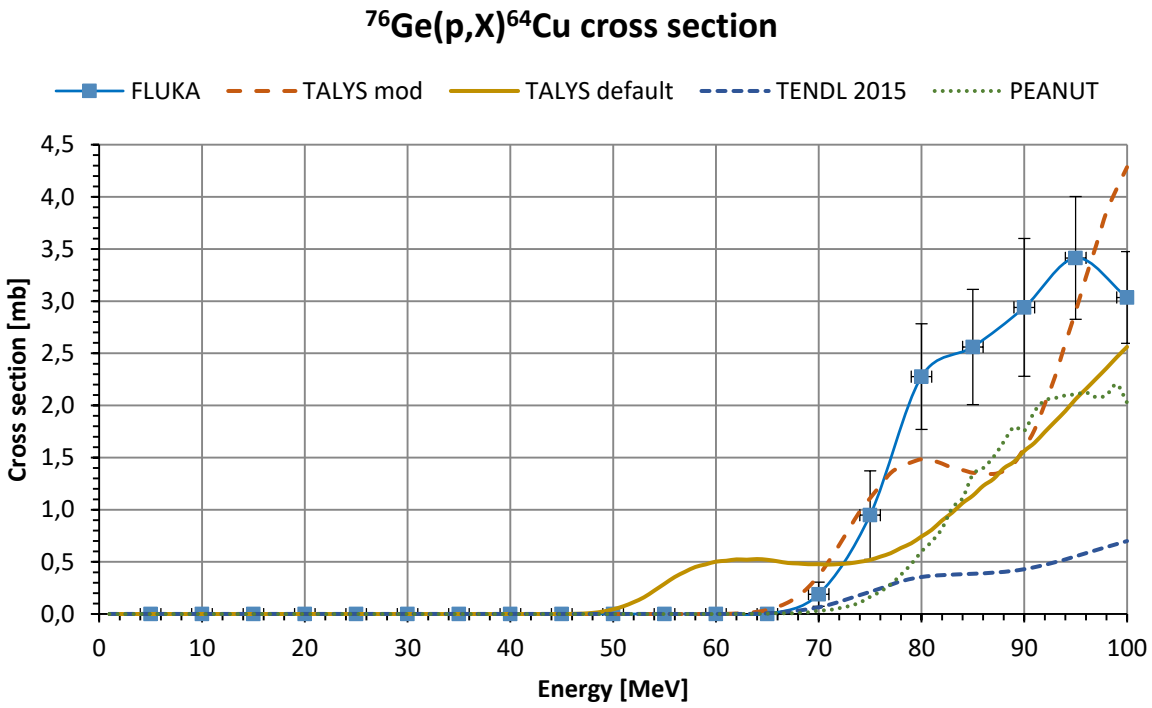

Figure C.5: *cross section for the $^{76}Ge(p,X)^{64}Cu$ reaction according to various models*

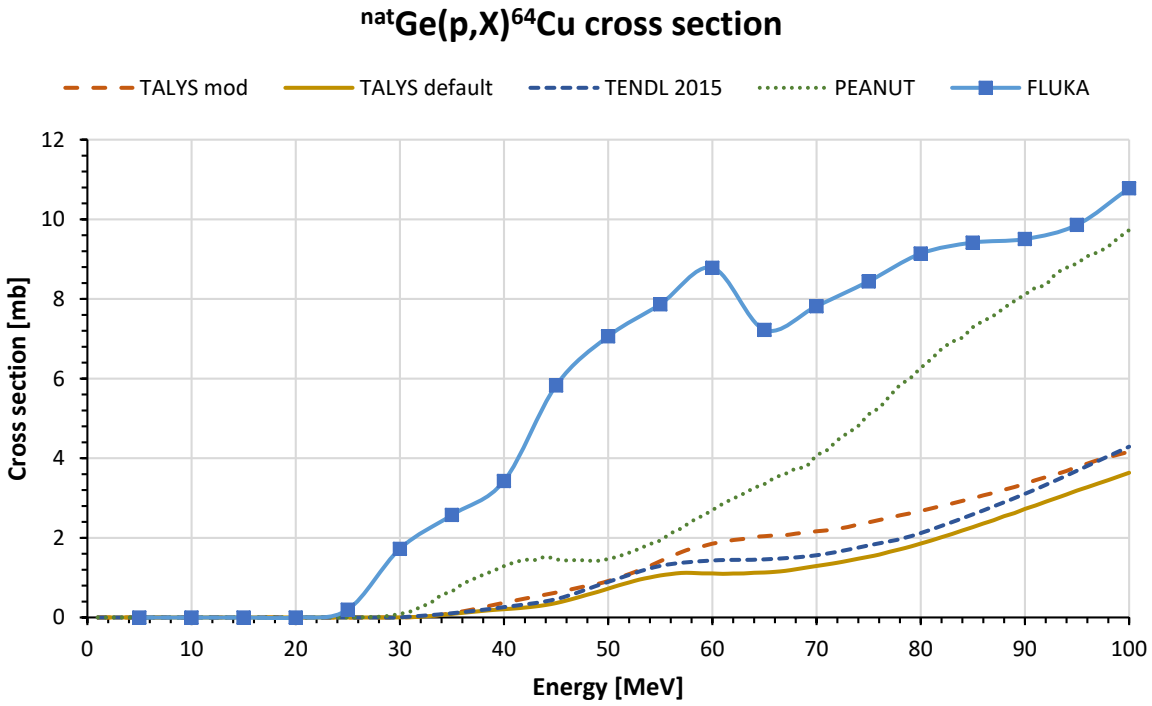

Figure C.6: *cross section for the $^{nat}Ge(p,X)^{64}Cu$ reaction according to various models*

C.3 Cross sections for the production of ^{67}Cu

In figures C.7, C.8, C.9, C.10 and C.11 are reported the cross sections for the reactions ^{70}Ge(p,X)^{67}Cu, ^{72}Ge(p,X)^{67}Cu, ^{73}Ge(p,X)^{67}Cu, ^{74}Ge(p,X)^{67}Cu and ^{76}Ge(p,X)^{67}Cu according to the different models. Such data were finally used to produce the plot for the ^{nat}Ge(p,X)^{64}Cu reaction, reported in figure C.12.

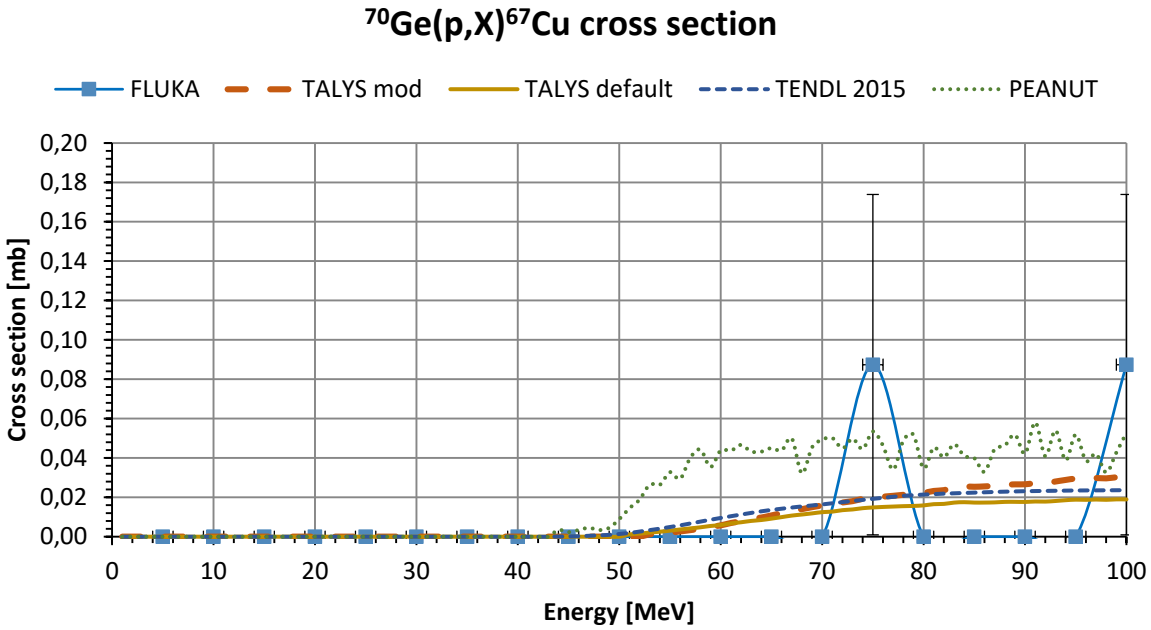

Figure C.7: *cross section for the ^{70}Ge(p,X)^{67}Cu reaction according to various models*

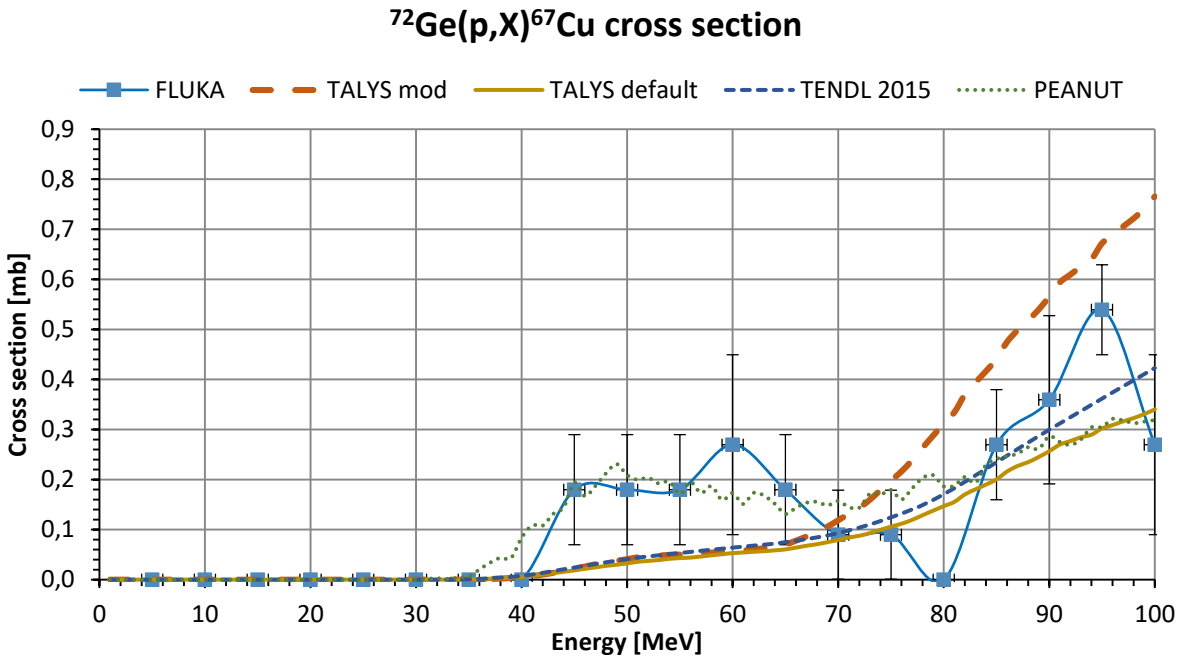

Figure C.8: *cross section for the ^{72}Ge(p,X)^{67}Cu reaction according to various models*

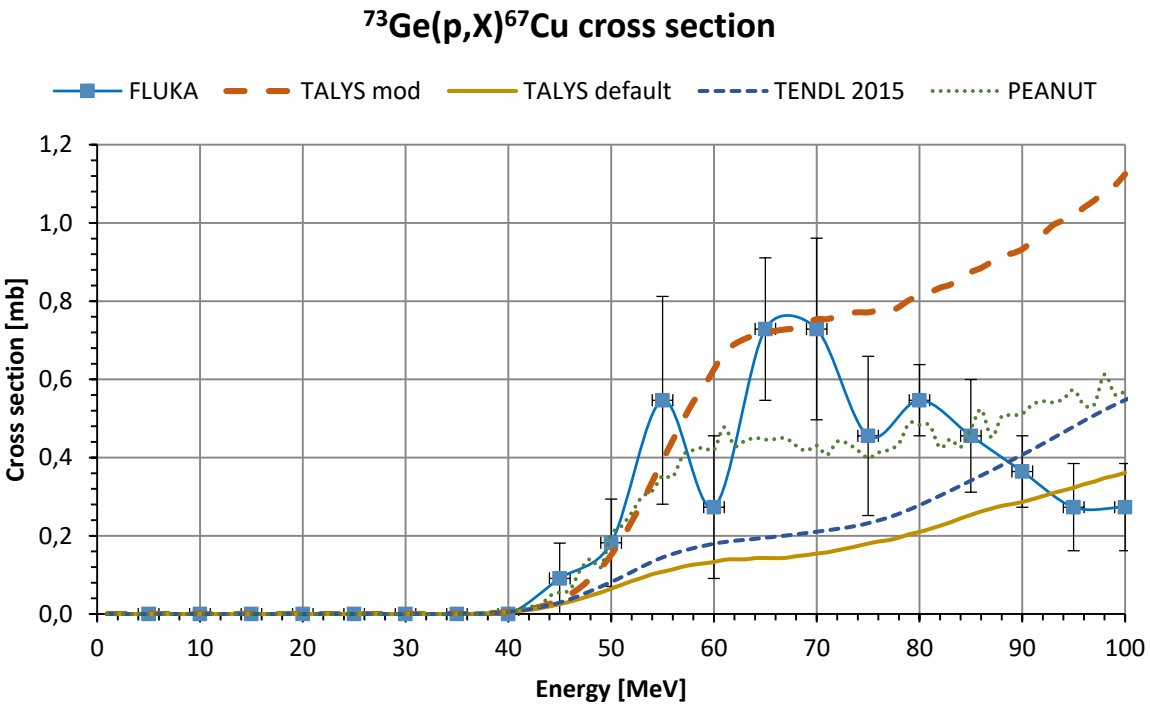

Figure C.9: *cross section for the $^{73}Ge(p,X)^{67}Cu$ reaction according to various models*

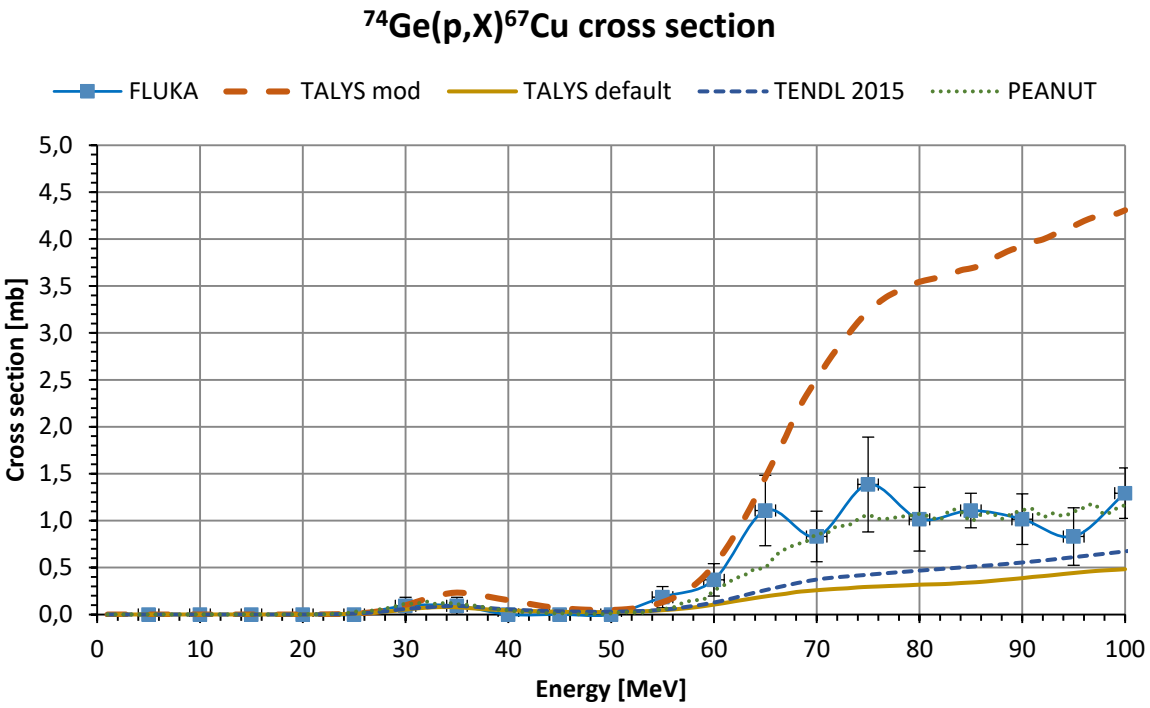

Figure C.10: *cross section for the $^{74}Ge(p,X)^{67}Cu$ reaction according to various models*

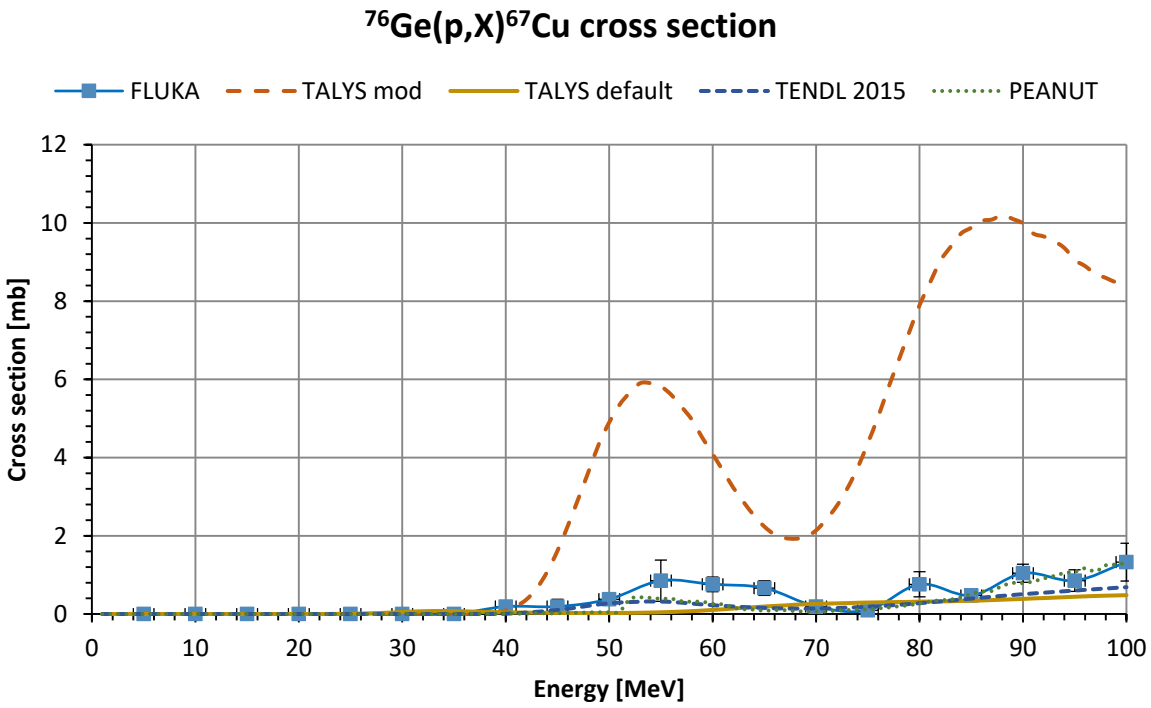

Figure C.11: *cross section for the $^{76}Ge(p,X)^{67}Cu$ reaction according to various models*

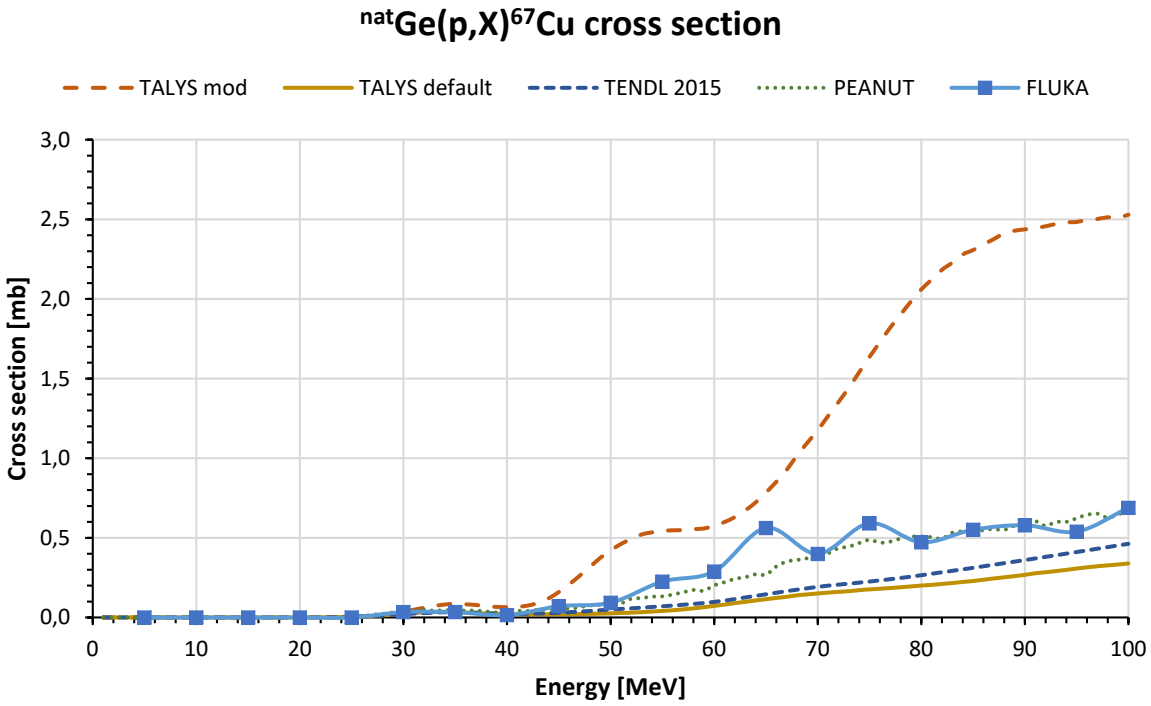

Figure C.9: *cross section for the $^{nat}Ge(p,X)^{67}Cu$ reaction according to various models*

C.4 Cross sections for the production of ^{65}Zn

In figures C.13, C.14, C.15, C.16 and C.17 are reported the cross sections for the reactions ^{70}Ge(p,X)^{65}Zn, ^{72}Ge(p,X)^{65}Zn, ^{73}Ge(p,X)^{65}Zn, ^{74}Ge(p,X)^{65}Zn and ^{76}Ge(p,X)^{65}Zn according to the different models. Such data were finally used to produce the plot for the ^{nat}Ge(p,X)^{65}Zn reaction, reported in figure C.18, compared with data found in EXFOR [C.7].

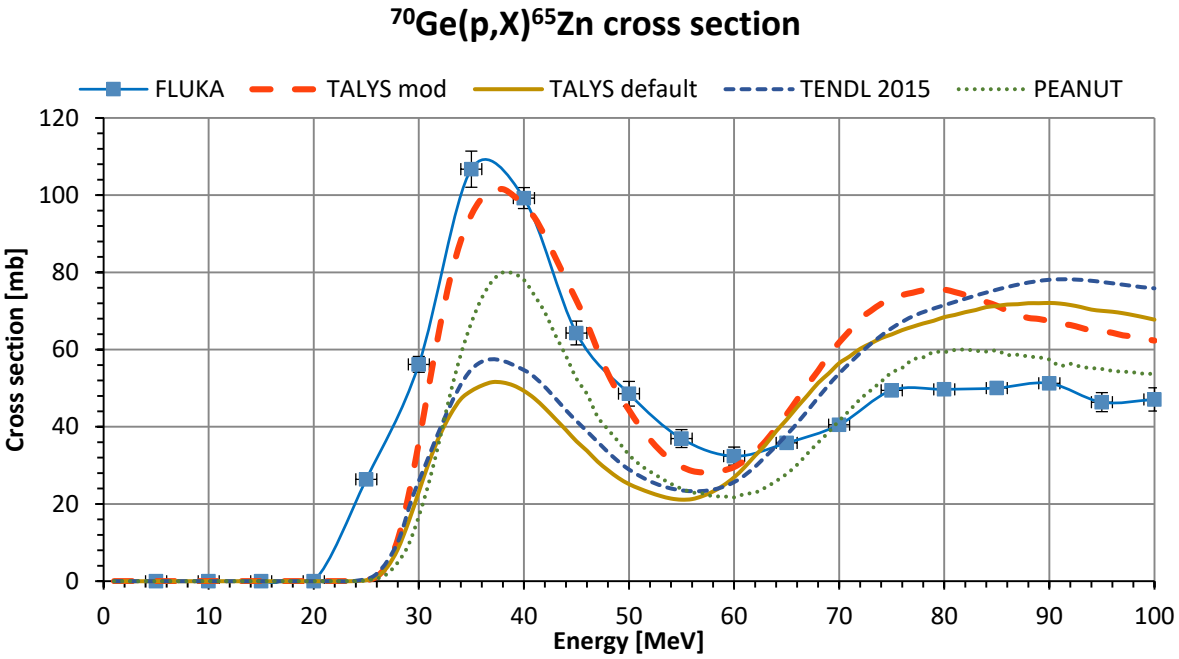

Figure C.13: *cross section for the ^{70}Ge(p,X)^{65}Zn reaction according to various models*

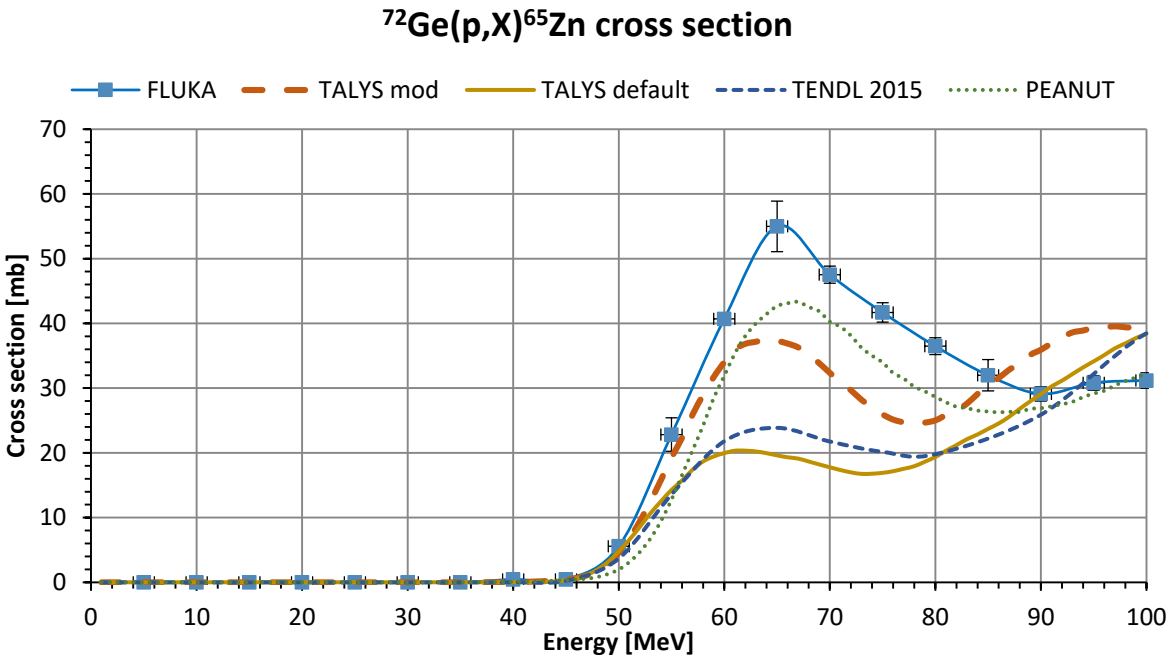

Figure C.14: *cross section for the ^{72}Ge(p,X)^{65}Zn reaction according to various models*

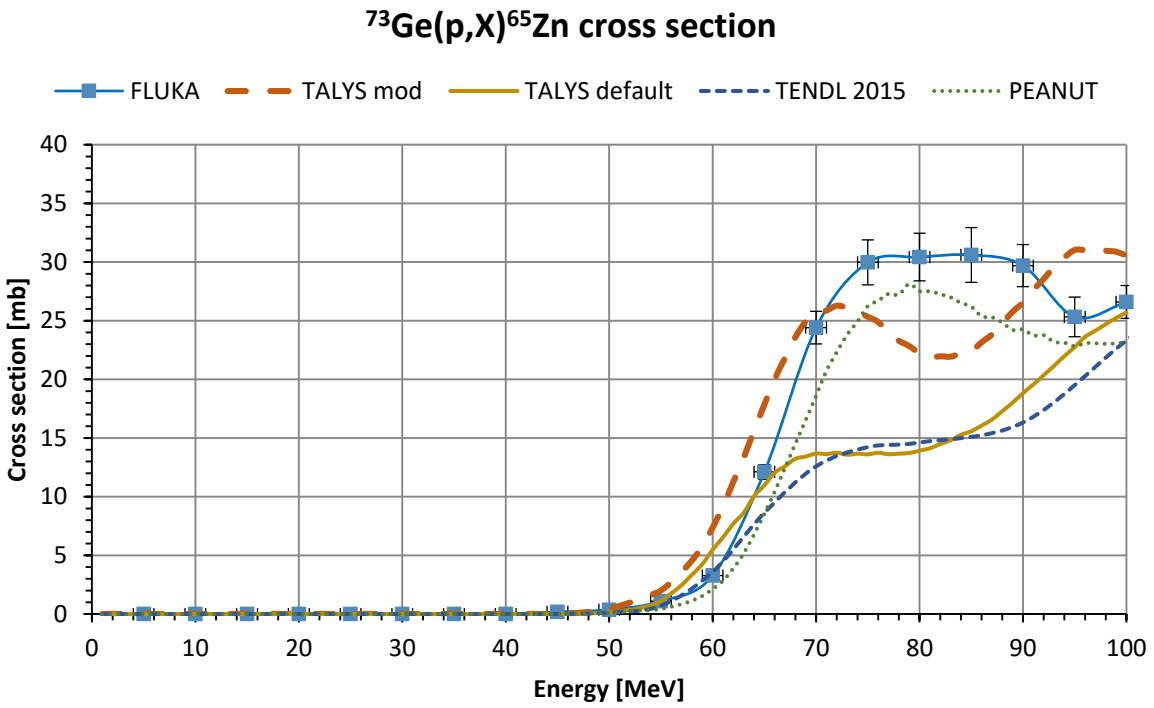

Figure C.15: *cross section for the $^{73}Ge(p,X)^{65}Zn$ reaction according to various models*

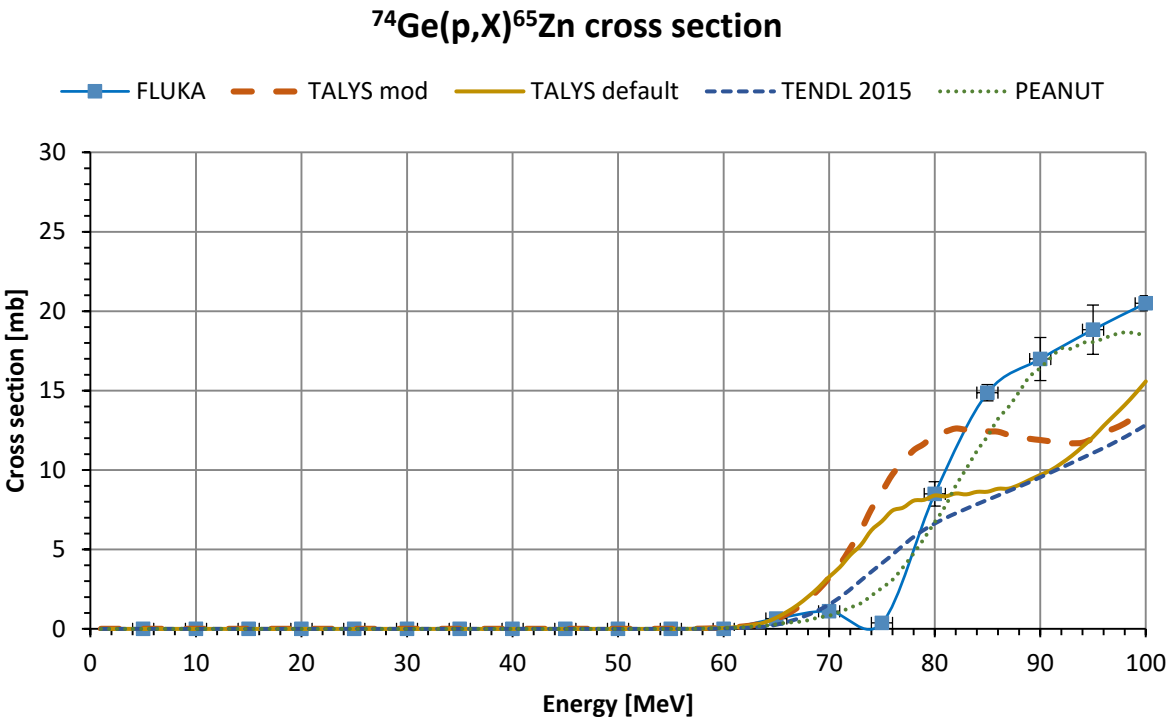

Figure C.16: *cross section for the $^{74}Ge(p,X)^{65}Zn$ reaction according to various models*

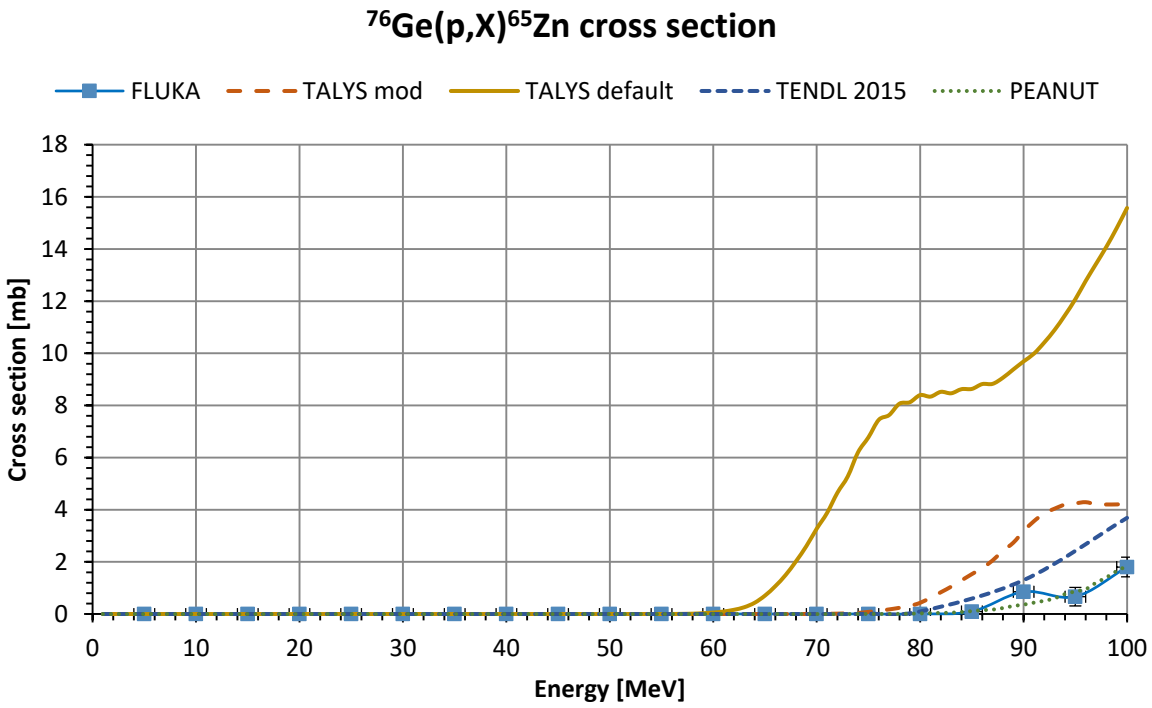

Figure C.17: *cross section for the $^{76}Ge(p,X)^{65}Zn$ reaction according to various models*

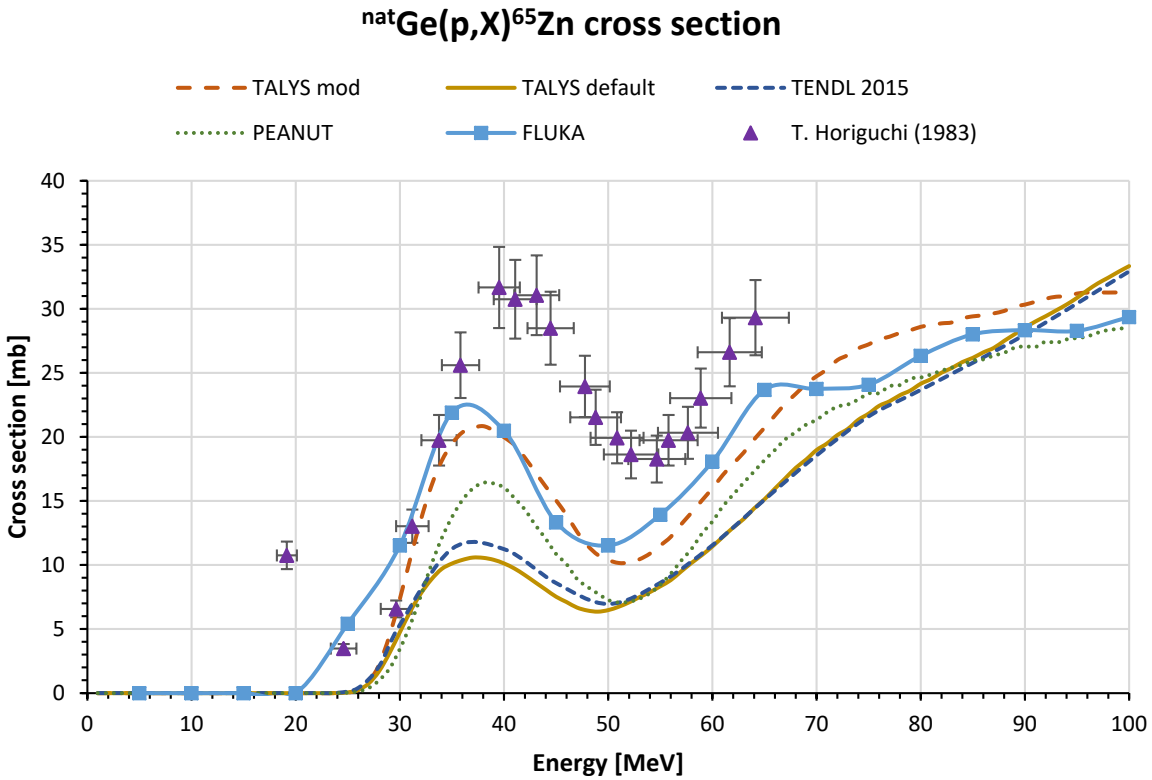

Figure C.18: *cross section for the $^{nat}Ge(p,X)^{65}Zn$ reaction according to various models and experimental data* [C.7]

C.5 Cross sections for the production of ^{65}Ga

In figures C.19, C.20, C.21, C.22 and C.23 are reported the cross sections for the reactions ^{70}Ge(p,X)^{65}Ga, ^{72}Ge(p,X) ^{65}Ga, ^{73}Ge(p,X) ^{65}Ga, ^{74}Ge(p,X) ^{65}Ga and ^{76}Ge(p,X) ^{65}Ga according to the different models. Such data were finally used to produce the plot for the ^{nat}Ge(p,X) ^{65}Ga reaction, reported in figure C.24, compared with data found in EXFOR [C.8].

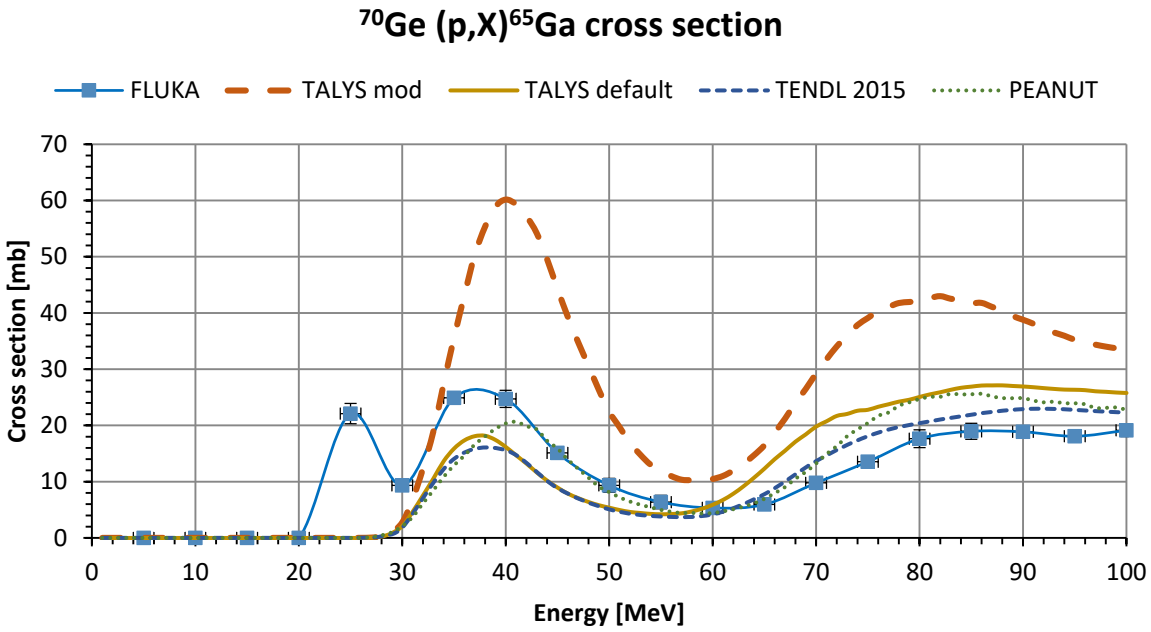

Figure C.19: *cross section for the ^{70}Ge(p,X)^{65}Ga reaction according to various models*

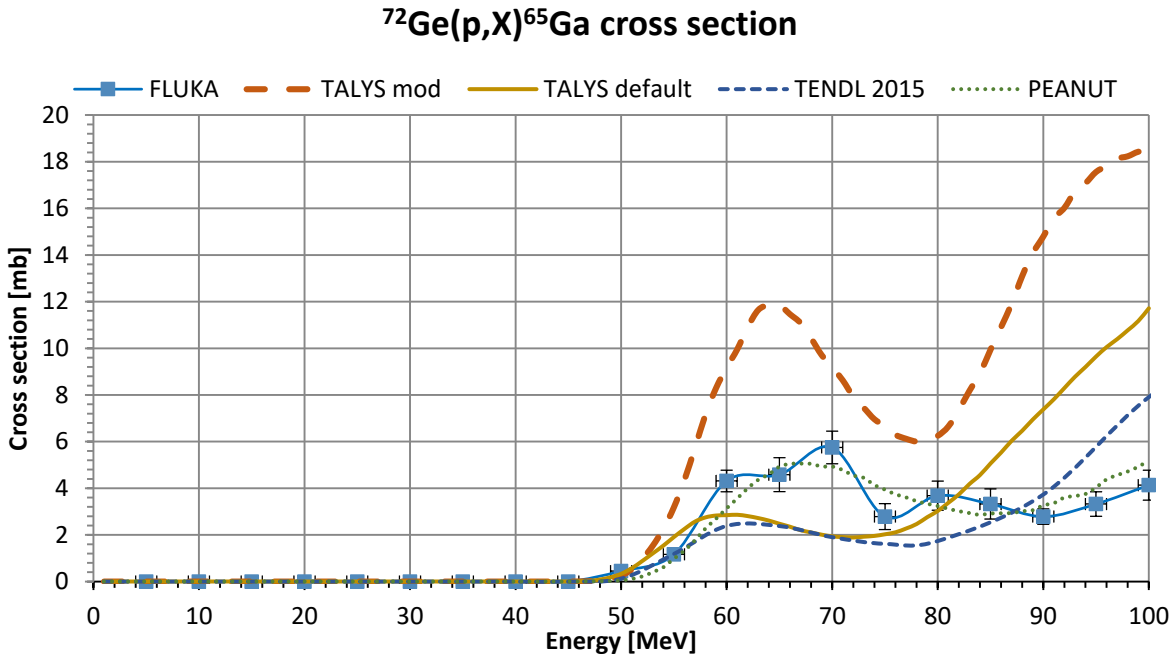

Figure C.20: *cross section for the ^{72}Ge(p,X)^{65}Ga reaction according to various models*

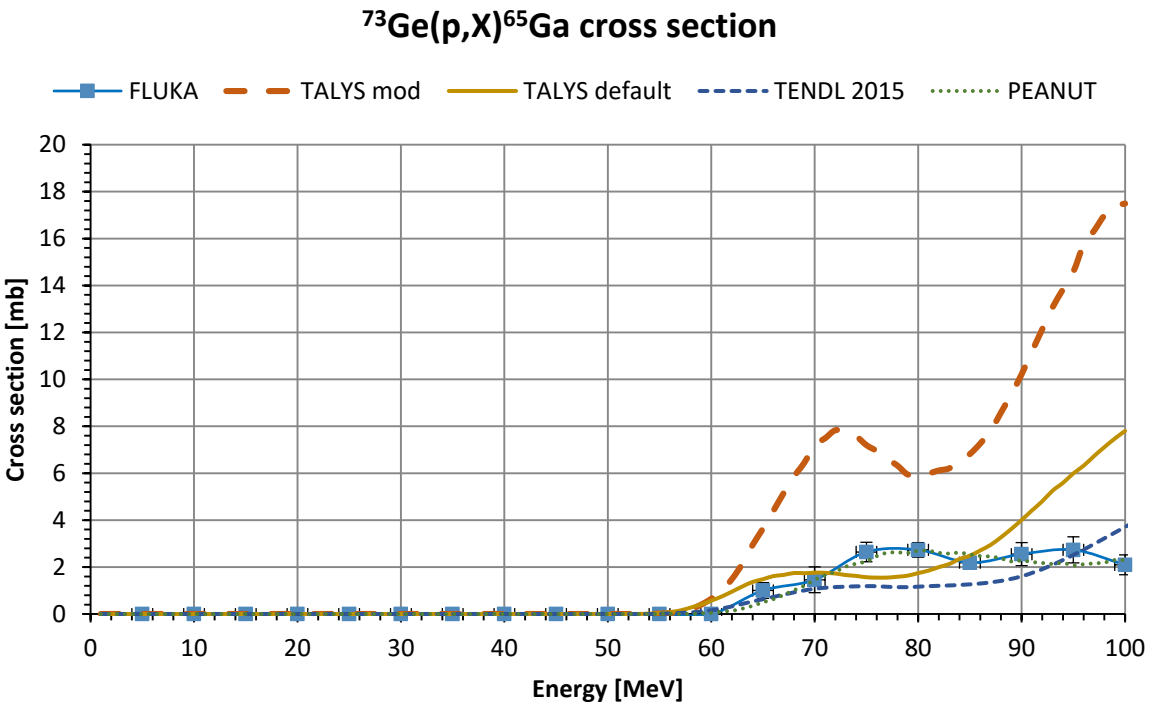

Figure C.21: *cross section for the $^{73}Ge(p,X)^{65}Ga$ reaction according to various models*

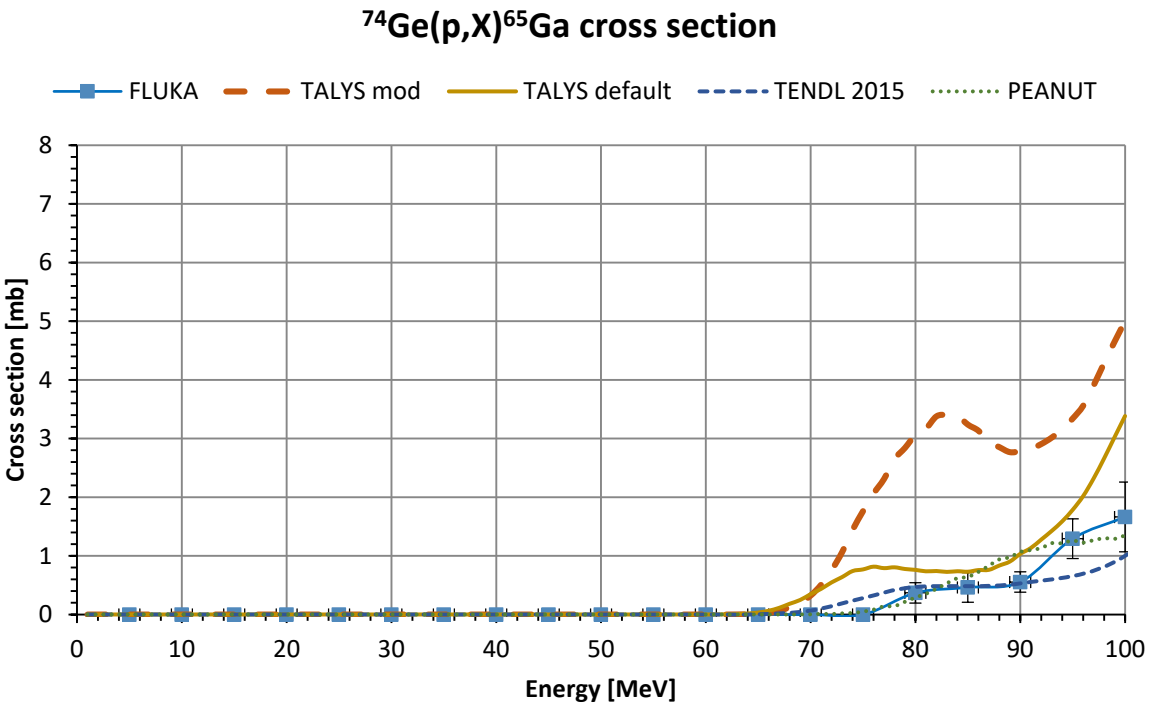

Figure C.22: *cross section for the $^{74}Ge(p,X)^{65}Ga$ reaction according to various models*

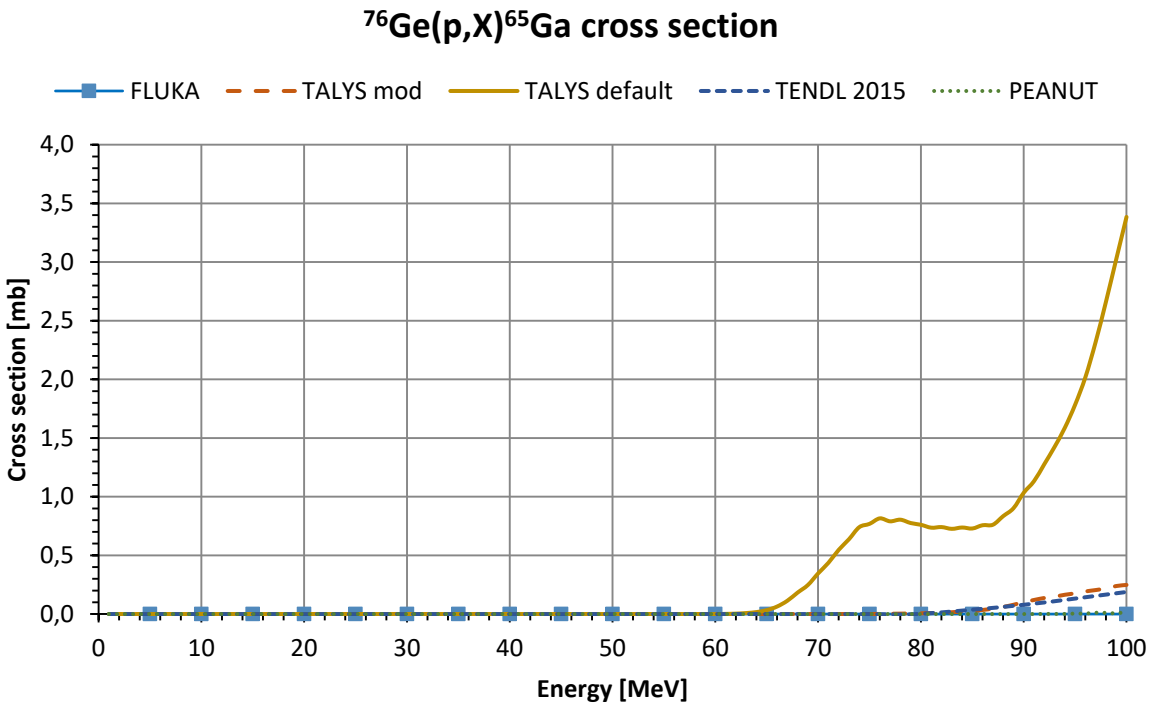

Figure C.23: *cross section for the $^{76}Ge(p,X)^{65}Ga$ reaction according to various models*

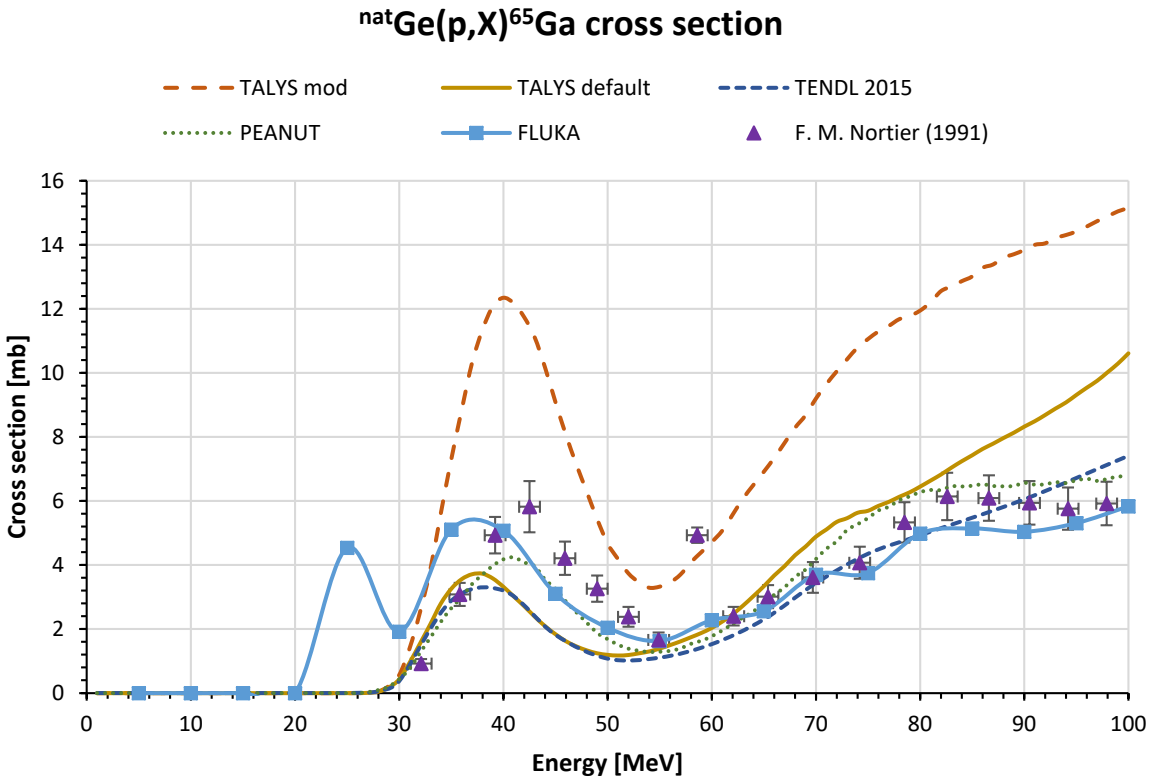

Figure C.24: *cross section for the $^{nat}Ge(p,X)^{65}Ga$ reaction according to various models and experimental data* [C.8]

C.6 Cross sections for the production of ^{67}Ga

In figures C.25, C.26, C.27, C.28 and C.29 are reported the cross sections for the reactions ^{70}Ge(p,X)^{65}Ga, ^{72}Ge(p,X) ^{65}Ga, ^{73}Ge(p,X) ^{65}Ga, ^{74}Ge(p,X) ^{65}Ga and ^{76}Ge(p,X) ^{65}Ga according to the different models. Such data were finally used to produce the plot for the ^{nat}Ge(p,X) ^{65}Ga reaction, reported in figure C.30. Data in EXFOR were found for the reactions ^{70}Ge(p,X)^{65}Ga [C.9] and ^{nat}Ge(p,X) ^{65}Ga [C.7, C.8].

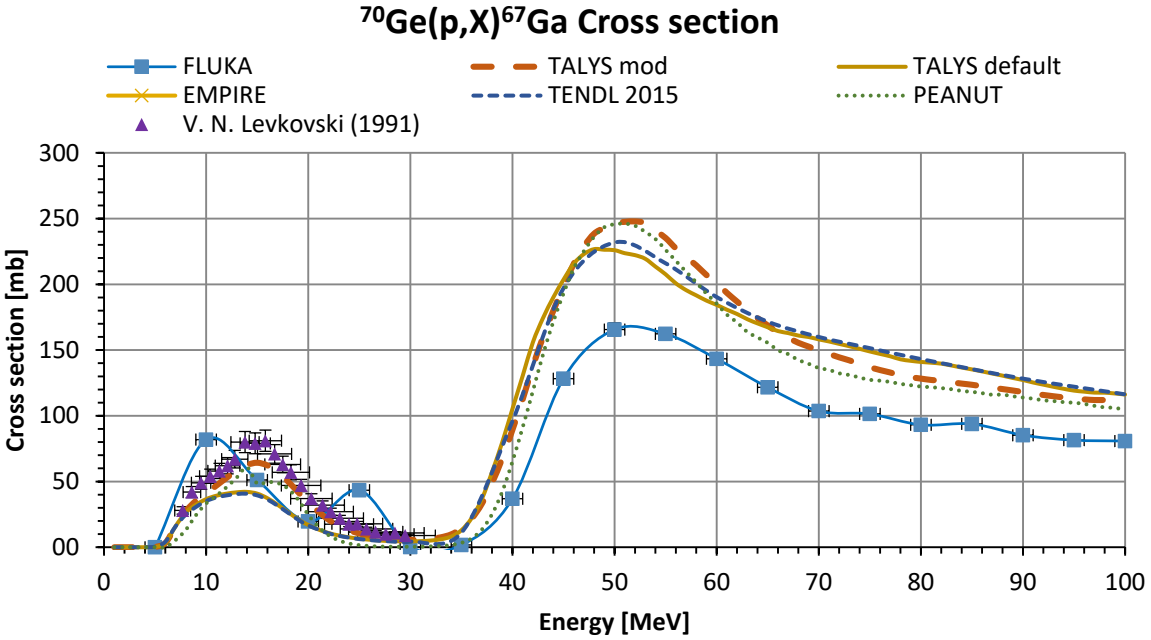

Figure C.25: *cross section for the ^{70}Ge(p,X)^{67}Ga reaction according to various models and experimental data* [C.9]

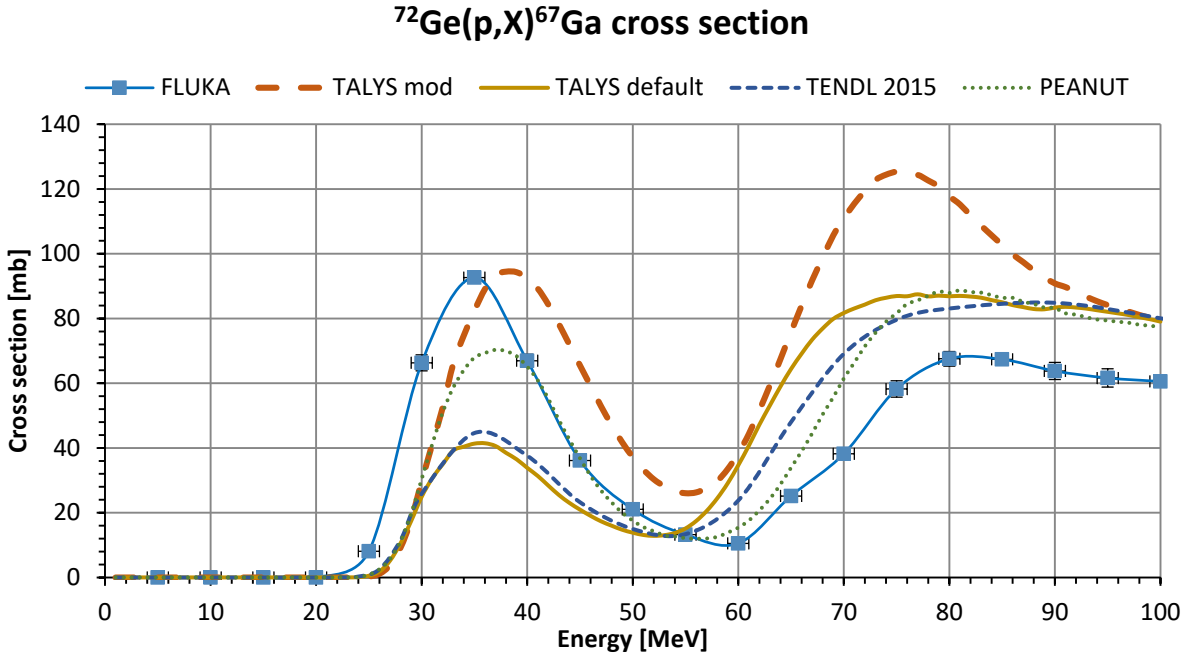

Figure C.26: *cross section for the ^{72}Ge(p,X)^{67}Ga reaction according to various models*

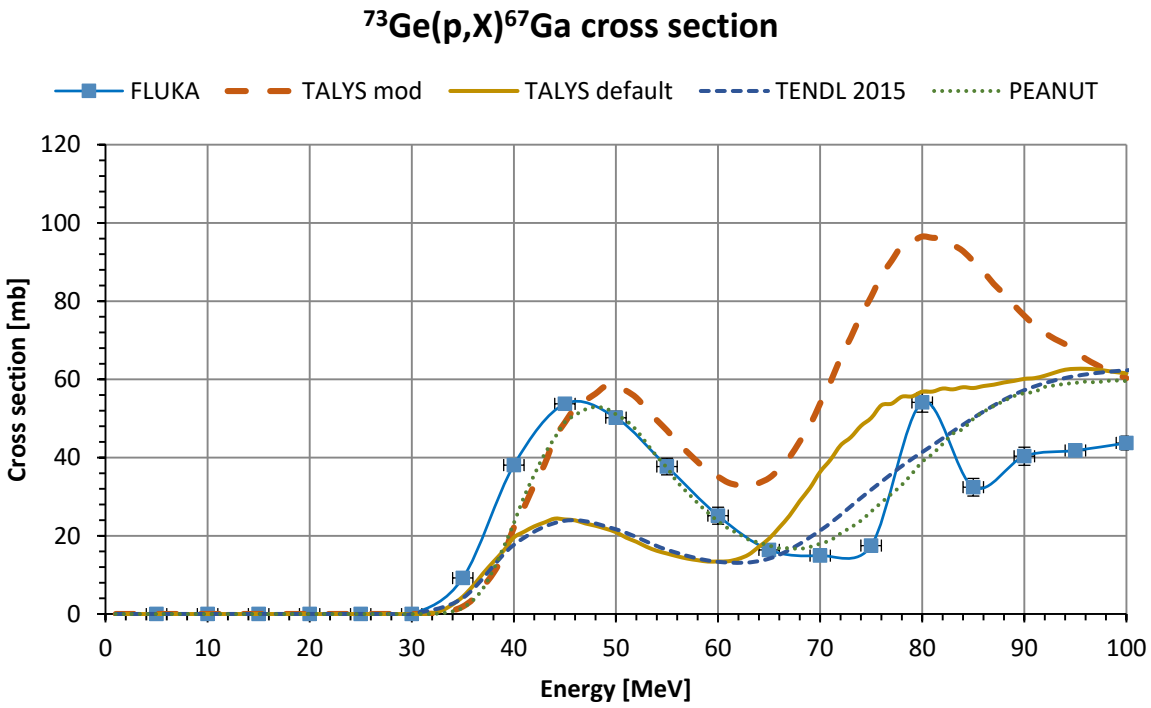

Figure C.27: *cross section for the ^{73}Ge(p,X)^{67}Ga reaction according to various models*

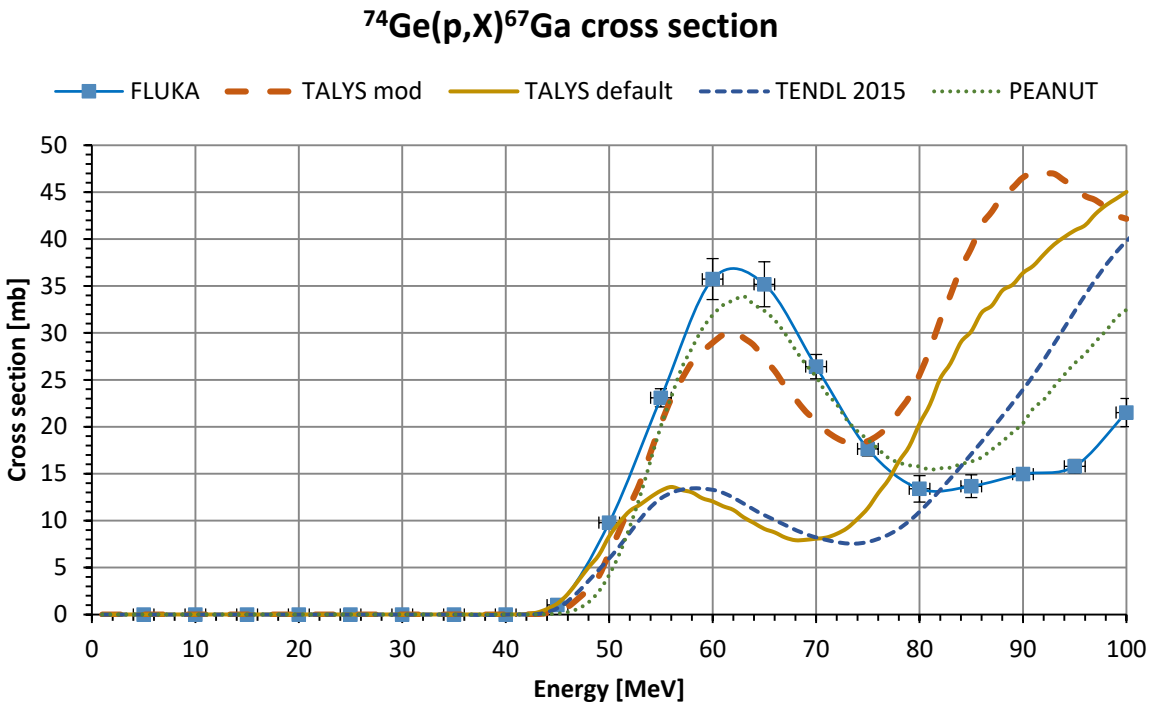

Figure C.28: *cross section for the ^{74}Ge(p,X)^{67}Ga reaction according to various models*

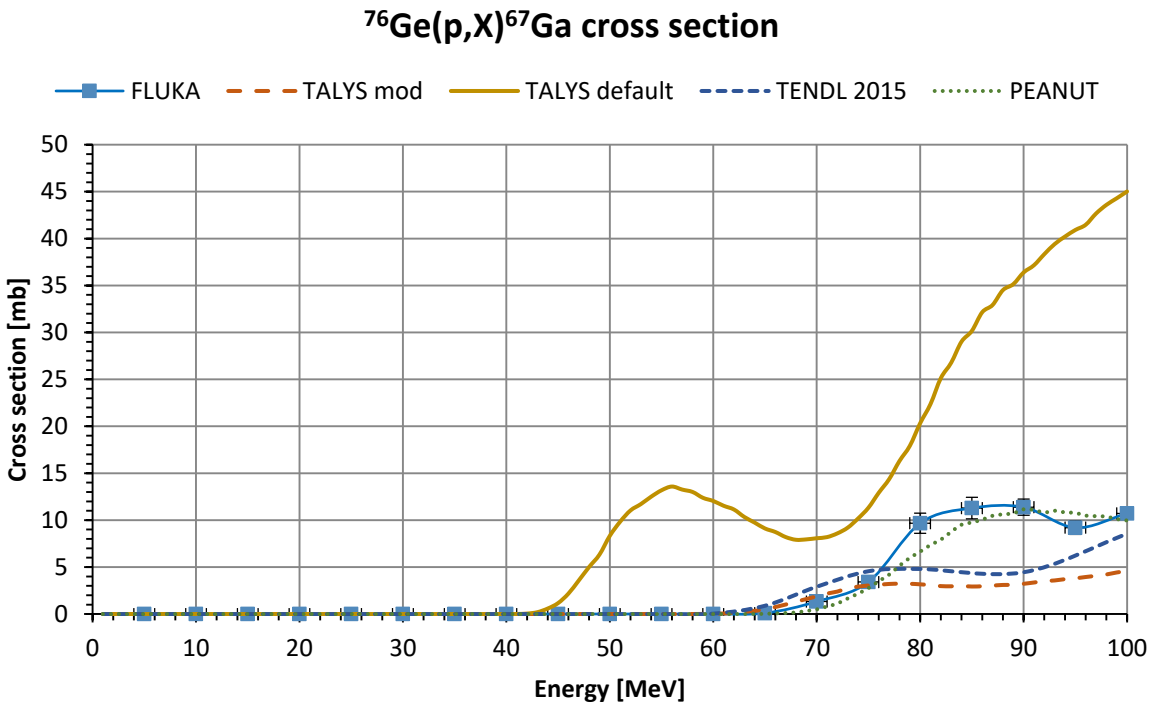

Figure C.29: *cross section for the $^{76}Ge(p,X)^{67}Ga$ reaction according to various models*

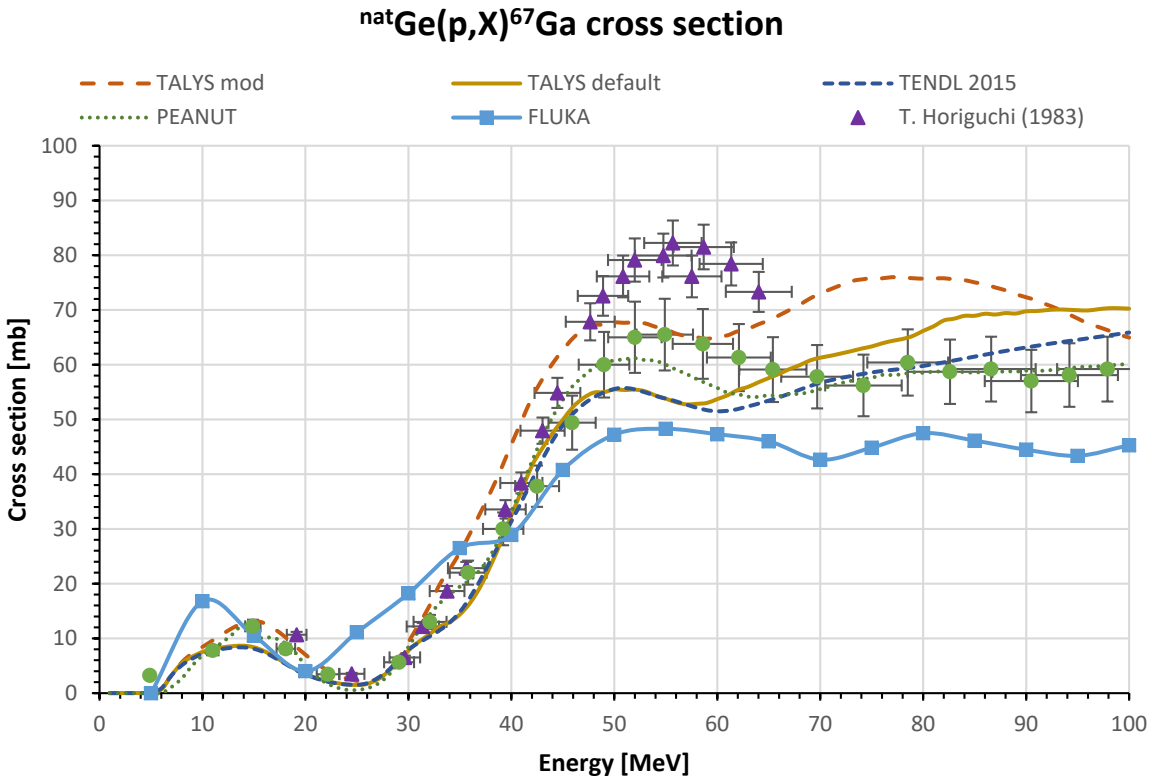

Figure C.30: *cross section for the $^{nat}Ge(p,X)^{67}Ga$ reaction according to various models and experimental data* [C.7, C.8]

C.7 Discussion and conclusions

In this work the cross sections for a large variety of nuclear reactions were calculated by means of both the FLUKA-PEANUT and the TALYS codes.

From the comparison of the produced data it was possible to highlight a general congruence of the various models for the less "exotic" reactions, thus when the involved product was ^{67}Ga, and good match with the few existing experimental data for all considered models. Therefore, for such reactions all models can be considered relatively consistent.

On the other hand, regarding the reactions producing ^{64}Cu and ^{67}Cu, main focus of this study, the models outputted less consistent trends in most cases, thus making difficult to assess the reliability of the calculated cross sections.

Provided that in any case the experimental results might be obsolete, since such measurements were performed almost thirty years ago, the effective reliability of the calculated cross section could be evaluated with an appropriate experimental campaign. Anyway, in addition to the presented codes, other calculations are being performed considering additional models, such as EMPIRE III [C.10].

C.8 References

[C.1] F. Borgna *et al.*, "Early Evaluation of Copper Radioisotope Production at ISOLPHARM," *Molecules*, vol. 23, no. 10, 2018.

[C.2] N. Otuka *et al.*, "Towards a More Complete and Accurate Experimental Nuclear Reaction Data Library (EXFOR): International Collaboration Between Nuclear Reaction Data Centres (NRDC)," *Nucl. Data Sheets*, vol. 120, pp. 272–276, Jun. 2014.

[C.3] A. J. Koning and D. Rochman, "Modern Nuclear Data Evaluation with the TALYS Code System," *Nucl. Data Sheets*, vol. 113, no. 12, pp. 2841–2934, Dec. 2012.

[C.4] M. Brugger, A. Ferrari, S. Roesler, and P. R. Sala, "Calculation of radionuclide production cross sections with FLUKA and their application in high energy hadron collider studies," in *ND2007*, 2007.

[C.5] D. Rochman *et al.*, "The TENDL library: Hope, reality and future," *EPJ Web Conf.*, vol. 146, p. 02006, Sep. 2017.

[C.6] C. Duchemin, A. Guertin, F. Haddad, N. Michel, and V. Métivier, "Production of medical isotopes from a thorium target irradiated by light charged particles up to 70 MeV," *Phys. Med. Biol.*, vol. 60, no. 3, p. 931, 2015.

[C.7] T. Horiguchi, H. Kumahora, H. Inoue, and Y. Yoshizawa, "Excitation function of Ge(p,xnyp) reactions and production of 68Ge," *Int. J. Appl. Radiat. Isot.*, vol. 34, no. 11, pp. 1531–1535, Nov. 1983.

[C.8] F. M. Nortier, S. J. Mills, and G. F. Steyn, "Excitation functions and yields of relevance to the production of 67Ga by proton bombardment of natZn and natGe up to 100 MeV," *Int. J. Radiat. Appl. Instrumentation. Part A. Appl. Radiat. Isot.*, vol. 42, no. 4, pp. 353–359, Jan. 1991.

[C.9] V.N.Levkovski, "Cross sections of medium mass nuclide activation (A=40-100) by medium energy protons and alpha-particles (E=10-50 MeV)," 1991.

[C.10] M. Herman *et al.*, "EMPIRE: Nuclear Reaction Model Code System for Data Evaluation," *Nucl. Data Sheets*, vol. 108, no. 12, pp. 2655–2715, Dec. 2007.